Amelioration of systemic inflammation via the display of two different decoy protein receptors on extracellular vesicles

Dhanu Gupta[1,†], Oscar P.B Wiklander[1†], André Görgens[1,2], Mariana Conceição[3], Giulia Corso[1], Xiuming Liang[1], Yiqi Seow[4], Sriram Balusu[5], Ulrika Feldin[1], Beklem Bostancioglu[1], Rim Jawad[1], Doste R Mamand[1], Yi Xin Fiona Lee[1,7], Justin Hean[8], Imre Mäger[3], Thomas C. Roberts[3,9], Manuela Gustafsson[1], Dara K Mohammad[1,10], Helena Sork[1], Alexandra Backlund[11], C.I. Edvard Smith[12], Matthew J.A. Wood[3,9], Roosmarijn E. Vandenbroucke[5], Joel Z. Nordin[1,ø] and Samir EL Andaloussi[1,ø]

Affiliations

[1]Biomolecular Medicine, Clinical Research Center, Department of Laboratory Medicine, Karolinska Institutet, Stockholm, Sweden
[2]Institute for Transfusion Medicine, University Hospital Essen, University of Duisburg-Essen, Essen, Germany
[3]Department of Paediatrics, University of Oxford, Oxford, UK
[4]Molecular Engineering Laboratory, Institute for Bioengineering and Nanotechnology, A*STAR, Singapore
[5]VIB Center for Inflammation Research, VIB, Ghent, Belgium and Department of Biomedical Molecular Biology, Ghent University, Ghent, Belgium
[6]Biology department, Cihan University-Erbil, Kurdistan Region, Iraq
[7]Genome Institute of Singapore, Agency for Science, Technology and Research, Singapore, Singapore
[8]Evox Therapeutics Limited, Oxford, United Kingdom
[9]MDUK Oxford Neuromuscular Centre, University of Oxford, Oxford, UK
[10]College of Agricultural Engineering Sciences, Salahaddin University-Erbil, 44002 Erbil, Kurdistan Region, Iraq
[11]Cardiovascular Medicine Unit, Department of Medicine, Solna, Karolinska Institute, Stockholm, Sweden
[12]Department of Laboratory Medicine, Clinical Research Center, Karolinska Institutet, Karolinska University Hospital Huddinge, SE-141 86 Huddinge, Sweden
[†]These authors have contributed equally for first authorship.
[ø] These authors have contributed equally for last authorship.

Abstract

Extracellular vesicles (EVs) can be functionalized to display specific protein receptors on their surface. However, surface-display technology typically labels only a small fraction of the EV population. Here, we show that the joint display of two different therapeutically relevant protein receptors on EVs can be optimized by systematically screening EV-loading protein moieties. We used cytokine-binding domains derived from tumour necrosis factor receptor 1 (TNFR1) and interleukin-6 signal transducer (IL-6ST), which can act as decoy receptors for the pro-inflammatory cytokines tumour necrosis factor alpha (TNF-α) and IL-6, respectively. We found that the genetic engineering of EV-producing cells to express oligomerized exosomal

sorting domains and the N-terminal fragment of syntenin (a cytosolic adaptor of the single transmembrane domain protein syndecan) increased the display efficiency and inhibitory activity of TNFR1 and IL-6ST and facilitated their joint display on EVs. In mouse models of systemic inflammation, neuroinflammation and intestinal inflammation, EVs displaying the cytokine decoys ameliorated the disease phenotypes with higher efficacy as compared with clinically approved biopharmaceutical agents targeting the TNF-α and IL-6 pathways.

Keywords: Engineered Extracellular Vesicles, Drug delivery, EV therapeutics, Exosomes, Synthetic biology, Cytokine decoy, Protein engineering.

Introduction

Extracellular vesicles (EVs) hold great potential as therapeutic agents with the ability to functionally deliver therapeutic cargos[1]. We and others have utilized the display of surface ligands to achieve targeted delivery of nucleic acid species in hard-to-reach tissues, such as the central nervous system (CNS)[2–5]. While being a highly promising strategy, recent studies have highlighted the limitations associated with conventional endogenous surface display technologies, as they typically label only a fraction of the EV population and thus limit the targeting capabilities to a sub-set of EVs. Emerging evidence indicates that EVs have numerous subpopulations aside from the classical separation into exosomes, microvesicles, and apoptotic bodies[6–9]. This heterogeneity is critically important in EV engineering, especially when delivery of a therapeutic cargo is required in combination with a targeting ligand approach for a successful therapeutic effect.

Here, we present a engineering strategy to display different protein therapeutics simultaneously on the surface of EVs achieved by synthetic biology and a systematic screening of loading moieties. As proof-of-concept, we targeted inhibition of IL6 and TNFα signaling pathway using an extracellular decoy strategy. Various studies have emphasized that both cytokines play a key role in stimulating inflammation and tissue damage[10,11]. Hence, these pathways are correspondingly targeted by clinically used drugs, including blockers of TNFα (Etanercept, Infliximab and many more) and IL6 receptor (IL6R)(Tocilizumab), to alter the adaptive immune response in autoimmune and inflammatory diseases[12,13]. The soluble TNFα homotrimers exert diverse biological functions, such as cell proliferation, differentiation, and apoptotic signaling, through binding to one of its two receptors, TNF-

receptor 1 (TNFR1) and TNFR2[14]. The cytokine IL6 has broad, pleiotropic biological activities and has been shown to exert both anti-inflammatory and pro-inflammatory signals in deregulated adaptive immune responses[15]. Studies have highlighted that the trans-signaling activation by IL6 complexed to soluble IL6R through IL6 signaling transducer (IL6ST), is linked to inflammation, whereas classical IL6 *cis*-signaling has been shown to be anti-inflammatory and involved in regenerative processes[12]. In this study, we thus aimed to express TNFR1 and IL6ST on EVs as a clinically relevant approach that enable us to assess the display of the therapeutic proteins on a functional level rather than the mere presence on EV surfaces. Furthermore, the therapeutic relevance of these two cytokines in various inflammatory diseases allowed us to investigate the potency of these receptor decoy systems *in vivo*. Here, a screen of multiple endogenous display strategies was conducted for the decoration of the EV surface with cytokine binding domains of TNFR1 and IL6ST, which can decoy the pro-inflammatory cytokines TNFα and IL6, respectively.

This approach provides the ability to display more than one receptor type simultaneously in multimeric form and subsequently enhance their inhibitory activity as compared to conventional therapeutics against the same cytokines. In addition, this approach elicits efficient anti-inflammatory effects *in vivo* by significantly improving survival and disease phenotype in three inflammatory mouse models: lipopolysaccharide (LPS)-induced systemic inflammation, experimental autoimmune encephalomyelitis (EAE), and 2,4,6-Trinitrobenzenesulfonic acid (TNBS)-induced colitis, which mimic sepsis, multiple sclerosis (MS), and inflammatory bowel disease (IBD) respectively. The versatility of this engineering approach was further confirmed by efficacious treatment of EAE using EVs displaying an IL23-alphabody. This work shows great promise for developing engineered, combinatorial EV-based protein therapeutics, as the flexibility of this approach allows robust and efficient surface display of therapeutic proteins and potentially also targeting ligands.

Results

Systemic comparison of engineering strategies for surface display of biologics on EVs

To develop an efficient EV surface display technology, which can be adapted for targeting domains or therapeutic proteins, we designed numerous surface display designs using luminal EV proteins found to be highly enriched in EV proteomic data sets published by us and others[16–18]. As a proof-of-concept model for the display of therapeutic proteins on EVs, we fused these

EV domains to the cytokine binding domains of either TNFR1 or to IL6ST, for decoy sequestration of TNFα or IL6/IL6R heterodimeric complexes respectively, and further engineered these receptors to be signaling incompetent. This enabled evaluation of various surface display designs in a semi-high throughput workflow by assessing the ability of engineered EVs to decoy their respective cytokine (see schematic illustration of decoy EVs in (Extended Data Figure 1A). An array of genetic constructs was designed using different exosomal sorting proteins, or their respective domains annotated for EV sorting (Figure 1A-B).

HEK293T cells were transiently transfected with plasmids encoding the different display constructs and engineered EVs were purified by ultracentrifugation and quantified by nanoparticle tracking analysis (NTA) (Extended Data Figure 1B and 1C). The potency of the purified EVs was assessed using an *in vitro* reporter system for the respective cytokine, either by detecting luciferase activity driven by a NF-κB minimal promoter (TNFα, Extended Data Figure 1D) or secreted alkaline phosphatase (SEAP) driven by a STAT3 minimal promoter (IL6/sIL6R, Extended Data Figure 1E). We observed inhibitory activity of engineered decoy EVs with various designs in a dose-dependent manner (Figure 1C, D). Constructs with inclusion of the N-terminal sorting domain derived from Syntenin (TNFR1-N term Syntenin and IL6ST-N term Syntenin), a protein implicated in sorting of protein cargo into EVs, significantly and reproducibly exhibited the best inhibitory activity for both IL6ST and TNFR1 signaling incompetent receptor constructs (Figure 1A-D and Supp. Figure 1A). Furthermore, the quantitative assessment of EVs by western blot (WB) probing for the respective decoy receptor (TNFR1 or IL6ST) or the fused His-Tag on the C terminus of each construct mirrored the functionality of cytokine decoy EVs. Notably, TNFR1-N term Syntenin (Supp. Figure 1B & 2) and IL6ST-N term Syntenin (Supp. Figure 3 & 4) displayed a clear band in both parental cells and EVs of respective decoy receptor. Interestingly, we moreover observed cleavage products of the TNFR1 fusion protein only upon probing the WB with the His-Tag antibody and not with the hTNFR1 antibody. We hypothesized that a matrix metalloprotease (MMP) cleavage site previously annotated[19] in TNFR1 resulted in cleavage of the receptor from the decoy EV surface, hence reducing the efficacy of the TNFR1-decoy EVs. Deletion of the MMP cleavage site on the TNFR1 extracellular domain reduced the levels of the cleaved product and resulted in a further 10-fold increase of the inhibitory activity in reporter cells (Supp. Figure 5A-B).

To further increase efficiency, multimerization domains were introduced in different positions within the constructs to increase the number of decoy receptors per EV and to mimic the natural receptor state *in situ*[12,13]. A trimerization domain 'Foldon' derived from T4 fibritin protein of the T4 bacteriophage[20] was introduced to the lead TNFR1 design either in the extracellular- or intracellular region (Figure 2A), which further increased the efficiency of the decoy EVs to sequester TNFα (Figure 2B-C). Similarly, we introduced a dimerization domain 'GCN4 L.Z', derived from yeast[21], and a tetramerization domain 'Fragment X', derived from Phosphoprotein P of the human metapneumovirus[22], to the IL6ST-N term Syntenin construct in the intracellular domain (Figure 2D). Both designs showed a significant enhancement over their predecessors (Figure 2E and 2F). However, addition of the dimerization domain both in the extracellular and intracellular domain simultaneously decreased the efficacy of the display, potentially because it affects the cytokine binding properties of the receptor. Furthermore, a sorting domain derived from transferrin receptor (TfR) along with GCN4 L.Z dimerization domain showed similar efficacy as compared to Syntenin in our screen when it was fused to IL6ST. Importantly, the variation in active dose among the different sets of experiments is primarily due to large-scale transfection and therefore a relative comparison with multiple doses was performed in every screen to account for this variation.

Based on these findings, the N-term-Syntenin was selected as the EV-sorting domain for both TNFR1 and IL6ST decoy EVs with the intracellular dimerization domain included for IL6ST (IL6STΔ-LZ-NST) and with the intracellular trimerization domain and deletion of MMP-cleavage site for TNFR1 (TNFR1ΔΔ-FDN-NST) (Figure 2A and 2D). As foreign protein sequences in the extracellular domains might lead to immune responses that could affect multi-dosing strategies, designs with intracellular multimerization domains were chosen for subsequent work[23].

Moreover, to further benchmark these optimized designs to established surface display technologies, the optimized TNFR1ΔΔ-FDN-NST construct was compared to TNFR1ΔΔ-Lamp2b and TNFR1ΔΔ-PTGFRN since both Lamp2b[24] and PTGFRN[25] have been used as efficient display approach in recent publications. TNFR1ΔΔ-FDN-NST outperformed both these display scaffolds in the functional TNFα reporter assay (Figure 3A). The TNFR1ΔΔ-FDN-NST engineered EVs showed 50% inhibition of TNFα induced NF-kB activation at a

dose as low as $5x10^8$/ml. In contrast, the PTGFRN showed moderate activity only at the highest dose ($2X10^9$/ml), and Lamp2b fused constructs failed to show any bioactivity at the doses tested in this dose-range. This is in line with unpublished work from us showing that although peptide display is efficient on Lamp, the protein can be less amenable to engineering with larger proteins (unpublished data). Furthermore, single vesicle flow cytometry analysis of the different display strategies indicated that the TNFR1ΔΔ-FDN-NST could engineer 60% of the total EV population (Supp. Figure 5C), whereas PTGFRN and Lamp2b fusion protein was detected only on 16% and 6% of the EVs, respectively, thus collaborating the results observed in the functional assay. Notably, the positive 6% of TNFR1ΔΔ-Lamp2b EVs showed a higher abundance of the fusion protein than TNFR1ΔΔ-FDN-NST and TNFR1ΔΔ-PTGFRN engineered EVs. Hence Lamp2b is efficient for EV engineering but is restricted to a small subset of EVs.

After establishing the potency of our lead constructs using transient transfections, we next generated stable cells to allow for production scale-up and reduced variability emanating from transient transfection of cells. Hence, we stably engineered HEK293T producer cells for production of IL6STΔ-LZ-NST- and TNFR1ΔΔ-FDN-NST-decoy EVs using lentiviral transduction. HEK293T IL6STΔ-LZ-NST decoy EVs inhibited IL6/IL6R induced trans-signaling with reduced STAT3 activation and TNFR1ΔΔ-FDN-NST-decoy EVs could inhibit TNFα stimulated NF-kB activation in a dose-dependent manner (Supp. Figure 6A and 6B). To further validate whether our EV engineering strategy is applicable to other cell types, we validated the approach in a more therapeutically relevant cell source, mesenchymal stem cells (MSC), which were engineered to stably produce the respective decoy EVs (Supp. Figure 6C). MSC TNFR1ΔΔ-FDN-NST and IL6STΔ-LZ-NST EVs displayed a dose response to decoy the cytokines similar to what was observed using HEK293T cell-derived decoy EVs (Figure 3B-C). The engineered MSC-derived EVs were characterized using NTA, showing that the majority of the EVs were in the size range of exosomes with a peak of around 100 nm (Supp. Figure 6D), and the yield of the EVs were unaltered by the engineering strategy (Supp. Figure 6E).

Characterization by WB of isolated EVs from the respective cell source confirmed expression of both common EV markers ALIX and TSG101, absence of apoptotic body marker calnexin and presence of the respective decoy proteins (Figure 3D)[26]. In addition, the presence of decoy

receptors (TNFR1 or IL6ST) on EVs was confirmed by immunogold electron microscopy, using primary antibodies against the respective decoy receptor (Figure 3E). To accurately determine the number of engineered receptors on EVs, image-based flow cytometry was performed. Using this method, we estimated that, an average of 600 TNFR1 receptors are displayed per vesicle (Supp. Fig 6F-H).

The EV engineering strategy is highly efficient and maintain the innate properties of EVs

To determine the impact on the EV surface proteomic profile possibly caused by the engineering, a multiplex bead-based flow cytometry assay was applied for simultaneous flowcytometric detection of 37 surface proteins on CD63/CD81/CD9 positive vesicles[27] (Figure 3F). MSC-derived TNFR1ΔΔ-FDN-NST and IL6STΔ-LZ-NST decoy EVs exhibited a highly similar surface protein profile as compared to MSC Ctrl EVs for 37 different surface markers on tetraspanins positive vesicles (Figure 3G and Supp. Figure 8A-C). Additionally, to determine whether the decoy receptors are present on the tetraspanins positive subpopulation of EVs, we modified the bead-based assay by using decoy receptor-based detection instead of tetraspanins-based detection of the 37 different capture beads. Upon using hTNFR1 antibody as a detection antibody for assessing the 37 different antigens, CD63 and CD81 were observed to be the most enriched surface markers on TNFR1ΔΔ-FDN-NST positive vesicles, whereas Ctrl EVs and IL6STΔ-LZ-NST EVs were negative for all markers, since only TNFR1 positive EVs is detected (Figure 3H and Supp. Figure 8D-F). A similar trend was observed for IL6STΔ-LZ-NST EVs upon using mIL6ST antibody as the detection antibody (Figure 3I and Supp. Figure 8G-I). Importantly, this engineering strategy preserved the angiogenic potential of MSC EVs as determined using an endothelial cells tube formation assay (Supp. Figure 9).

Next, an *in vivo* toxicity assessment was conducted to ensure that the engineered EVs are safe. A genetic disease model was utilized to avoid variability caused by chemically inducing the disease and with a phenotype independent of the target cytokine. Mice with a Duchenne muscular dystrophy (DMD) phenotype were selected as they have been shown to be IL-6 independent[28] and were injected with IL6TΔ-LZ-NST MSC EVs either intravenously (I.V) or subcutaneously (S.C) twice per week for two weeks using three different doses. No significant differences between PBS and IL6STΔ-LZ-NST EVs were observed in terms of hematological (Supp. Figure 10A-F) and physiological parameters (Supp. Figure 10G-H). These results clearly indicate that our engineering strategy allows for highly efficient engineering of EVs

with negligible disruption of the endogenous surface protein profile and the engineered EVs are furthermore well tolerated with a good *in vivo* toxicity profile in diseased mice. These observations are in line with previous reports on exogenous EVs immunogenicity and toxicity[29,30].

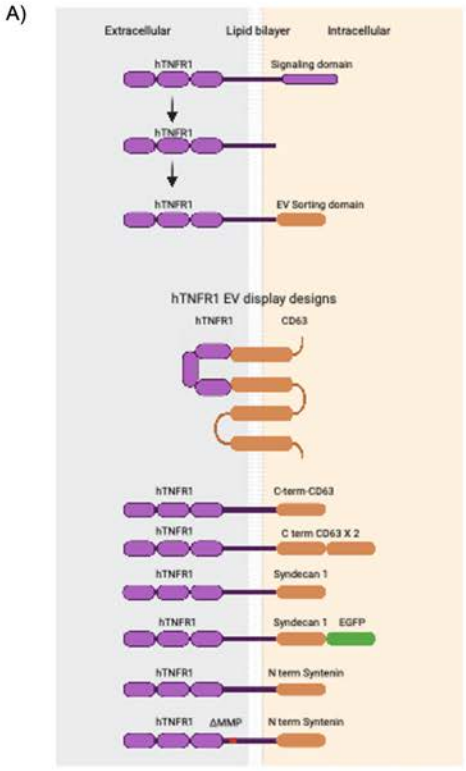
A)
Extracellular
Lipid bilayer
Intracellular
hTNFR1
Signaling domain
hTNFR1
hTNFR1
EV Sorting domain
hTNFR1 EV display designs
hTNFR1
CD63
hTNFR1
C-term-CD63
hTNFR1
C term CD63 X 2
hTNFR1
Syndecan 1
hTNFR1
Syndecan 1
EGFP
hTNFR1
N term Syntenin
hTNFR1
ΔMMP
N term Syntenin

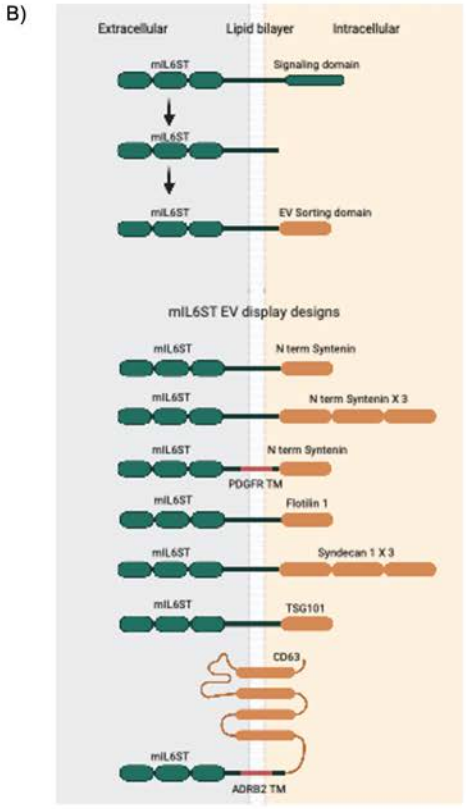
B)
Extracellular
Lipid bilayer
Intracellular
mIL6ST
Signaling domain
mIL6ST
mIL6ST
EV Sorting domain
mIL6ST EV display designs
mIL6ST
N term Syntenin
mIL6ST
N term Syntenin X 3
mIL6ST
N term Syntenin
PDGFR TM
mIL6ST
Flotilin 1
mIL6ST
Syndecan 1 X 3
mIL6ST
TSG101
CD63
mIL6ST
ADRB2 TM

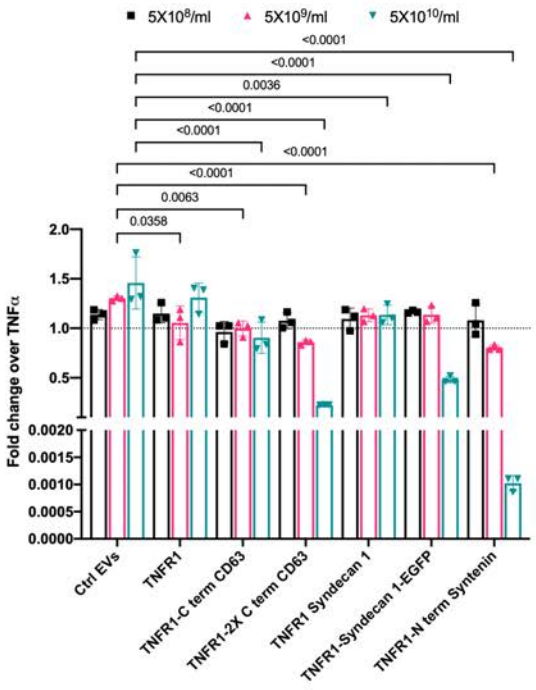
C)
5X10^8/ml
5X10^9/ml
5X10^10/ml
<0.0001
<0.0001
0.0036
<0.0001
<0.0001
<0.0001
<0.0001
0.0063
0.0358
Fold change over TNFα
2.0
1.5
1.0
0.5
0.0020
0.0015
0.0010
0.0005
0.0000
Ctrl EVs
TNFR1
TNFR1-C term CD63
TNFR1-2X C term CD63
TNFR1 Syndecan 1
TNFR1-Syndecan 1-EGFP
TNFR1-N term Syntenin

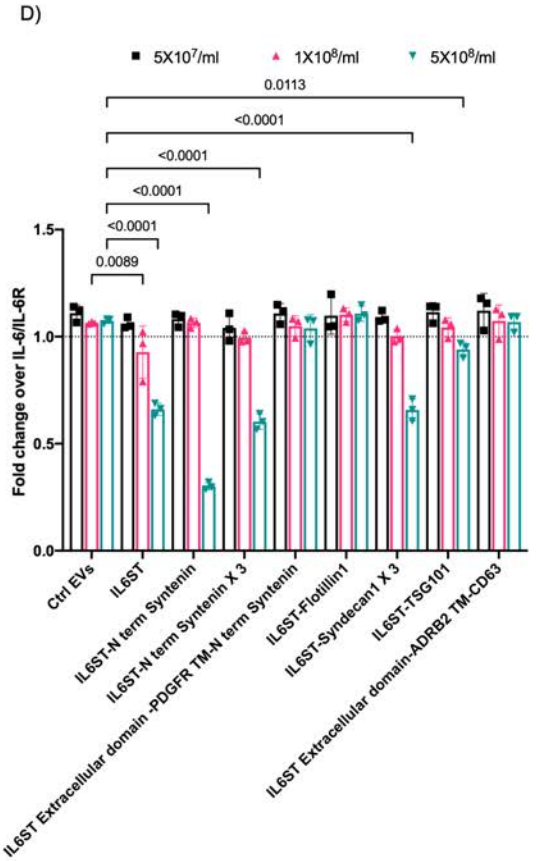
D)
5X10^7/ml
1X10^8/ml
5X10^8/ml
0.0113
<0.0001
<0.0001
<0.0001
<0.0001
0.0089
Fold change over IL-6/IL-6R
1.5
1.0
0.5
0.0
Ctrl EVs
IL6ST
IL6ST-N term Syntenin
IL6ST-N term Syntenin X 3
IL6ST Extracellular domain -PDGFR TM-N term Syntenin
IL6ST-Flotillin1
IL6ST-Syndecan1 X 3
IL6ST-TSG101
IL6ST Extracellular domain-ADRB2 TM-CD63

Figure 1. Systematic screening of multiple endogenous EV display strategies for cytokine decoys. A) and B) List of various TNFR1 or IL6ST sorting domain fusions assessed in the initial screen. **C)** Engineered decoy EVs displaying TNFR1 purified from HEK293T cells transfected with the constructs encoding the different display constructs (Figure1D) evaluated for TNFα decoy in an *in vitro* cell assay responsive to TNFα induced NF-κB activation. Data were normalized to control cells treated with TNFα only (5 ng/ml). **D)** Engineered EVs displaying IL6ST purified from HEK293T cells transfected with constructs encoding the different display constructs (Figure1G) evaluated for IL6/sIL6R decoy in an *in vitro* cell assay respondent to IL6/sIL6R induced STAT3 activation. Data were normalized to control cells treated with IL6/sIL6R (5 ng/ml). **C, D,** Central Value: Mean, Error bars: S.D (*Biological replicate, n*=3), statistical significance calculated by two-way ANOVA with Dunnett's post-test compared with response of Ctrl EVs at the respective dose.

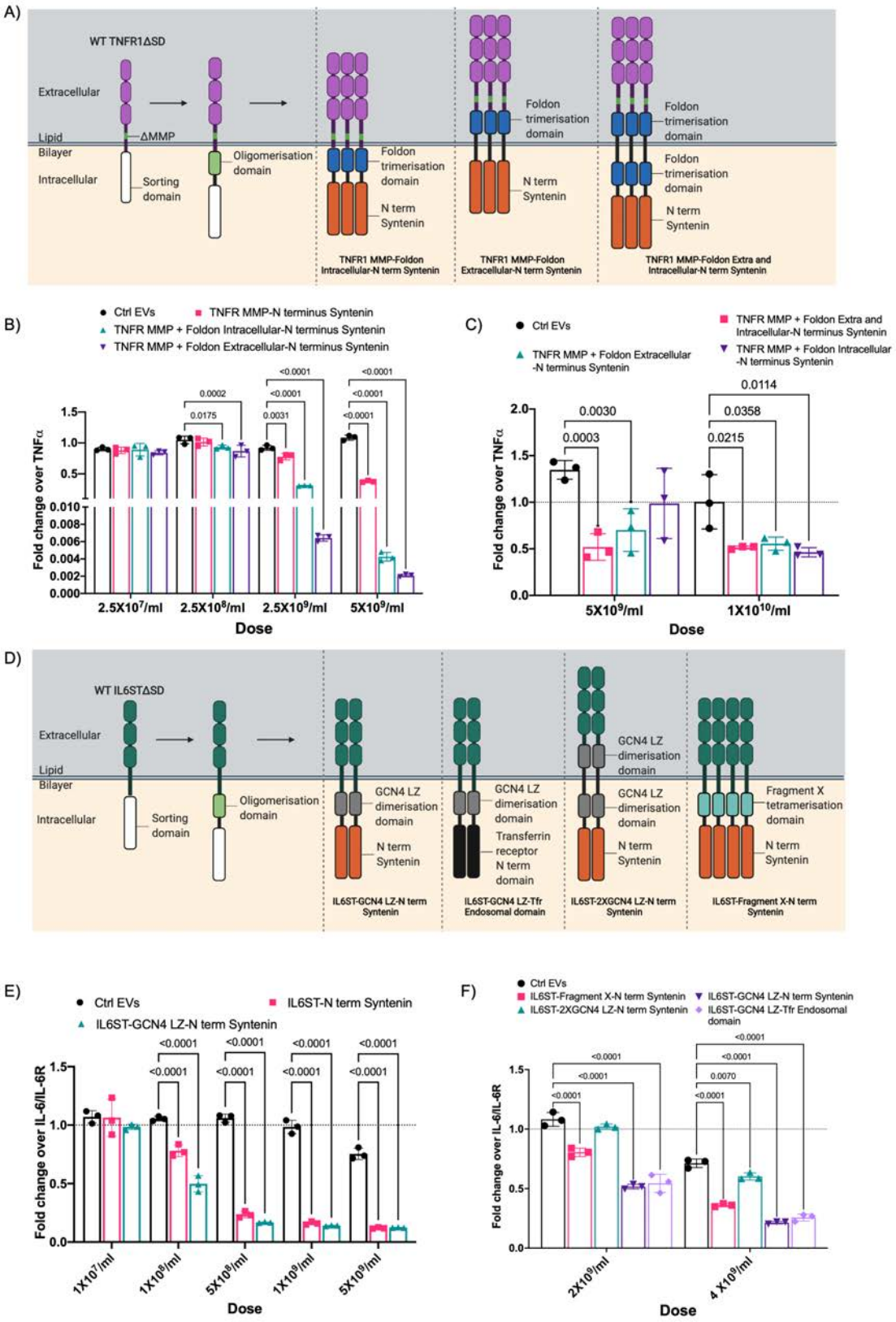

Figure 2. Multimerization of decoy fusion proteins improves loading and activity A) Schematic illustration showing the evolution of TNFR1 design by addition of trimerization

domains to enhance loading and binding efficiency of the EV- displayed decoy receptors. **B) and C)** Systematic comparison of various TNFR1 designs with multimerization domains. Engineered EVs displaying TNFR1 purified from HEK293T cells transfected with constructs encoding TNFR1 multimerization sorting domain fusion proteins (as listed in Figure 2A) evaluated for TNFα neutralisation in an *in vitro* cell assay responsive to TNFα induced NF-κB activation. Data were normalized to control cells treated with TNFα only (5 ng/ml). **D)** Schematic illustration showing the evolution of IL6ST designs by addition of different multimerization domain to enhance loading and binding efficiency of displayed decoy receptors on EVs. **E) and F)** Engineered EVs displaying IL6ST purified from HEK293T cells transfected with constructs encoding IL6ST multimerization sorting domain fusion constructs (as listed in Figure 2D) respectively evaluated for IL6/sIL6R decoy in an *in vitro* cell assay respondent to IL6/sIL6R induced STAT3 activation. Data were normalized to control cells treated with IL6/sIL6R (5 ng/ml). **B, C, E, F,** Central Value: Mean, Error bars: S.D (*Biological replicate, n*=3), statistical significance calculated by two-way ANOVA with Dunnett's post-test compared with response of Ctrl EVs at the respective dose.

Engineered decoy EVs display improved efficacy compared to conventional biologics

Next, we sought to investigate the efficacy of engineered EVs and benchmark them to a clinically approved biologic against TNFα, Etanercept (a dimeric TNFR2 protein)[13]. Using the aforementioned TNFα reporter model, HEK293T TNFR1ΔΔ-FDN-NST decoy EVs showed a 10-fold lower IC50 value compared to Etanercept (Figure 4A-B). To further evaluate our natural engineered vesicles, their ability to decoy TNFα *in vitro* was compared to a synthetic proteoliposome displaying hTNFR1 protein (provided by Creative Biolabs). With concentrations of hTNFR1 proteoliposomes as high as 100 ng/ml we did not observe any inhibition of TNFα activity in our functional assay (Supp. Figure 11). This lack of activity could potentially be due to various factors ranging from choice of *in vitro* translation system to reverse orientation of hTNFR1 protein on the surface of proteoliposomes[31], hence the synthetic system require more rigorous optimization before displaying efficient decoy activity. In addition, in our experience cost of manufacturing the proteoliposome compared to EVs was orders of magnitude higher. Moreover, there is naturally a possibility that the synthetic system is not suitable for displaying proteins in large enough quantities.

Nevertheless, in order to further validate the potency of engineered EVs, a physiologically more relevant *in vitro* model of inflammation was utilized. Using RAW 246.7 macrophages challenged with LPS, HEK293T TNFR1ΔΔ-FDN-NST decoy EVs significantly decreased secreted TNFα levels by RAW 246.7 macrophages, in a dose-dependent manner both at 6 hours and 24 hours post stimulation (Figure 4C and Supp. Figure 12A and 12B). After these encouraging *in vitro* results, the potency of decoy EVs was assessed *in vivo* using an LPS-

induced systemic inflammation mouse model. Intravenous (I.V) injection of HEK293T decoy EVs along with LPS challenge in mice resulted in significantly improved survival (100% up to 60 hours post injection) of TNFR1ΔΔ-FDN-NST- and IL6STΔ-LZ-NST EV treated mice compared to 0% survival of mock treated mice (Figure 4B). This was further corroborated with MSC-derived TNFR1ΔΔ-FDN-NST decoy EVs (1×10^{11}), which showed improved survival (100% up to 60 hours) compared to 160 μg Etanercept (25% at 60 hours) and 1×10^{11} Ctrl EVs (50% at 60 hours) (Figure 4E). Despite enhancement in the survival rate of the animals treated with engineered EVs, the therapeutic effect was not evident based on the change in body weight (Supp. Figure 10C). This could be due to a lower dose of therapeutic EVs in relation to the severity of the disease model. Therefore, in a separate experiment, we increased the therapeutic dose of engineered EVs. Mice treated with 6.5×10^{11} MSC IL6STΔ-LZ-NST and/or 6.5×10^{11} MSC TNFR1ΔΔ-FDN-NST decoy EVs and displayed significant reduced weight loss as compared to Ctrl EV treatment (Figure 4F). Notably, the protective effect in mice with LPS-induced inflammation was improved by combinatorial treatment with both decoy EVs, as compared to 6.5×10^{11} unmodified MSC-EVs. These results collectively underpin the therapeutic potential of decoy EVs and led us to continue assessing the therapeutic anti-inflammatory potential of decoy EVs in an autoimmune MS disease model.

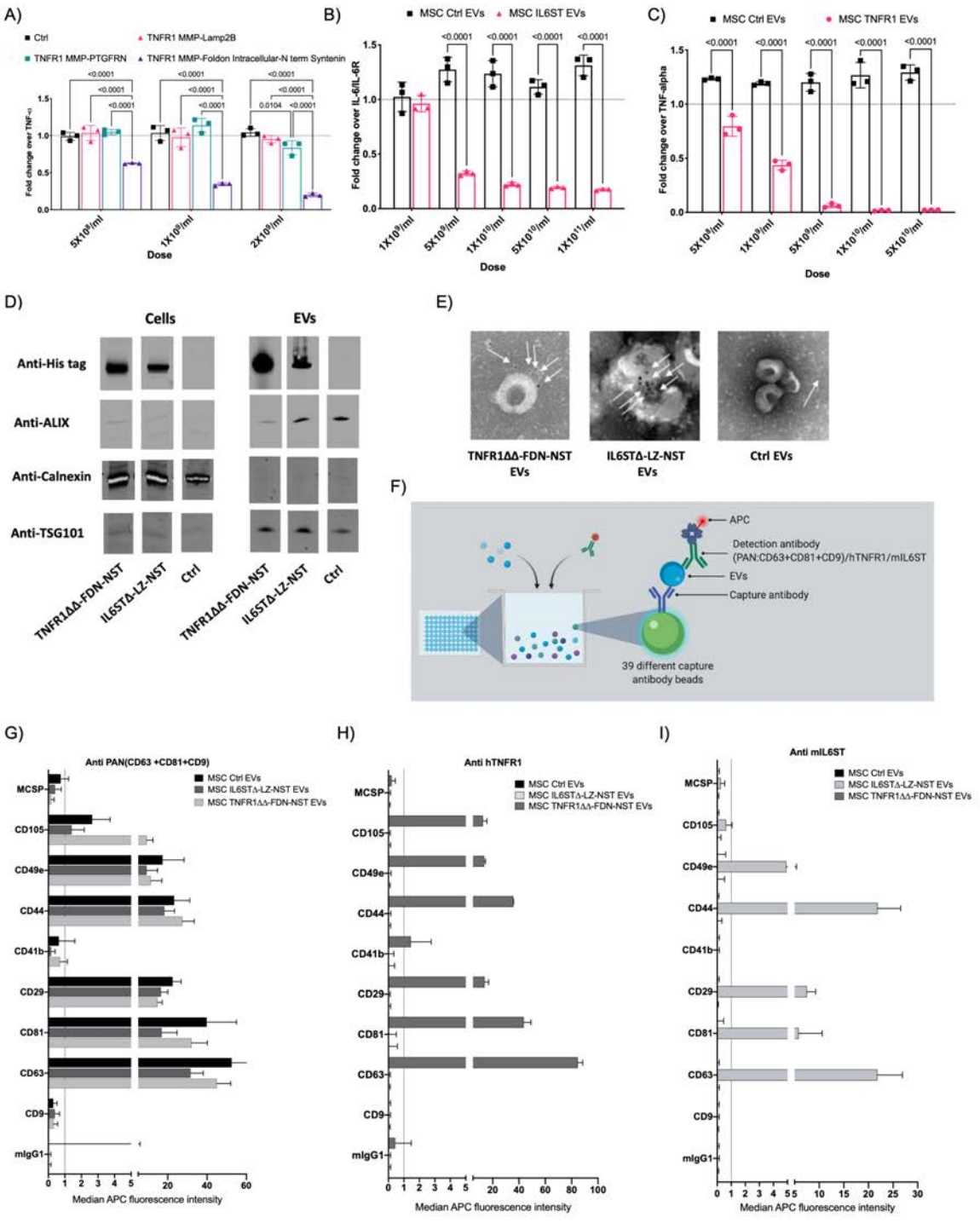

Figure 3. Multimeric decoy receptor EV sorting protein chimera is functionalized on several EV subpopulations. A) Comparison of the optimized TNFR1 display design with currently available EV engineering strategies. Engineered EVs, displaying TNFR1 purified from HEK293T cells transfected with constructs listed in the figure were evaluated for TNFα neutralisation in an *in vitro* cell assay responsive to TNFα induced NF-ϰB activation. Data were normalized to control cells treated with TNFα only (5 ng/ml). **B)** Engineered EVs

displaying IL6ST purified from MSC cells stably expressing the optimized IL6STΔ-LZ-NST display construct, evaluated for IL6/sIL6R decoy in an *in vitro* cell assay respondent to IL6/sIL6R induced STAT3 activation. EVs purified from MSC stably expressing Ctrl construct were used as control. Data were normalized to control cells treated with IL6/sIL6R (5 ng/ml). **C)** Engineered EVs displaying TNFR1 purified from MSC cells stably expressing the optimized TNFR1ΔΔ-FDN-NST display construct, evaluated for TNFα decoy in an *in vitro* cell assay responsive to TNFα induced NF-κB activation. EVs purified from MSC stably expressing Ctrl construct were used as control. Data were normalized to control cells treated with TNFα (5 ng/ml). **D)** WB of MSC TNFR1ΔΔ-FDN-NST, IL6STΔ-LZ-NST and Ctrl cells and EVs indicating the presence of EV markers; ALIX (96 kDa), TSG101 (44 kDa) and absence of Calnexin (67 kDa) in the isolated EVs. The WB results further demonstrate the presence of respective His-tagged decoy receptors; TNFR1ΔΔ-FDN-NST (48 kDa) and IL6STΔ-LZ-NST (94 kDa) both on cells and EVs. Uncropped gel images included in Supp. Figure 7. **E)** Transmission electron microscopy of MSC TNFR1ΔΔ-FDN-NST, IL6STΔ-LZ-NST and Ctrl-EVs with nanogold labelled antibody staining of respective decoy receptor indicated by white arrows. **F)** Schematic illustration showing the workflow of the multiplex bead-based flow cytometry assay. Isolated EVs incubated with up to 39 different bead populations coated with different capture antibodies, which are distinguishable by flow cytometry due to their different fluorescence intensities. EVs captured by the different beads are detected with detection PAN (CD63-APC, CD81-APC and CD9-APC), mIL6ST-APC, or hTNFR1-APC antibodies. **G-I)** Characterization of EV surface protein composition by using G) anti-PAN (CD63, CD81 and CD9), H) anti-hTNFR1 and I) anti-mIL6ST detection antibodies in multiplex bead-based assays to confirm marker co-expression on MSC TNFR1ΔΔ-FDN-NST, IL6STΔ-LZ-NST and ctrl EVs. Data represented as background corrected median APC fluorescence intensity determined by flow cytometry of EVs bound to respective capture bead and upon using APC labelled detection antibody. **A, B, C** Central Value: Mean, Error bars: S.D (*Biological replicate, n=*3), statistical significance calculated by two-way ANOVA with Dunnett's post-test compared with response of Ctrl EVs at the respective dose. **G, H, I** Central Value: Mean, Error bars: S.D *(Technical replicate, n=5000-15000)*.

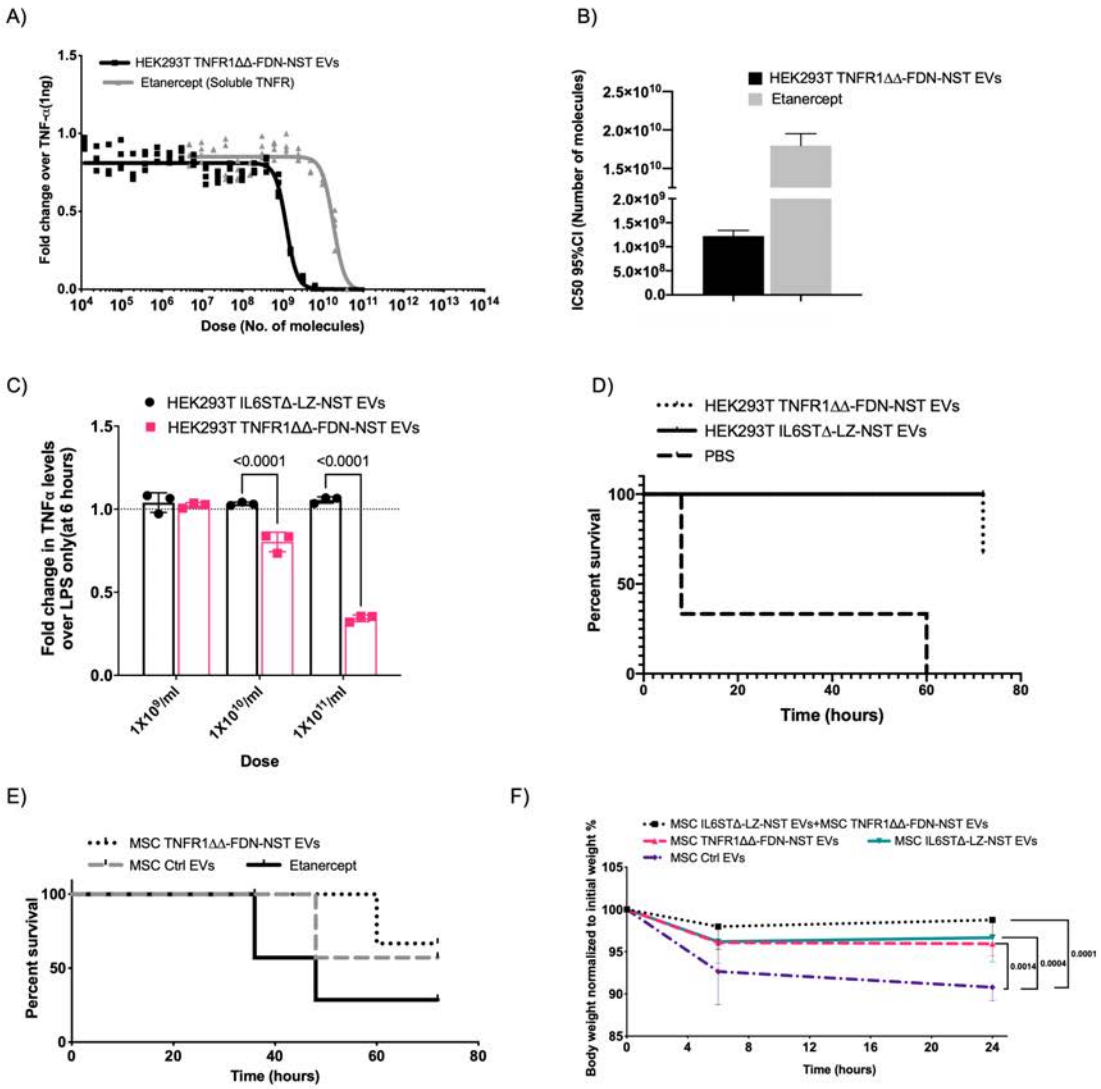

Figure 4. Benchmarking Engineered decoy EVs against clinically approved biologics both *in vitro and in vivo*. Comparison of **A)** inhibitory dose response curves and **B)** calculated IC50 values (95% Confidence interval) for TNFα sequestration by HEK293T TNFR1ΔΔ-FDN-NST EVs and Etanercept. HEK293T NF-kB reporter cells were challenged with 10 ng/ml (1 ng) of TNFα along with increasing doses of either HEK 293T TNFR1ΔΔ-FDN-NST EVs or Etanercept. **C)** Effect of HEK293T TNFR1ΔΔ-FDN-NST EVs and IL6STΔ-LZ-NST EVs on TNFα levels in conditioned medium determined by ELISA at 6 hours post LPS stimulation of RAW 246.7 macrophages. Data were normalized to control cells treated with LPS only. **D)** Survival curve of LPS (15 mg/kg) induced systemic inflammation in mice treated with I.V injection of either $1x10^{11}$ HEK 293T TNFR1ΔΔ-FDN-NST EVs (n=3) or 2×10^{11} HEK293T IL6STΔ-LZ-NST EVs (n=4) or PBS (n=5) 3 hours post induction. P = (0.0120) based on Gehan-Breslow-Wilcoxon test. **E)** Survival curve of LPS (15 mg/kg) induced systemic inflammation in mice treated with I.V injection of either 1×10^{11} MSC TNFR1ΔΔ-FDN-NST

EVs (n=7) or 1×10^{11} MSC Ctrl EVs (n=7) or 160 μg Etanercept (n=7) 3 hours post LPS induction. P = (0.0140) based on Gehan-Breslow-Wilcoxon Test. **F)** Percent relative bodyweight to initial bodyweight over time of mice induced with LPS (15 mg/kg). Mice were treated with I.V injection of either 3.25×10^{11} MSC IL6STΔ-LZ-NST EVs + 3.25×10^{11} MSC TNFR1ΔΔ-FDN-NST EVs (n=6), 6.5×10^{11} MSC TNFR1ΔΔ-FDN-NST EVs (n=6), 6.5×10^{11} MSC IL6STΔ-LZ-NST EVs (n=6), 6.5×10^{11} MSC Ctrl EVs (n=6), or PBS (n=6) 3 hours post induction. **A, (***Biological replicate, n*=3), Central line: Non-linear fit derived from 4 parameter logistic regression model. **B,** IC50 range with 95% confidence interval derived from same data set as plotted in **A**, Central Value: Mean, Error Bars: upper and lower limit. **C,** Central Value: Mean, Error bars: S.D (*Biological replicate, n*=3), Statistical significance calculated by two-way ANOVA with Dunnett's post-test compared with response of both groups at respective dose. **F,** Central Value: Mean, Error bars: S.D, Statistical significance calculated by two-way ANOVA with Dunnett's post-test compared with response of Ctrl EVs at the respective observation time.

Engineered decoy EVs inhibit progression of neuroinflammation

We have previously shown that EVs can be used to treat hard-to-reach tissues, including the ability to cross the blood-brain-barrier and exhibit therapeutic effects in the central nervous system (CNS)[4]. To explore the potential effect of decoy EVs in neuroinflammation, the experimental autoimmune EAE mouse model, mimicking MS in humans, was used. To evaluate the effect of the treatment, clinical scores 0-5 are used that reflect the disease severity (EAE-score, Supp. Table 1). Upon repeat Subcutaneous (S.C) administration of control MSC EVs, as depicted in Figure 5A, no effect was observed on disease progression compared to mock treatment. However, as hypothesized, TNFR1ΔΔ-FDN-NST decoy EVs (4×10^{10}) S.C injected significantly reduced disease progression over time (Figure 5B). At the endpoint (day 16), mice treated with decoy EVs could still move freely, with only minor tail and/or hind limb weakness, as compared to mock treated mice that were hind limb paralyzed. Additionally, significantly lower EAE-scores were observed in mice treated with TNFR1ΔΔ-FDN-NST decoy EVs (EAE-score 1.7/5) compared to control EVs (EAE score 3.0), which was similar to mock treatment (EAE score 2.9/5) (Figure 5C). In addition, mock treated EAE mice displayed a gradual decrease in body weight after symptom onset, reflecting disease progression (Supp. Figure 13A). Mice treated with TNFR1ΔΔ-FDN-NST decoy EVs displayed sustained bodyweight over time, with increased weight at the endpoint (4.2%) compared to mock treated mice (Supp. Figure 13B). In addition, treatment with TNFR1ΔΔ-FDN-NST decoy EVs reduced the levels of the pro-inflammatory cytokines TNFα and IL6 in spinal cord compared to mock treatment (Extended Data Figure 2A and 2B).

In a similar set-up, depicted in Figure 5D, we next tested the therapeutic potential of blocking IL6 signaling in neuroinflammation, but instead of a prolonged release route we opted for I.V administration for an immediate treatment effect. This is based on our previous work where we observed prolonged release of EVs in plasma with S.C injection as compared to rapid EV uptake in different tissues including CNS, after I.V adminsitration[32]. Repeated injection of IL6STΔ-LZ-NST EVs (5×10^9) in mice induced with EAE until onset of symptoms, showed significant reduction in clinical score at day 16 (EAE score 1.33/5) as compared to mock treatment (EAE score 4.4/5) (Figure 5E-F). In contrast, MSC control EVs showed only minimal therapeutic effect (EAE score 3/5). Both TNFR1ΔΔ-FDN-NST and IL6STΔ-LZ-NST decoy EVs thus significantly reduced disease progression in a neuroinflammatory MS model.

To further test the versatility of this display system, we designed constructs using IL6ST-LZ-NST as a backbone and replaced the cytokine binding region of IL6ST with an alphabody against IL23[33], another pro-inflammatory cytokine implicated in the pathophysiology of MS[34]. Repeated injection of IL23B-LZ-NST EVs (1×10^{10}) purified from transiently transfected HEK293T cells, after the induction of disease, showed significantly lower EAE scores (EAE score 0.4/5) (Figure 5G-I and Extended Data Figure 2C). Importantly, administration of a single dose of IL23 decoy EVs (6×10^{10}) in EAE mice after onset of symptoms reduced the clinical score compared to mock treatment (Figure 5I). Taken together, these data clearly reflect the adaptability of the engineering approach and the potential of using EVs to display therapeutic receptors in inflammatory diseases including hard-to-treat CNS inflammation.

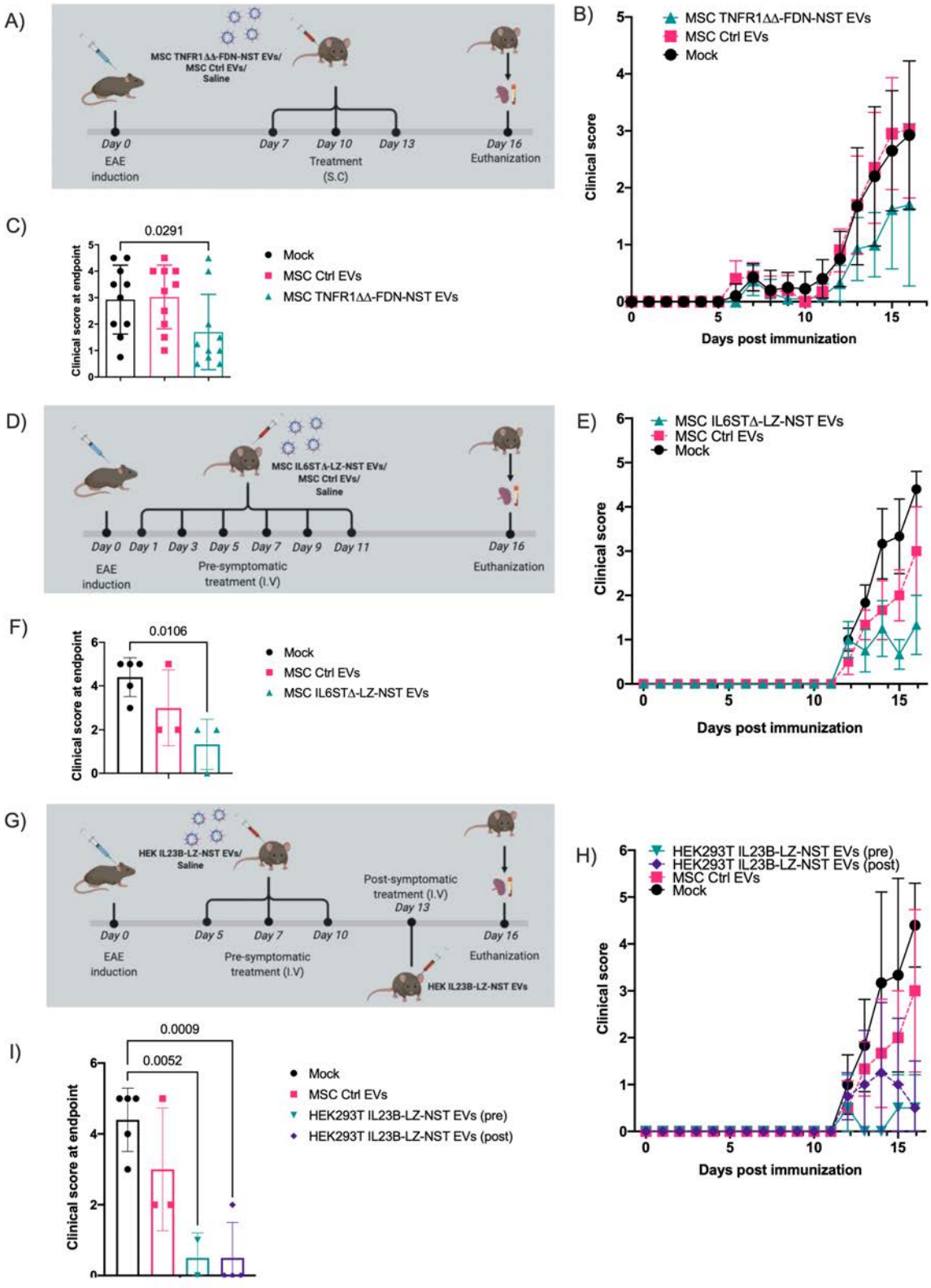
A)
MSC TNFR1ΔΔ-FDN-NST EVs/
MSC Ctrl EVs/
Saline
Day 0
EAE
induction
Day 7
Day 10
Day 13
Treatment
(S.C)
Day 16
Euthanization
B)
MSC TNFR1ΔΔ-FDN-NST EVs
MSC Ctrl EVs
Mock
Clinical score
Days post immunization
C)
0.0291
Clinical score at endpoint
Mock
MSC Ctrl EVs
MSC TNFR1ΔΔ-FDN-NST EVs
D)
MSC IL6STΔ-LZ-NST EVs/
MSC Ctrl EVs/
Saline
Day 0
Day 1
Day 3
Day 5
Day 7
Day 9
Day 11
EAE
induction
Pre-symptomatic
treatment (I.V)
Day 16
Euthanization
E)
MSC IL6STΔ-LZ-NST EVs
MSC Ctrl EVs
Mock
Clinical score
Days post immunization
F)
0.0106
Clinical score at endpoint
Mock
MSC Ctrl EVs
MSC IL6STΔ-LZ-NST EVs
G)
HEK IL23B-LZ-NST EVs/
Saline
Post-symptomatic
treatment (I.V)
Day 13
Day 0
Day 5
Day 7
Day 10
Day 16
EAE
induction
Pre-symptomatic
treatment (I.V)
Euthanization
HEK IL23B-LZ-NST EVs
H)
HEK293T IL23B-LZ-NST EVs (pre)
HEK293T IL23B-LZ-NST EVs (post)
MSC Ctrl EVs
Mock
Clinical score
Days post immunization
I)
0.0009
0.0052
Clinical score at endpoint
Mock
MSC Ctrl EVs
HEK293T IL23B-LZ-NST EVs (pre)
HEK293T IL23B-LZ-NST EVs (post)

Figure 5. Targeting TNF-alpha, IL6 and IL23 signalling axis with engineered decoy EVs suppress neuroinflammation. A) Description of the treatment protocol for TNFα decoy EVs in EAE. **B)** Clinical score (EAE-score, see Supplementary table 1) of disease progression over time and **C)** EAE-score at endpoint (day 16) in mice induced with EAE using MOG_{35-55} peptide and treated with S.C administration of either 4×10^{10} MSC TNFR1ΔΔ-FDN-NST EVs (*n*=5), MSC Ctrl EVs (*n*=5), or saline (*n*=5) (on day 7, 10 & 13). **D)** Schematic description of treatment protocol for IL6 decoy EVs in EAE. **E)** Clinical score of disease progression over time and **F**) EAE-score at endpoint (day 16) in mice induced with EAE using MOG_{35-55} peptide and treated with I.V administration of either 5×10^{9} MSC IL6STΔ-LZ-NST EVs (*n*=5), MSC Ctrl EVs (*n*=5), or saline (*n*=6) (on day 1,3,5,7,8,9 & 11). **G)** Schematic description of treatment protocol for IL23 decoy EVs in EAE. **H)** Clinical score of disease progression over time and **I)** EAE-score at endpoint (day 16) in mice induced with EAE using MOG_{35-55} peptide and treated I.V with either 1×10^{10} HEK293TIL23B-LZ-NST EVs pre symptomatic (*n*=5) (on day 5, 7 & 10), 6×10^{10} HEK293TIL23B-LZ-NST EVs post symptomatic (*n*=5) (on day 13), or saline (*n*=6). **C, F, I,** Central Value: Mean, Error bars: S.D, statistical significance calculated by two-way ANOVA with Dunnett's post-test compared with response to mock treated animal.

Double decoy EVs display two receptors simultaneously and effectively abrogate colitis in mice

After successful application of engineered EVs displaying single biologics, we next sought to generate combinatorically engineered EVs displaying two different surface proteins simultaneously. To this end, MSC cells stably expressing both TNFR1ΔΔ-FDN-NST and IL6STΔ-LZ-NST were generated (Supp. Figure 14A). The optimized engineered EVs isolated from conditioned medium were characterized using NTA, showing that the majority of the EVs were in the size range of exosomes with a peak of around 100 nm (Supp. Figure 14B). Characterization of isolated EVs from the respective cell source confirmed surface expression of both common EV markers ALIX and TSG101, absence of the apoptotic body marker calnexin, and co-expression of both decoy proteins by WB (Supp. Figure 15). To validate the extent of engineering and to identify populations of EVs displaying both, or a single version, of the decoy receptors, single vesicle imaging flow cytometry[35] was performed after labelling of EVs with anti-TNFR and anti-IL6ST antibodies (Extended Data Figure 3A). As expected, we observed a heterogenous pool of engineered EVs in our analysis, where 23% of the population of engineered EVs were found to carry both decoy receptors simultaneously, whereas 37% and 40% of engineered EVs were determined to carry either TNFR1 or IL6ST respectively (Figure 6A and Supp. Figure 16A). This was further validated by immuno-gold EM, where double positive EVs could be detected (Figure 6B). Furthermore, a similar trend as with single engineered EVs in the multiplex bead-based flow cytometry assay was observed, where the surface protein profile was similar to MSC Ctrl EVs, and the decoy receptors could

be detected on several sub-populations (Extended Data Figure 3B and Supp. Figure 16B-E). Decoy EVs purified from the double stable cells showed similar potency to decoy both cytokines in the *in vitro* cell assays as compared to their single decoy EV counterparts (Figure 6C-D).

The unique ability of EVs to achieve body-wide distribution, including hard-to-reach tissues, makes them a versatile delivery vector. We and others have previously shown that upon systemic administration, EVs distribute to the gastro-intestinal tract and deliver therapeutic cargo[4,36]. However, the biodistribution of EVs could differ in a diseased state. Therefore we evaluated the *in vivo* biodistribution of EVs using luciferase labelling as previously described[37] to precisely track EVs biodistribution in an intestinal inflammation model chemically induced by TNBS to mimic inflammatory bowls disease (IBD). Surprisingly, EV accumulation was significantly increased in almost every organ analyzed in contrast to healthy mice. Importantly, the increment levels were specifically higher in the intestine (85-fold) as compared to lungs (16-fold), heart (30-fold), spleen (30-fold) and kidneys (32-fold) (Figure 6E and Extended Data Figure 4A). This unique ability of EVs to enrich into pathogenic tissues *in vivo* rendered us to validate the therapeutic effect of double decoy EVs to inhibit intestinal inflammation *in vivo*. Again, the TNBS mouse model was utilized to evaluate the decoy EVs in the IBD model and a single injection of double decoy EVs 24 hours post symptom onset (Figure 6F), showed a significant dose-dependent reduction of weight loss at 96 hours (-1.34% for the highest dose (3×10^{11}) and -3.2% for the lowest dose (3×10^{10})) compared to untreated mice (-6.8%) (Figure 6G). Importantly, the survival was also improved by double decoy EV treatment (92.3% survival) compared to untreated mice (66.7% survival) (Figure 6H). Furthermore, double decoy EVs outperformed equivalent doses (in terms of IC50 of mouse counterparts) of clinically used soluble TNFR protein (Etanercept) and anti-IL6R (Tocilizumab) in combination, with improved survival (92.3% for double decoy highest dose, 80.0% for the lowest dose vs 73.3% for 10 μg Etanercept + 1 μg Tocilizumab) and improved weight gain (1.8% weight for double decoy, highest dose, 0.8% for the lowest dose vs 0.2% for Etanercept + Tocilizumab) (Supp. Extended Data Figure 4B). We also observed a similar protective effect of double decoy EVs in a separate experiment with improved survival (50% at 120 h) and weight change (+1.1%) compared to PBS treatment (20% survival, -1.3% weight) (Extended Data Figure 4C-D). Collectively, this again confirmed the therapeutic potential of decoy EVs in inflammatory

settings and further demonstrated the versatility of the engineering approach with the possibility of displaying multiple therapeutic receptors with improved efficacy.

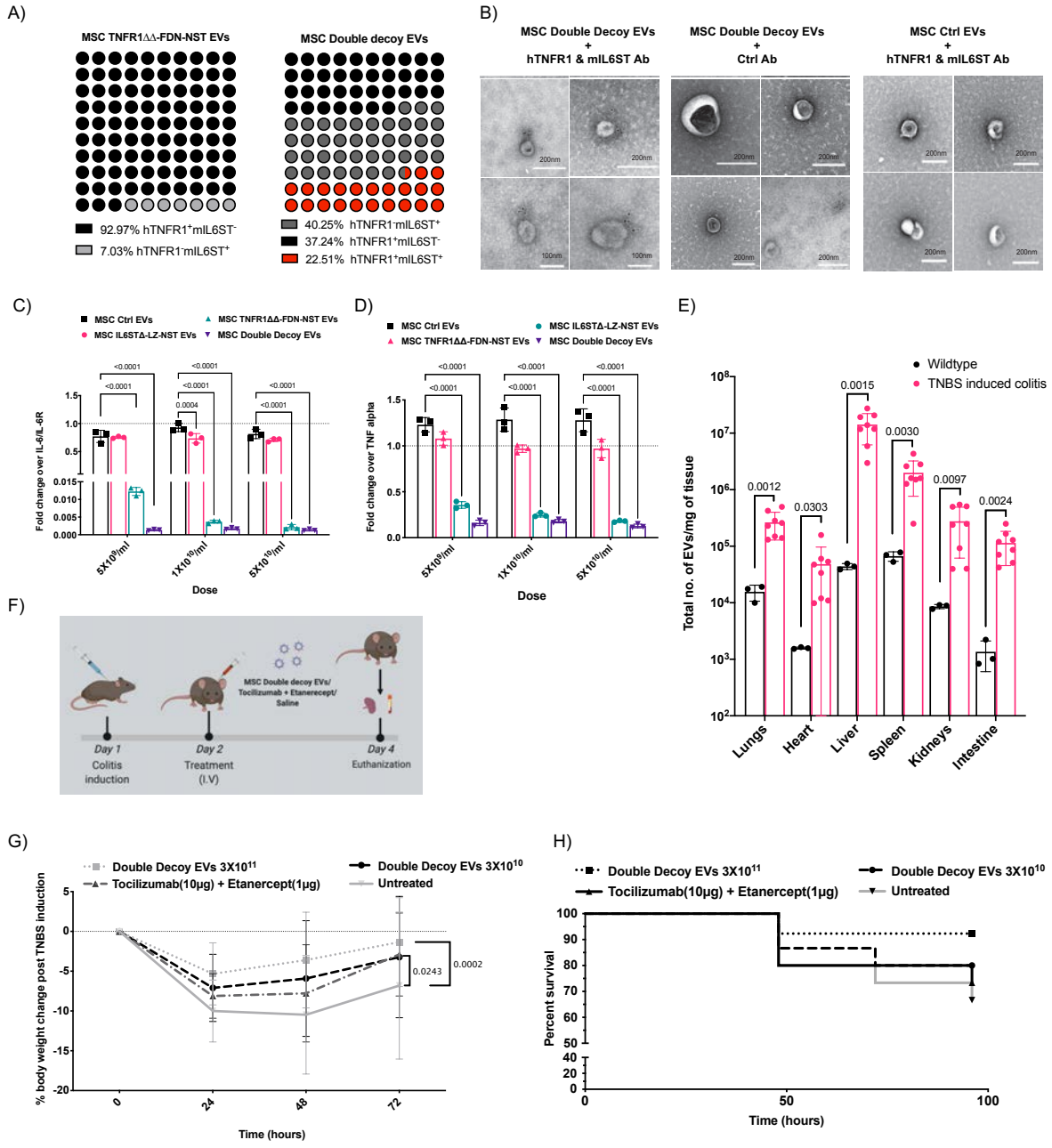

Figure 6. Dual functionalized Engineered EVs protect against intestinal inflammation. **A)** Percentage of detected events positive for either hTNFR1 or mIL6ST or both in Imaging flow cytometry analysis of MSC TNFR1ΔΔ-FDN-NST and MSC double decoy EVs stained with mIL6ST APC conjugated and hTNFR1 PE conjugated antibody. Percentage values determined from objects/ml in different gates. **B)** Transmission electron microscopy of double decoy EVs with nanogold labelled antibody staining of hTNFR1 (10 nm) and mIL6ST (5 nm). **C)**

Engineered EVs displaying TNFR1 purified from MSC cells stably expressing either the optimized TNFR1ΔΔ-FDN-NST display construct or TNFR1ΔΔ-FDN-NST and IL6STΔ-LZ-NST construct, evaluated for TNFα decoy in an *in vitro* cell assay responsive to TNFα induced NF-κB activation. EVs purified from MSC stably expressing either the IL6STΔ-LZ-NST display construct or Ctrl construct were used as control. Data were normalized to control cells treated with TNFα (5 ng/ml). **D)** Engineered EVs displaying IL6ST purified from MSC cells stably expressing either the optimized IL6STΔ-LZ-NST display construct or TNFR1ΔΔ-FDN-NST, evaluated for IL6/sIL6R decoy in an *in vitro* cell assay responsive to IL6/sIL6R induced STAT3 activation. EVs purified from MSC stably expressing either the TNFR1ΔΔ-FDN-NST display construct or Ctrl construct were used as control. Data were normalized to control cells treated with IL6/sIL6R (5 ng/ml). **E**) EVs *in vivo* biodistribution of the EVs differ significantly in a diseased animal. 1 X 10^{11} EVs labelled with CD63 NanoLuc were injected I.V in a wildtype *(n=3)* or in a TNBS-induced colitis Balbc mice *(n=8)*, 2 hours post-injection and animals were sacrificed, and organs were analysed *ex vivo* for EV accumulation per mg/tissue. **F)** Schematic of the treatment protocol for double decoy EVs in TNBS induced colitis. **G)** Percent change in relative bodyweight to initial weight over the disease course and **H)** survival curve in mice induced with colitis by intrarectal injection of TNBS and treated I.V with either 3×10^{11} MSC double decoy EVs (*n*=13), 3×10^{10} MSC double decoy EVs (*n*=15), 10 μg Tocilizumab and 1 μg Etanercept (*n*=14), or saline (n=15) 24 hours post disease induction. **C, D,** Central Value: Mean, Error bars: S.D (*Biological replicate, n*=3), Statistical significance calculated by two-way ANOVA with Dunnett's post-test compared with response of Ctrl EVs at the respective dose. **E.** Central Value: Mean, Error bars: S.D, Statistical significance calculated by Mann-Whitney two tailed t test. **G,** Central Value: Mean, Error bars: S.D, Statistical significance calculated by two-way ANOVA with Dunnett's post-test compared with response of Saline treated animal.

Discussion

With growing evidence on the critical role of EVs in a multitude of physiological processes, the potential of using EVs as a therapeutic modality has been increasingly explored. We and others have used various engineering strategies to achieve efficient loading of therapeutic cargos, such as nucleic acids and proteins, into EVs as well as to decorate them with various targeting ligands[1,2,5,38–41]. The approaches developed this far rely on multi-modular engineering strategies, where one protein is used to achieving drug loading and another protein imparting targeting moieties. Recent work by our group shows that the majority of these proteins, especially Lamp2b and CD63, fail to co-localize in the same vesicle subpopulation upon overexpression in producer cells[39]. Furthermore, Lamp2b, one of the most widely used EV engineering proteins for displaying small targeting peptides, labelled only a fraction of EVs in this study and in our previously published work [39]. This could be because we herein use a larger protein fusion which may affect the degree of engineering. As a result of heterogeneity in EV engineering with different scaffolds, there is a risk that multi-modular strategies (e.g.,

therapeutic and targeting) are distributed between mutually exclusive EV subpopulations, thereby negatively affecting the therapeutic efficacy of the EVs. Therefore, various exogenous engineering strategies based on chemical functionalization and lipid anchors have been devised for efficient engineering of EVs with small peptides or ligands but the applicability to bigger protein is still limited. In addition, these technologies lack specificity, potentially affecting the surface proteome and integrity of the EVs[42]. Furthermore, there is also a considerable risk of labelling soluble protein contaminants co-eluting with EVs.

Here, we explored various EV engineering approaches for devising an efficient strategy to surface display therapeutic proteins. To assess the efficacy of the surface decoration and as a therapeutic application, we used the cytokine receptors TNFR1 or IL6ST, lacking their respective signaling domains. These engineered EVs were able to inhibit TNFα or IL6/sIL6R complexes and hence decrease the activation of NF-κB and STAT3 signaling, respectively.

The focus of this study was to optimize the loading of the decoy receptors onto the surface of EVs by genetically modifying their producer cells. In the initial screenings, we observed the most efficient loading of decoy receptors onto EVs with the N-terminal fragment of Syntenin. Syntenin is a cytoplasmic adaptor of Syndecan proteoglycans and aids in the interaction of Syndecan to ALIX, a key component of the ESCRT machinery, which induces membrane budding and abscission[43]. To further enhance the efficiency of the decoy EVs, we introduced oligomerization, dimerization and trimerization domains on the IL6ST and TNFR1, respectively. These were hypothesized to increase receptor decoy EV potency in two ways. First, oligomerization of exosomal sorting domains enhances the active shuttling of the cargo into EVs[44] and second, it mimics the natural state of the receptors during ligand binding on the cell surface[12,13]. This addition of an oligomerization domain in combination with N-Terminal syntenin increased the inhibitory activity of TNFR1 decoy EVs by a further 10-fold and allowed us to decorate up to 600 receptors on an EV surface. This clearly showed the importance of rigorous engineering to increase the efficacy of the EVs.

To determine the therapeutic utility of the engineered EVs to suppress inflammation, we assessed the efficacy in three different inflammation models *in vivo*; LPS induced systemic inflammation, EAE, and TNBS induced colitis, which mimic sepsis, MS and IBD, respectively. In the preclinical model of sepsis, decoy EV treatments led to a higher survival rate, thus

indicating a dampening of the cytokine storm associated with systemic inflammation. We also observed similar effects in the preclinical model of MS, whereby systemic delivery of IL6STΔ-LZ-NST and TNFR1ΔΔ-FDN-NST decoy EVs reduced the clinical score in animals induced with EAE. Further, we demonstrated the applicability of this engineering strategy for display of other protein biologics, by simply replacing the cytokine binding region of IL6ST in IL6STΔ-LZ-NST with an alphabody against IL23. Therapeutic targeting of IL23 with IL23 targeting EVs in EAE effectively inhibited the CNS inflammation, in both prophylactic and therapeutic treatment settings. Application of this approach was additionally recently showcased by us in another study, where targeting IL-6 trans signaling axis in IL-6 overexpressing DMD model downregulated inflammation cascade signaling[45]. The flexibility of this approach thus allows for therapeutic applications spanning beyond decoying cytokines and could be adapted to decoy other deleterious signals, or for the display of other therapeutic and/or targeting moieties on the EV surface.

To explore the potential of displaying multiple therapeutic moieties on EVs, the same engineering strategy was used to generate double engineered EVs, carrying both TNFR1ΔΔ-FDN-NST and IL6STΔ-LZ-NST decoy receptors. These double decoy EVs showed similar efficacy as compared to single decoy EVs in *in vitro* assays for both cytokines assessed one by one, which demonstrate that the loading of both receptors was efficient despite using the same engineering approach. Importantly, this points to the fact that the overexpression of the receptors does not reach the limit of the Syntenin dependent loading machinery. Furthermore, we also identified the TfR derived endosomal sorting domain to be equally efficacious compared to N-term Syntenin for IL6ST display. Although beyond the scope of this study, future developments could include conjugation of TfR domains beside Syntenin to achieve display of two or more different biologics on the EV surface. However, the co-localization of these two-sorting domains into the same EV population must first be confirmed. Importantly, in the preclinical model of IBD, mice treated with double decoy EVs show improved survival and improvement in clinical symptoms as compared to a combination of clinically approved biologics against these cytokines, underpinning the benefit of decoying both cytokines simultaneously. Overall, these engineered EVs improved survival, reduced weight loss, improved clinical symptoms and down-regulated cytokine levels in the preclinical inflammation models.

EVs unique ability to penetrate hard to reach tissues have been showcased by us and others [4,37,46] but the precise mechanism of the therapeutic action of decoy EVs in case of localized inflammation still remains to be elucidated. Notably, the majority of the EV pharmacokinetics studies have typically been performed in wild type mice, and EV biodistribution may vary in a disease-relevant model. This fact was clearly reflected in our *in vivo* biodistribution results, where we observe a distinct biodistribution pattern of EVs in the intestinal inflammation model. These results corroborated well with a highlighted recent study by Perets et al., where MSC EVs showed accumulation in pathological CNS regions for longer durations of time than in a healthy mouse[47]. Based on this, we speculate that cytokine decoy EVs primarily could accumulate in pro-inflammatory microenvironments upon administration. This phenomenon may explain why decoy EVs display better efficacy *in vivo* as compared to clinically used biologics.

It was recently described that EVs can be a part of an innate immune response in humans where EVs decoy bacterial toxins using ADAM10 decorated EVs[48]. Furthermore, a similar mechanism is also utilized by CD4+ T cells to decoy HIV viruses by secreting EVs enriched in CD4[49]. These studies further strengthen the therapeutic applicability of these engineered EVs for decoying toxins, soluble proteins or viruses for various clinical applications.

In conclusion, the approach described here has the potential to be implemented in several EV engineering strategies for displaying targeting ligands, decoy receptors, single chain antibodies, as well as other therapeutic modalities. By further modifying these designs, luminal therapeutic cargo loading, and display of targeting moiety can be achieved simultaneously, hence addressing the limitation of engineering applications imparted by the heterogeneity of released EVs. By combining protein therapeutics and a natural delivery vehicle that can overcome tissue barriers, engineered EVs have great potential to be the next generation biotherapeutics.

Acknowledgments

We would like to acknowledge Bavo Vanneste and Griet Van Imschoot for their indispensable assistance. AG is an International Society for Advancement of Cytometry Marylou Ingram Scholar 2019-2023. SELA is supported by H2020 EXPERT, the Swedish foundation of

Strategic Research (SSF-IRC; FormulaEx), ERC CoG (DELIVER) and the Swedish Medical Research Council.

Conflict of interest

MJAW and SEA are founders of, and consultants for, Evox Therapeutics. DG, OW, AG & JZN are consultant for Evox Therapeutics. DG, OW, AG, JZN, MJAW and SEA have stock interest in Evox Therapeutics. The remaining authors declare no conflicts of interest.

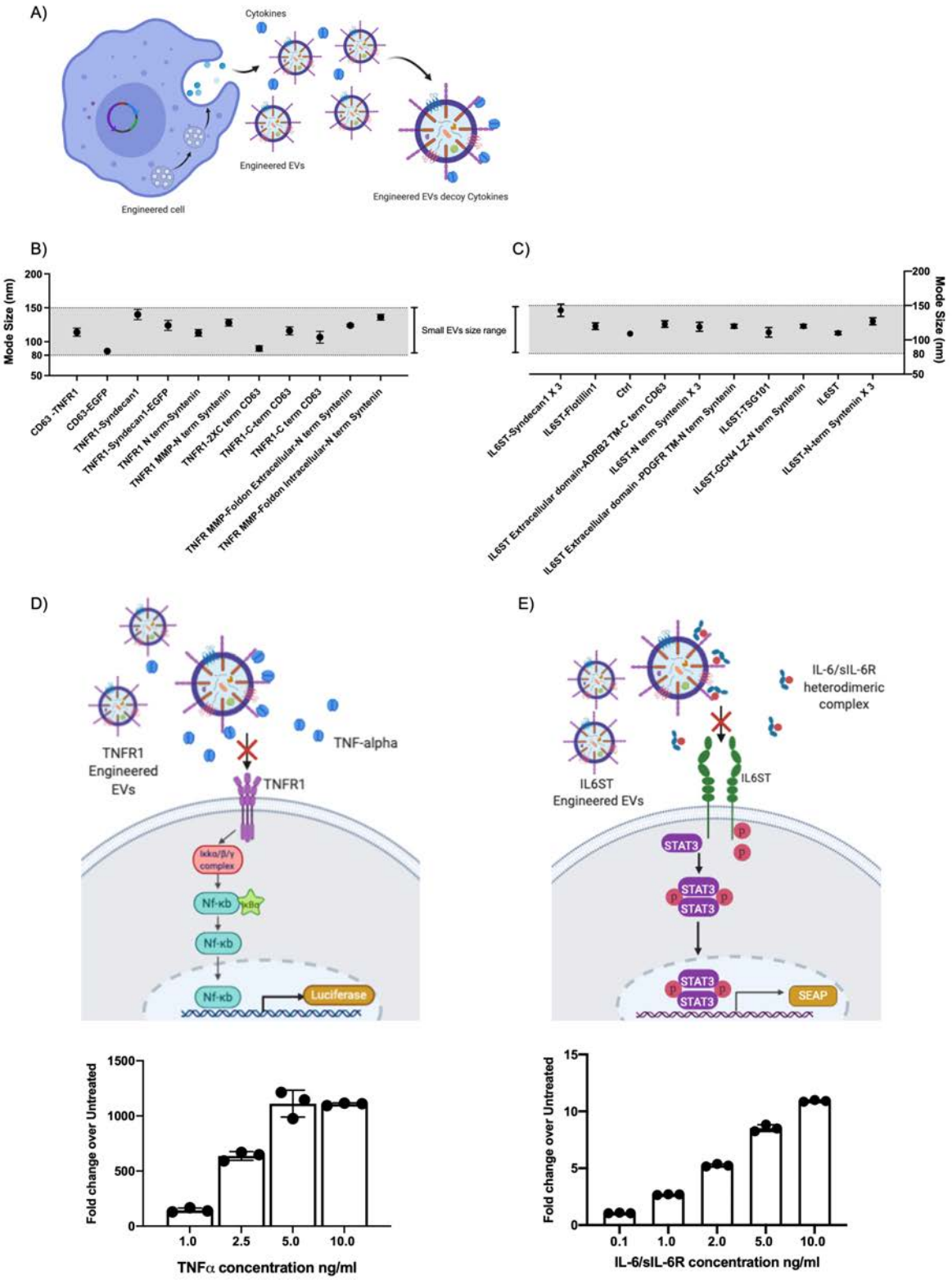

Extended Data Figure 1. Functionalizing EV surface with cytokine decoy receptors. **A)** Schematic illustration showing the generation of engineered decoy EVs at the cellular level.

Producer cells are genetically modified to express cytokine receptors without the signalling domain fused to an EV sorting domain for efficient display of cytokine receptors on the surface of the secreted EVs (decoy EVs), which can decoy cytokines specifically. **B-C)** Mode size determined by NTA of indicated engineered HEK293T EVs purified from cells transfected with various B) TNFR1 display constructs and C) IL6ST display constructs. Central Value: Mean, Error bars: S.D (*Technical replicate, n*=5). **D)** Fold change in signal over untreated HEK293T NF-κB reporter cells, upon incubation of different doses of TNFα for 4 hours. Central Value: Mean, Error bars: S.D (*Biological replicate, n*=3). **E)** Fold change in signal over untreated HEK293T STAT3 reporter cells, upon incubation of different doses of IL6/sIL6R for 12 hours. Central Value: Mean, Error bars: S.D (*Biological replicate, n*=3).

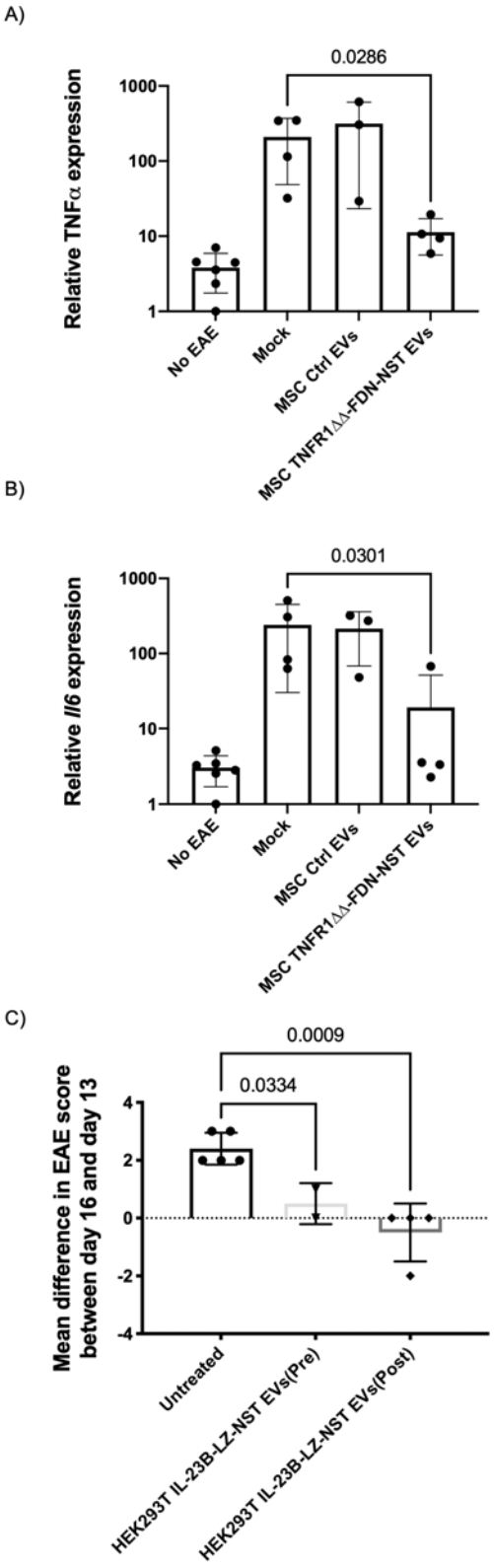

Extended Data Figure 2. Amelioration of neuroinflammation by cytokine decoy engineered EVs. Relative mRNA expression of pro inflammatory cytokines determined

by qPCR **(A)** TNFα, **(B)** IL6 in the spinal cord at day 16 in mice induced with EAE using MOG_{35-55} peptide and treated with S.C administration of either 4×10^{10} MSC TNFR1ΔΔ-FDN-NST EVs (*n*=5) or MSC Ctrl EVs (*n*=5) or Saline (*n*=5) (On day 7, 10 & 13). For the same dataset as shown in Figure 5B-C**.** Central Value: Mean, Error bars: S.D, Statistical significance calculated by one-way ANOVA compared with response of Saline treated animal. **C)** Relative change in clinical score of disease progression between day 16 and 13 in mice induced with EAE using MOG_{35-55} peptide and treated with I.V administration of either 1×10^{10} HEK293T IL23B-LZ-NST EVs pre symptomatic (On day 5, 7 & 10) or 6×10^{10} HEK293T IL23B-LZ-NST EVs post symptomatic (On day 13) or Saline. For the same dataset as shown in Figure 5H-I. Central Value: Mean, Error bars: S.D, Statistical significance calculated by two-way ANOVA with Dunnett's post-test compared with response of Saline treated animal.

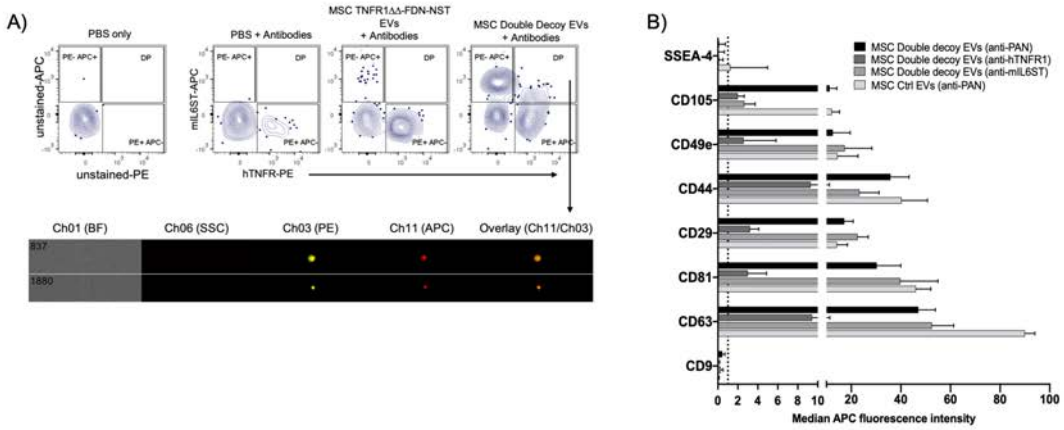

Extended Data Figure 3. Surface proteome is unaltered by Dual functionalization of engineered EVs. A) Imaging flow cytometry analysis (IFCM) with dot plots and example event images in the double positive (DP) gate of MSC TNFR1ΔΔ-FDN-NST and MSC double decoy EVs stained with mIL6ST APC conjugated and hTNFR1 PE conjugated antibody. PBS + antibodies were used for background adjustment and for determining the gating strategy. **B)** Multiplex EV surface characterization of PAN (CD63, CD81, and CD9) positive, hTNFR1 positive and mIL6ST positive population in MSC double decoy EVs and MSC Ctrl EVs. Data represented as background corrected median APC fluorescence intensity determined by flow cytometry of EVs bound different capture beads and upon using APC labelled detection antibody. Central Value: Mean, Error bars: S.D, *(Technical replicate, n=5000-15000).*

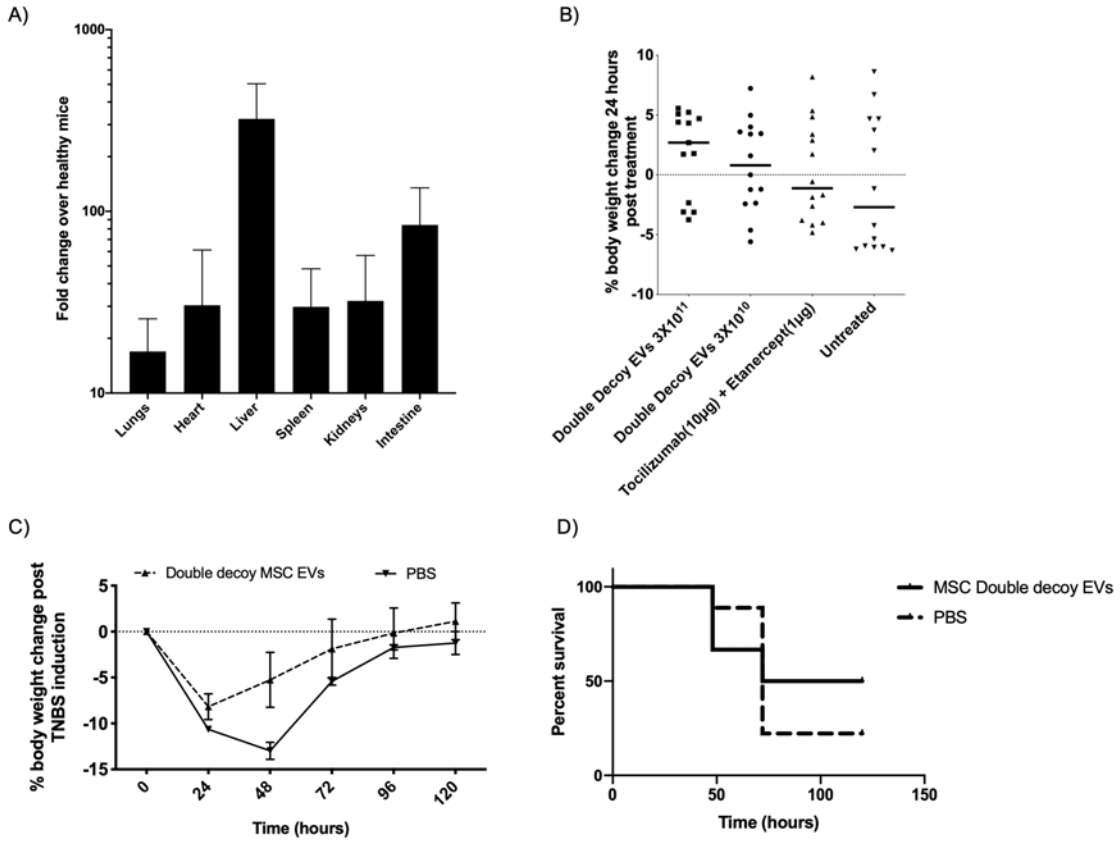

Extended Data Figure 4. Engineered EVs show therapeutic benefit in intestinal inflammation. A) Increment in EV accumulation in various tissues in animal induced with IBD over healthy animal. **B)** Change in body weight 24 hours after treatment with different groups in mice induced with TNBS colitis. For the same data set as shown in Figure 6G-H. **C)** Survival curve and **D)** percent change in relative bodyweight to initial weight over the disease course in mice induced with colitis by intrarectal injection of TNBS and treated with I.V administration (at 24 hours post disease induction) of either 3×10^{11} MSC double decoy EVs (n=8) or PBS (n=9).

References

1. Armstrong JPK, Holme MN, Stevens MM. Re-Engineering Extracellular Vesicles as Smart Nanoscale Therapeutics. *ACS Nano*. 2017;11(1):69-83. doi:10.1021/acsnano.6b07607
2. Alvarez-Erviti L, Seow Y, Yin H, Betts C, Lakhal S, Wood MJA. Delivery of siRNA to the mouse brain by systemic injection of targeted exosomes. *Nat Biotechnol*. 2011;29(4):341-345. doi:10.1038/nbt.1807
3. El-Andaloussi S, Lee Y, Lakhal-Littleton S, et al. Exosome-mediated delivery of siRNA

in vitro and in vivo. *Nat Protoc*. 2012;7(12):2112-2126. doi:10.1038/nprot.2012.131

4. Wiklander OPB, Nordin JZ, O'Loughlin A, et al. Extracellular vesicle in vivo biodistribution is determined by cell source, route of administration and targeting. *J Extracell Vesicles*. Published online 2015. doi:10.3402/jev.v4.26316
5. Cooper JM, Wiklander PBO, Nordin JZ, et al. Systemic exosomal siRNA delivery reduced alpha-synuclein aggregates in brains of transgenic mice. *Mov Disord*. 2014;29(12):1476-1485. doi:10.1002/mds.25978
6. Jeppesen DK, Fenix AM, Franklin JL, et al. Reassessment of Exosome Composition. *Cell*. 2019;177(2):428-445.e18. doi:10.1016/j.cell.2019.02.029
7. Willms E, Johansson HJ, Mäger I, et al. Cells release subpopulations of exosomes with distinct molecular and biological properties. *Sci Rep*. 2016;6. doi:10.1038/srep22519
8. Vagner T, Chin A, Mariscal J, Bannykh S, Engman DM, Di Vizio D. Protein Composition Reflects Extracellular Vesicle Heterogeneity. *Proteomics*. 2019;19(8):1800167. doi:10.1002/pmic.201800167
9. Crescitelli R, Lässer C, Jang SC, et al. Subpopulations of extracellular vesicles from human metastatic melanoma tissue identified by quantitative proteomics after optimized isolation. *J Extracell Vesicles*. 2020;9(1). doi:10.1080/20013078.2020.1722433
10. Kim EY, Moudgil KD. Immunomodulation of autoimmune arthritis by pro-inflammatory cytokines. *Cytokine*. 2017;98:87-96. doi:10.1016/j.cyto.2017.04.012
11. Moudgil KD, Choubey D. Cytokines in autoimmunity: Role in induction, regulation, and treatment. *J Interf Cytokine Res*. 2011;31(10):695-703. doi:10.1089/jir.2011.0065
12. Garbers C, Heink S, Korn T, Rose-John S. Interleukin-6: Designing specific therapeutics for a complex cytokine. *Nat Rev Drug Discov*. 2018;17(6):395-412. doi:10.1038/nrd.2018.45
13. Kalliolias GD, Ivashkiv LB. TNF biology, pathogenic mechanisms and emerging therapeutic strategies. *Nat Rev Rheumatol*. 2016;12(1):49-62. doi:10.1038/nrrheum.2015.169
14. Sedger LM, McDermott MF. TNF and TNF-receptors: From mediators of cell death and inflammation to therapeutic giants - past, present and future. *Cytokine Growth Factor Rev*. 2014;25(4):453-472. doi:10.1016/j.cytogfr.2014.07.016
15. Wolf J, Rose-John S, Garbers C. Interleukin-6 and its receptors: A highly regulated and dynamic system. *Cytokine*. 2014;70(1):11-20. doi:10.1016/j.cyto.2014.05.024
16. Simpson RJ, Kalra H, Mathivanan S. Exocarta as a resource for exosomal research. *J*

Extracell Vesicles. 2012;1(1). doi:10.3402/jev.v1i0.18374

17. Hurwitz SN, Rider MA, Bundy JL, Liu X, Singh RK, Meckes DG. Proteomic profiling of NCI-60 extracellular vesicles uncovers common protein cargo and cancer type-specific biomarkers. *Oncotarget*. 2016;7(52):86999-87015. doi:10.18632/oncotarget.13569
18. Sork H, Corso G, Krjutskov K, et al. Heterogeneity and interplay of the extracellular vesicle small RNA transcriptome and proteome. *Sci Rep*. 2018;8(1). doi:10.1038/s41598-018-28485-9
19. Xanthoulea S, Pasparakis M, Kousteni S, et al. Tumor necrosis factor (TNF) receptor shedding controls thresholds of innate immune activation that balance opposing TNF functions in infectious and inflammatory diseases. *J Exp Med*. 2004;200(3):367-376. doi:10.1084/jem.20040435
20. Meier S, Güthe S, Kiefhaber T, Grzesiek S. Foldon, the natural trimerization domain of T4 fibritin, dissociates into a monomeric A-state form containing a stable β-hairpin: Atomic details of trimer dissociation and local β-hairpin stability from residual dipolar couplings. *J Mol Biol*. 2004;344(4):1051-1069. doi:10.1016/j.jmb.2004.09.079
21. Ellenberger TE, Brandl CJ, Struhl K, Harrison SC. The GCN4 basic region leucine zipper binds DNA as a dimer of uninterrupted α Helices: Crystal structure of the protein-DNA complex. *Cell*. 1992;71(7):1223-1237. doi:10.1016/S0092-8674(05)80070-4
22. Jensen MR, Yabukarski F, Communie G, et al. STRUCTURAL DESCRIPTION OF THE NIPAH VIRUS PHOSPHOPROTEIN AND ITS INTERACTION WITH STAT1. *Biophys J*. Published online April 18, 2020. doi:10.1016/j.bpj.2020.04.010
23. Sliepen K, Van Montfort T, Melchers M, Isik G, Sanders RW. Immunosilencing a highly immunogenic protein trimerization domain. *J Biol Chem*. 2015;290(12):7436-7442. doi:10.1074/jbc.M114.620534
24. Alvarez-Erviti L, Seow Y, Yin H, Betts C, Lakhal S, Wood MJA. Delivery of siRNA to the mouse brain by systemic injection of targeted exosomes. *Nat Biotechnol*. 2011;29(4):341-345. doi:10.1038/nbt.1807
25. Dooley K, McConnell RE, Xu K, et al. A versatile platform for generating engineered extracellular vesicles with defined therapeutic properties. *Mol Ther*. 2021;29(5):1729-1743. doi:10.1016/j.ymthe.2021.01.020
26. Théry C, Witwer KW, Aikawa E, et al. Minimal information for studies of extracellular vesicles 2018 (MISEV2018): a position statement of the International Society for

Extracellular Vesicles and update of the MISEV2014 guidelines. *J Extracell Vesicles*. 2018;7(1). doi:10.1080/20013078.2018.1535750

27. Wiklander OPB, Bostancioglu RB, Welsh JA, et al. Systematic Methodological Evaluation of a Multiplex Bead-Based Flow Cytometry Assay for Detection of Extracellular Vesicle Surface Signatures. *Front Immunol*. 2018;9:1326. doi:10.3389/fimmu.2018.01326
28. Pelosi L, Berardinelli MG, Forcina L, et al. Increased levels of interleukin-6 exacerbate the dystrophic phenotype in mdx mice. *Hum Mol Genet*. 2015;24(21):6041-6053. doi:10.1093/hmg/ddv323
29. Saleh AF, Lázaro-Ibáñez E, Forsgard MAM, et al. Extracellular vesicles induce minimal hepatotoxicity and immunogenicity. *Nanoscale*. 2019;11(14):6990-7001. doi:10.1039/c8nr08720b
30. Zhu X, Badawi M, Pomeroy S, et al. Comprehensive toxicity and immunogenicity studies reveal minimal effects in mice following sustained dosing of extracellular vesicles derived from HEK293T cells. *J Extracell Vesicles*. 2017;6(1). doi:10.1080/20013078.2017.1324730
31. Sejwal K, Chami M, Baumgartner P, Kowal J, Müller SA, Stahlberg H. Proteoliposomes - A system to study membrane proteins under buffer gradients by cryo-EM. *Nanotechnol Rev*. 2017;6(1):57-74. doi:10.1515/ntrev-2016-0081
32. Gupta D, Liang X, Pavlova S, et al. Quantification of extracellular vesicles in vitro and in vivo using sensitive bioluminescence imaging. *J Extracell Vesicles*. 2020;9(1). doi:10.1080/20013078.2020.1800222
33. Desmet J, Verstraete K, Bloch Y, et al. Structural basis of IL-23 antagonism by an Alphabody protein scaffold. *Nat Commun*. 2014;5(1):1-12. doi:10.1038/ncomms6237
34. Lovett-Racke AE, Racke MK. Role of IL-12/IL-23 in the Pathogenesis of Multiple Sclerosis. In: *Neuroinflammation*. Elsevier; 2018:115-139. doi:10.1016/b978-0-12-811709-5.00005-3
35. Görgens A, Bremer M, Ferrer-Tur R, et al. Optimisation of imaging flow cytometry for the analysis of single extracellular vesicles by using fluorescence-tagged vesicles as biological reference material. *J Extracell Vesicles*. 2019;8(1). doi:10.1080/20013078.2019.1587567
36. Reshke R, Taylor JA, Savard A, et al. Reduction of the therapeutic dose of silencing RNA by packaging it in extracellular vesicles via a pre-microRNA backbone. *Nat*

Biomed Eng. Published online January 14, 2020. doi:10.1038/s41551-019-0502-4

37. Gupta D, Liang X, Pavlova S, et al. Quantification of extracellular vesicles in vitro and in vivo using sensitive bioluminescence imaging. *J Extracell Vesicles*. 2020;9(1):1800222. doi:10.1080/20013078.2020.1800222
38. Kamerkar S, Lebleu VS, Sugimoto H, et al. Exosomes facilitate therapeutic targeting of oncogenic KRAS in pancreatic cancer. *Nature*. 2017;546(7659):498-503. doi:10.1038/nature22341
39. Corso G, Heusermann W, Trojer D, et al. Systematic characterization of extracellular vesicle sorting domains and quantification at the single molecule – single vesicle level by fluorescence correlation spectroscopy and single particle imaging. *J Extracell Vesicles*. 2019;8(1):1663043. doi:10.1080/20013078.2019.1663043
40. Gao X, Ran N, Dong X, et al. Anchor peptide captures, targets, and loads exosomes of diverse origins for diagnostics and therapy. *Sci Transl Med*. 2018;10(444). doi:10.1126/scitranslmed.aat0195
41. Wiklander OPB, Brennan M, Lötvall J, Breakefield XO, Andaloussi SEL. Advances in therapeutic applications of extracellular vesicles. *Sci Transl Med*. 2019;11(492). doi:10.1126/scitranslmed.aav8521
42. Rayamajhi S, Aryal S. Surface functionalization strategies of extracellular vesicles. *J Mater Chem B*. 2020;8(21):4552-4569. doi:10.1039/d0tb00744g
43. Baietti MF, Zhang Z, Mortier E, et al. Syndecan-syntenin-ALIX regulates the biogenesis of exosomes. *Nat Cell Biol*. 2012;14(7):677-685. doi:10.1038/ncb2502
44. Fang Y, Wu N, Gan X, Yan W, Morrell JC, Gould SJ. Higher-Order Oligomerization Targets Plasma Membrane Proteins and HIV Gag to Exosomes. Walter P, ed. *PLoS Biol*. 2007;5(6):e158. doi:10.1371/journal.pbio.0050158
45. Conceição M, Forcina L, Wiklander OPB, et al. Engineered extracellular vesicle decoy receptor-mediated modulation of the IL6 trans-signalling pathway in muscle. *Biomaterials*. 2021;266. doi:10.1016/j.biomaterials.2020.120435
46. Lai CP, Mardini O, Ericsson M, et al. Dynamic biodistribution of extracellular vesicles in vivo using a multimodal imaging reporter. *ACS Nano*. 2014;8(1):483-494. doi:10.1021/nn404945r
47. Perets N, Betzer O, Shapira R, et al. Golden Exosomes Selectively Target Brain Pathologies in Neurodegenerative and Neurodevelopmental Disorders. *Nano Lett*. 2019;19(6):3422-3431. doi:10.1021/acs.nanolett.8b04148

48. Keller MD, Ching KL, Liang FX, et al. Decoy exosomes provide protection against bacterial toxins. *Nature*. 2020;579(7798):260-264. doi:10.1038/s41586-020-2066-6
49. de Carvalho J V., de Castro RO, da Silva EZM, et al. Nef Neutralizes the Ability of Exosomes from CD4+ T Cells to Act as Decoys during HIV-1 Infection. Pöhlmann S, ed. *PLoS One*. 2014;9(11):e113691. doi:10.1371/journal.pone.0113691
50. Corso G, Mäger I, Lee Y, et al. Reproducible and scalable purification of extracellular vesicles using combined bind-elute and size exclusion chromatography. *Sci Rep*. 2017;7(1). doi:10.1038/s41598-017-10646-x
51. Tertel, T., Bremer, M., Maire, C.L., Lamszus, K., Peine, S., Jawad, R., El Andaloussi, S., Giebel, B., Ricklefs, F.L., and Gorgens A. High-Resolution Imaging Flow Cytometry Reveals Impact of Incubation Temperature on Labelling of Extracellular Vesicles with Antibodies. *Cytom Part A*. Published online 2020.
52. Brkic M, Balusu S, Van Wonterghem E, et al. Amyloid β oligomers disrupt blood–CSF barrier integrity by activating matrix metalloproteinases. *J Neurosci*. 2015;35(37):12766-12778. doi:10.1523/JNEUROSCI.0006-15.2015
53. Scheiffele F, Fuss IJ. Induction of TNBS Colitis in Mice. In: *Current Protocols in Immunology*. John Wiley & Sons, Inc.; 2002. doi:10.1002/0471142735.im1519s49

Materials and Methods

Cells

Human embryonic kidney cells (HEK293T) and immortalized human bone marrow derived mesenchymal stem cells (MSCs) were grown at 37°C, 5% CO_2 atmosphere. HEK293T cells were cultured in Dulbecco's Modified Eagle's Medium (DMEM) (Invitrogen), supplemented with 10% Fetal Bovine Serum (FBS) (Invitrogen), 20 mM L-Glutamine and 1% penicillin (100 U/ml) and streptomycin (100 µg/ml) (P/S) (Sigma). MSCs were cultured in Roswell Park Memorial Institute (RPMI-1640) (Invitrogen) medium supplemented with 10% FBS, 10^{-6} mol/l hydrocortisone, and 1% P/S. 48 hours prior to harvest of conditioned medium (CM) for EV isolation, the cells were washed with PBS and media was changed to OptiMem (Invitrogen).

RAW264.7 cells were grown in DMEM supplemented with 10% FBS and 1× Antibiotic-Antimycotic at 37°C in 5% CO_2.

RAW264.7 macrophages were seeded in a 24 well-plate, at a density of 80,000 cells per well. The next day, cells were treated with 100 ng/ml of lipopolysaccharide (LPS) (L-5886, Sigma), in the presence or absence of EVs. The supernatant was collected 6 hours and 24 hours after treatment, and TNFα levels were evaluated by ELISA (BioLegend, San Diego, CA), following the manufacturer's protocol.

Reporter cell lines

NF-κB reporter (Luc)-HEK293 cells (BPS Bioscience, catalogue no. 60650) were cultured and used as proposed by the manufacturer. 30,000 cells per well were seeded to a 96-well plate with culture medium (DMEM + 10% FBS + 1% P/S) and incubated at 37°C with 5% CO_2. After 24 hours, the cells were treated with or without EVs, and with hTNFα (5 ng/ml, NordicBiosite) in 50 μl of complete DMEM. 6 hours after treatment the cells were lysed using 0.1% Triton X-100 in PBS (Sigma) and mixed with D-Luciferin assay (Promega) prior to luminescence measurement by Luminometer (Promega) following the manufacturer's instructions.

HEK-Blue IL6 Cells (Invivogen, catalogue no. hkb-hil6) were cultured and used as proposed by the manufacturer. 30,000 cells per well were seeded in a 96-well plate with culture medium (DMEM + 10% FBS + 1% P/S) and incubated at 37°C with 5% CO_2. After 24 hours, the cells were treated with or without EVs and 5 ng/ml IL6 or 5 ng/ml IL6-IL6R-complex (hyperIL6), kindly provided by Prof. Stefan Rose-John (University of Kiel, Germany). 6 hours later, an amount of 20 µl supernatant was transferred to a flat bottom 96-well plate and 180 µl of QUANTI Blue (InvivoGen) added to each well. After 3 hours incubation at 37°C the SEAP levels were quantified using a spectrophotometer (SpectraMax) at 620-655 nm.

Plasmid constructs and cloning

For the TNFR1 display constructs, cDNA was amplified by PCR and cloned downstream of CMV promoter into a pEGFP-C1 vector backbone using NheI and BamHI. For IL6ST display

constructs, codon optimized designs were synthesized (Gen9) and cloned downstream of CAG promoter into a pLEX vector backbone using EcoRI and NotI. The different constructs were assessed by transient transfection using branched polyethylenimine (PEI: total pDNA μg ratio 1.5:1). Next, the complete CDS of the different display constructs was cloned into the lentiviral p2CL9IPwo5 backbone downstream of the SFFV promoter using EcoRI and NotI, and upstream of an internal ribosomal entry site-Puromycin or Neomycin resistance cDNA cassette. All expression cassettes were confirmed by sequencing and the sequences are listed in Supplementary table 2. Magic™ Cell-free Wheat Germ System-based Membrane Protein Expression in Liposome (Creative Bioscience, US) was used to generate TNFR1 proteoliposomes.

Production of lentiviral vectors and stable-cell lines

Lentiviral supernatants were produced as described previously[27]. In brief, HEK293T cells were co-transfected with p2CL9IPw5 plasmids containing CD63 fused to luminescent proteins, the helper plasmid pCD/NL-BH, and the human codon-optimized foamy virus envelope plasmid pcoPE using the transfection reagent JetPEI (Polyplus, Illkrich Cedex). 16 hours post transfection gene expression from the human CMV immediate-early gene enhancer/promoter was induced with 10 mM sodium butyrate (Sigma-Aldrich) for 6 hours before fresh media was added to the cells, and the supernatant was collected 22 hours later. Viral particles were pelleted at 25,000 × *g* for 90 min at 4°C. The supernatant was discarded, and the pellet was re-suspended in 2 ml of Iscove's Modified Dulbecco's Media supplemented with 20% FBS and 1% P/S. Aliquots were stored at −80°C until usage. To generate stable cell lines, HEK293T cells or MSC cells were transduced by overnight exposure to virus stocks and passaged at least five times under puromycin selection (Sigma; 6 μg/ml)

EV isolation

EV isolation was based on the recently optimized isolation techniques utilized in our group and described in a recent publication[50]. Briefly, conditioned media (CM) was harvested and spun first at 500 *g* for 5 minutes to remove cells, followed by 2,000 *g* for 10 minutes to remove cell debris and thereafter filtrated through an 0.22 μm filter to remove any larger particles. The CM was then run through a hollow fiber filter (D06-E300-05-N, MIDIKROS 65CM 300K MPES 0.5MM, Spectrum Laboratories) using a tangential flow filtration (TFF) system (KR2i TFF

System, Spectrum Laboratories) at a flow rate of 100 ml/min (transmembrane pressure at 3.0 psi and shear rate at 3700 sec^{-1}) and concentrated down to approx. 40-50 ml after diafiltration of PBS. The pre-concentrated CM was subsequently loaded onto BE-SEC columns (HiScreen Capto Core 700 column, GE Healthcare Life Sciences) and connected to an ÄKTAprime plus or ÄKTA Pure 25 chromatography system (GE Healthcare Life Sciences). Flow rate settings for column equilibration, sample loading and column cleaning in place (CIP) procedure were chosen according to the manufacturer's instructions. The EV sample was collected according to the 280 nm UV absorbance chromatogram and concentrated using an Amicon Ultra-15 10 kDa molecular weight cut-off spin-filter (Millipore).

Nanoparticle tracking analysis

Nanoparticle tracking analysis (NTA) was performed with a NS500 nanoparticle analyzer (NanoSight, United Kingdom) to measure the size distribution of EVs. NTA is based on the motion of nanometer-sized particles (Brownian motion) and commonly used for quantifying the concentration and size distribution of submicron-sized particles. For all our recordings, we used a camera level of 10-13 and automatic functions for all post-acquisition settings except for the detection threshold which we fixed at 6-7. Samples were diluted in PBS between 1:500 to 1:5,000 to achieve a particle count of between 2×10^8 and 2×10^9 per ml. The camera focus was adjusted to make the particles appear as sharp dots. Using the *script control* function, five 30 seconds videos for each sample were recorded, incorporating a sample advance and a 5 seconds delay between each recording.

Western blot

Samples were treated with RIPA buffer and vortexed every 5 minutes for 30 minutes to lyse the EVs, subsequently the sample was spun at 12,000 *g* for 12 minutes to remove any lipids and the supernatant was collected. 30 µl of lysed sample was mixed with a sample buffer containing 0.5 M ditiothreitol (DTT), 0.4 M sodium carbonate (Na_2CO_3), 8% SDS and 10% glycerol, and heated at 65 °C for 5 minutes. Samples were then loaded on a NuPAGE® Novex® 4-12% Bis-Tris Gel and ran at 120 V in MOPES running buffer (Invitrogen). The proteins on the gel were transferred to an iBlot nitrocellulose membrane (Invitrogen) for 7

minutes with the iBlot system. The membranes were blocked with Odyssey blocking buffer (LiCor) diluted 1:1 in PBS for 60 minutes at room temperature with gentle shaking.

After the blocking step, the membrane was incubated with freshly prepared primary antibody solution (1:1,000 dilution for anti-Alix [ab117600, Abcam], anti-Tsg101 [ab30871, Abcam], anti-Calnexin [ab22595, Abcam], anti-His [34660, Qiagen], anti-hTNFR [ab19139, Abcam,], anti-mGp130 [R&D, #AF468] and 1:200 dilution for anti-CD81 [sc-9158, Santa Cruz]) overnight at 4°C. Membranes were washed four times, 5 minutes each using washing buffer (TBS-T 0.1%) with gentle shaking before adding the secondary antibody solution (anti-mouse IgG DyLight-800 at 1:15,000 dilution if detecting Alix or His and anti-rabbit IgG DyLight-800 at 1:15,000 dilution if detecting Calnexin or TSG101) and incubated for 1 hour at room temperature. After the secondary antibody incubation, membranes were washed four times, 5 minutes each and visualized by scanning both 700 nm and 800 nm channels on the LI-COR Odyssey CLx infrared imaging system.

Transmission Electron Microscopy

Purified TNFR1ΔΔ-FDN-NST EVs or double decoy EVs were incubated with 1 μl of 1% BSA diluted in PBS, for 5 minutes. 2 μl of primary antibodies (1 mg/ml, anti-hTNFR, Abcam, ab19139) were added and incubated for 45 minutes. For the immuno-gold labeling, 2 μl of protein A conjugated 10 nm gold nanoparticles (BBI Solutions) were added and incubated for 45 minutes.

Purified IL6STΔ-LZ-NST EVs or double decoy EVs were incubated with 1 μl of 1% Rabbit Serum (Sigma) diluted in PBS, for 5 minutes. 2 μl of primary antibody (0.2 mg/ml, anti-mGp130 from R&D, #AF468) were added and incubated for 45 minutes. For the immuno-gold labeling, 2 μl of rabbit anti-goat conjugated 5 nm gold nanoparticles (BBI Solutions) were added and incubated for 45 minutes.

Finally, 3 μl of labeled EVs were added onto glow-discharged formvar-carbon type B coated electron microscopy grids (Ted Pella Inc) for 3 minutes. The grid was dried with filter paper, washed twice with distilled water and blotted dry with filter paper. After the wash, the grid was

stained with 2% uranyl acetate in double distilled H_2O (Sigma) for 10 seconds and filter paper dried. The grid was air-dried and visualized on a transmission electron microscope (Tencai 10).

In vitro capillary tube formation assay

Tube formation assay was used to confirm the angiogenic potential of EVs by co-culturing with Human Heart Aortic Endothelial Cells (TELO-HAEC) on Matrigel (Corning, Belford, USA). Briefly, TELO-HAEC cells were cultured in a starving medium (Endothelial cell basal medium-2 with 2% FBS) for 4 hours. The serum-starved cells were plated at the density of 4x104 cells/well on Matrigel-coated 96-well plates. Cells were then equilibrated with EBM-2 medium along with EVs or as a control in PBS. Endothelial cells aligning into network structures were visually confirmed at 12 hours post-treatment. The results were then documented photographically using an inverted microscope (Olympus) at 10X magnification. Various angiogenic parameters such as length of tube, node numbers, Extremities and Branch length were calculated using ImageJ software (National Institutes of Health, Bethesda, Maryland).

Flow Cytometry

Surface expression of decoy constructs on engineered MSC lines was assessed by using either APC-conjugated rat-anti-mouse gp130 (IL6ST) antibodies (clone FAB4681A, R&D Systems) or AlexaFluor647-conjugated mouse-anti-human CD120a (TNFR1) antibodies (clone H398, Bio-Rad). DAPI was used for dead cell exclusion.

Multiplex bead-based flow cytometry analysis

Multiplex bead-based flow cytometry analysis (MACSPlex Exosome Kit, human, Miltenyi Biotec) was implemented to characterize general surface protein composition of decoy EVs and specific surface proteins co-expressed on engineered decoy receptor EVs. Assays were performed based on an optimized protocol described previously[27]. In brief, EVs were used at an input dose of 1×10^9 NTA-based particles per assay, diluted with MACSPlex buffer to a total volume of 120 μl and incubated with 15 μl of MACSPlex Exosome Capture Beads overnight in wells of a pre-wet and drained MACSPlex 96 well 0.22 μm filter plate at 450 *g* at room temperature. Beads were washed with 200 μl MACSPlex buffer and the liquid was removed

applying vacuum (Sigma-Aldrich, Supelco PlatePrep; -100 mBar). For counterstaining of captured EVs, either a mixture of APC-conjugated anti-CD9, anti-CD63 and anti-CD81 detection antibodies (supplied in the MACSPlex kit, 5 μl each) or anti-decoy receptor antibodies (AlexaFluor647-labelled anti-human TNFR1, Bio-Rad, cat #MCA1340A647, clone H398, lot 0410; or APC-labelled anti-mouse gp130, R&D Systems, cat #FAB4681A, clone 125623, lot AAOK0114071; 200 ng, respectively) were added to each well in a total volume of 135 μl and the plate was incubated at 450 *g* for 1 hours at room temperature. Next, the samples were washed twice, resuspended in MACSPlex buffer and analyzed by flow cytometry with a MACSQuant Analyzer 10 flow cytometer (Miltenyi Biotec). FlowJo software (version 10.6.2, FlowJo, LLC) was used to analyze flow cytometric data. Median fluorescence intensities (MFI) for all 39 capture bead subsets were background-corrected by subtracting respective MFI values from matched non-EV containing buffer controls (buffer + capture beads + antibodies) that were treated exactly like sEV-containing samples (buffer + capture beads + EVs + antibodies).

Single EV analysis by Imaging Flow Cytometry

TNFR-decoy EVs and double decoy EVs were analyzed by single EV Imaging Flow Cytometry (IFCM) on an ImageStreamX MkII instrument (ISX; Amnis/Luminex) to confirm decoy receptor co-expression on a portion of engineered EVs. Isolated EVs were stained with PE-labelled anti-human TNFR1 (Bio-Rad, cat #MCA1340PE, clone H398, lot 0407) and APC-labelled anti-mouse gp130 antibodies (R&D Systems, cat #FAB4681A, clone 125623, lot AAOK0114071; final concentration during staining 10 nM) at a concentration of 5×10^9 NTA-based particles in 60 μl total volume for 1 hour at room temperature. Samples (and buffer controls without EVs, i.e. PBS + antibodies) were diluted 200-fold in PBS post staining and analyzed on an ISX equipped with 5 lasers (70 mW 375 nm, 100 mW 488 nm, 200 mW 561 nm, 150 mW 642 nm, 70 mW 785 nm [SSC]) with a protocol and masking setting described and optimized previously[35,51]. Fluorescence parameters recorded and analyzed in this study comprise PE signals (MC_Or_NMC_Channel_03) and APC/AlexaFluor 647 (MC_Or_NMC_Channel_11). All analyses were performed by using the 60× objective and deactivated Remove Beads option. All lasers were set to maximum powers, and all data was acquired with a 7 µm core size and low flow rate (~0.38 µL/min). Data was recorded for 5 min and pre-gated on SSC (low) events as described previously. Dulbecco's PBS pH 7.4 (Gibco) was used as sheath fluid and for all dilution steps. Data was analyzed with optimized masking

settings and by excluding coincidence events as described before using Amnis IDEAS software (version 6.2.187.0) and FlowJo v. 10.6.2 (FlowJo, LLC). To estimate the amount of decoy receptors on the surface of engineered EVs, we performed similar analyses on a Cellstream Imaging Flow Cytometer (Amnis/Luminex). Isolated EVs were stained with AlexaFluor647 (AF647)-labelled anti-human TNFR1 (Bio-Rad, cat #MCA1340A647, clone H398, lot 1005) at a final ab concentration of 8 nM and a concentration of 1×10^{10} NTA-based particles/mL in a total volume of 25 μL over night. Sample and controls were diluted 2000-fold post staining and analyzed by IFCM (Amnis Cellstream, Luminex; equipped with 405, 488, 561 and 642 nm lasers; see Supplemental Figure 7 F-G). Fluorescence calibration was performed as described previously[45]. In brief, AF647 MESF (molecules of equivalent soluble fluorophores) beads (Bangs Laboratories, Inc, Cat #647A, Lot 12929) with known numbers of AF647 fluorophores for distinct bead populations were acquired with the same respective settings used for EV measurements with the exception that the SSC laser was turned off. Linear regression was performed (Supplemental Figure 7F) and the resulting equation was used to convert fluorescence intensity values measured in arbitrary units to MESF values of absolute fluorescence. Flow cytometry plots using MESF units on the x-axis were created with FlowJo v. 10.6.2 (FlowJo, LLC).

Reverse Transcription-quantitative PCR (RT-qPCR)

Total RNA was isolated using TRIzol reagent (Invitrogen) and Aureum Total RNA Isolation Mini Kit (Bio-Rad), according to manufacturer's instructions. cDNA synthesis was performed using iScript cDNA synthesis kit (Bio-Rad Laboratories), according to manufacturer's instructions. RT-qPCR was performed with the Light Cycler 480 system (Roche) using Sensifast Bioline Mix (Bio-Line). Expression levels in the spinal cord were normalized to the expression of the two most stable housekeeping genes, which were determined using geNorm[52]: ubiquitin-C (*Ubc*) and hypoxanthine-guanine phosphoribosyltransferase (*Hprt*).
Primer sequences:
Ubc (Fw 5′-AGGTCAAACAGGAAGACAGACGTA-
3', Rev 5'-TCACACCCAAGAACAAGCACA-3'),
Hprt (Fw 5'-AGTGTTGGATACAGGCCAGAC-3', Rev
5'-CGTGATTCAAATCCCTGAAGT-3'),
Il6 (Fw 5'-TAGTCCTTCCTACCCCAATTTCC-3', Rev

5’-TTGGTCCTTAGCCACTCCTTC-3’),
Tnf (Fw 5’-ACCCTGGTATGAGCCCATATAC-3’, Rev
5’-ACACCCATTCCCTTCACAGAG-3’),
Il17a (Fw 5’-TTTAACTCCCTTGGCGCAAAA-3’, Rev
5’-CTTTCCCTCCGCATTGACAC-3’),
Cxcl1 (Fw 5’-CTGGGATTCACCTCAAGAACATC-3’,
Rev 5’-CAGGGTCAAGGCAAGCCTC-3’).

Animal experiments

Systemic inflammation model

Systemic inflammation was induced using Lipopolysaccharide (LPS) as described by others. 20 g (±5 g) female C57BL/6 mice were injected intraperitoneally (I.P) with LPS (L-5886, Sigma). EVs were I.V injected via the tail vein subsequent to LPS induction and the animals were observed and weighed daily after induction. The animal experiments were approved by The Swedish Local Board for Laboratory Animals.

Experimental autoimmune encephalitis (EAE) model

EAE was induced as described previously[19]. 20 g (±5 g) female C57BL/6 mice were immunized by S.C injection of 100 μl of the MOG35-55-CFA emulsion, distributed to 3 different locations. I.P injections of 400 ng pertussis toxin were given on the day of and two days following immunization to induce disease. Mice were subsequently monitored for change in body weight and assessed using EAE-scoring, see Table 1. EVs were injected either S.C on day 7, 9 and 13 or given as single I.V injection. The animal experiments were approved by The Swedish Local Board for Laboratory Animals.

TNBS induced colitis model

Trinitrobenzene sulfonic acid (TNBS) induced Colitis was induced as described previously[53]. 20 g (±5 g) female BALB/c mice were pre-sensitized with peritoneum skin application of 60 μl 5% TNBS + 90 μl acetone-olive oil (4:1) mix per mouse. One week later, Colitis was induced by intra-rectal administration of 30 μl TNBS + 42.1 μl 95% ethanol + 27.9 μl H_2O per

mouse. Mice were subsequently monitored for change in body weight. For therapeutic treatment EVs were injected I.V. on day 1 as single I.V injection. For in vivo biodsitrbituon study, animals were injected with HEK293T CD63 Nanoluc EVs purified from HEK293T cells stable expressing CD63 Nanoluc on day 1 post disease induction as single I.V injection, 2 hours post injection animals were sacrificed and organs were analyzed as described earlier[37]. The animal experiments were approved by The Swedish Local Board for Laboratory Animals.

in vivo toxicity study

All animal experiments were performed in accordance with the ethical permission and designed to minimize the suffering and pain of the animals.

For the toxicity study, the mdx model was used. The work was conducted at the Jackson laboratory, Bar Harbor, ME, USA. 2-weeks old mice (14-16 days) were used. Hemizygous (mdx/Y) male mice were grouped into 8 groups receiving injections twice a week for two weeks comparing I.V vs. S.C route with different doses, as shown in the table xx. The mice were monitored daily for signs of toxicity. Two weeks following the first injection blood was collected by cardiocentesis and the mice were sacrificed. Body and spleen weight were recorded at necropsy. Whole blood was used for hematology assessment (CBC/Diff/Retic and smears) and processed for flow cytometry analysis. The flow panel used included MHC-II FITC, CD69 PE, CD45 PE-Cy7, CD11c APC, CD115 biotin/Streptavidin APC-Cy7, Ly6G V450, Ly6C BV570, CD11b BV650, CD8 BV711, CD4 BUV 737, and FVD780.

Statistical analysis

Statistical analyses of the data were performed using Prism 6.0 (GraphPad Software Inc.) by one-way ANOVA or two-way ANOVA for all *P*-values. All results are expressed as mean ±S.D. All graphs were made in Prism 8.0 (GraphPad Software Inc.).

A)

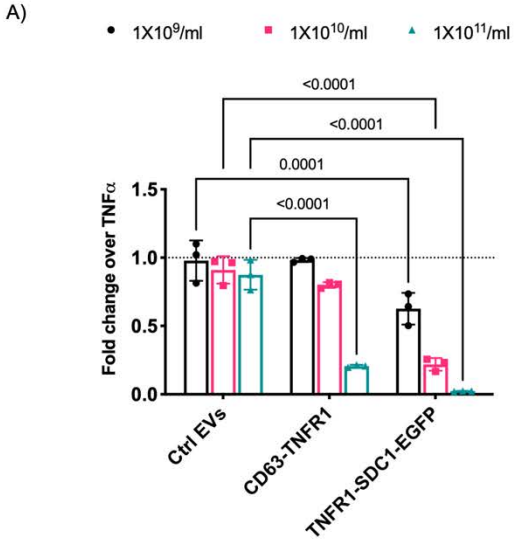

B)

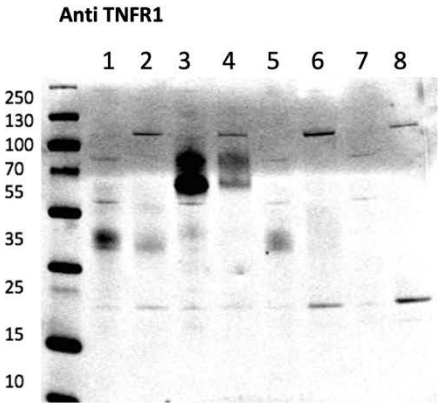

Lane	Sample Name	Predicted M.W kDa
1	TNFR1-Syndecan1 Cells	42
2	TNFR1-Syndecan1 EVs	42
3	TNFR1-Syndecan1-EGFP Cells	59
4	TNFR1-Syndecan1-EGFP EVs	59
5	CD63-TNFR1 Cells	40
6	CD63-TNFR1 EVs	40
7	Ctrl Cells	-
8	Ctrl EVs	-

Supplementary Figure 1. A) Engineered EVs displaying TNFR1 purified from HEK293T cells transfected with constructs listed in the figure legends, evaluated for TNFα decoy in an *in vitro* cell assay respondent to TNFα induced NF-ϰB activation. Data were normalized to control cells treated with TNFα (5ng/ml). Central Value = Mean, Error bars = S.D (*Biological replicate*, *n*=3). Statistical significance calculated by two-way ANOVA with Dunnett's post-test compared with response of Ctrl EVs at the respective dose. **B)** WB probed against human TNFR1 on engineered HEK293T EVs and their respective cells transfected with various EVs engineering designs. Predicted molecular weight (kDa) was calculated based on the amino acid sequence of the respective construct.

A)

Anti poly-Histidine tag

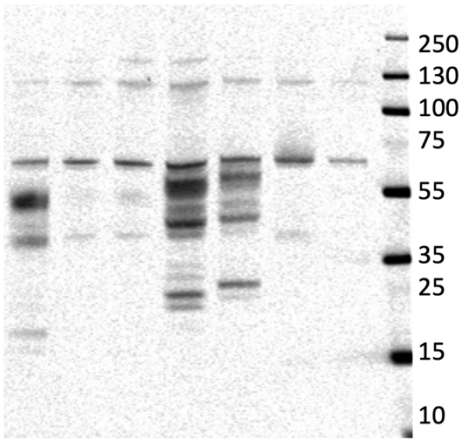

Lane	Sample Name	Predicted M.W kDa
1	TNFR1 Cells	38
2	TNFR1-C term CD63 Cells	40
3	TNFR1-2XC term CD63 Cells	42
4	TNFR1-Syndecan1 Cells	42
5	TNFR1-N term Syntenin Cells	59
6	TNFR1-Syndecan1-EGFP Cells	45
7	Ctrl Cells	-

B)

Anti poly-Histidine tag

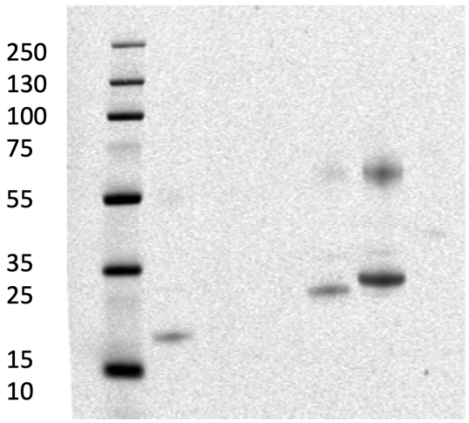

Lane	Sample Name	Predicted M.W kDa
1	TNFR1 EVs	38
2	TNFR1-C term CD63 EVs	40
3	TNFR1-2XC term CD63 EVs	42
4	TNFR1-Syndecan1 EVs	42
5	TNFR1-N term Syntenin EVs	59
6	TNFR1-Syndecan1-EGFP EVs	45
7	Ctrl EVs	-

Supplementary Figure 2. WB probed against poly Histidine tag on **A)** engineered HEK293T cells and their **B)** respective EVs. Cells were transfected with indicated genetic constructs. Predicted molecular weight (kDa) was calculated based on the amino acid sequence of the respective construct.

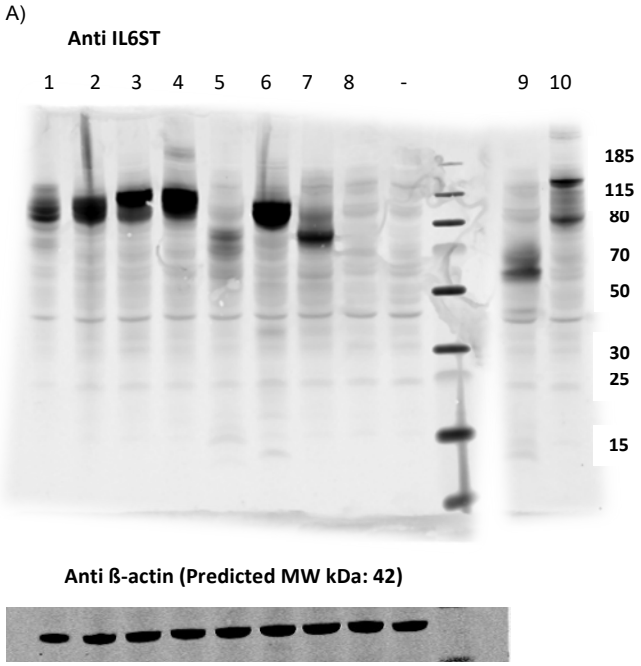

Lane	Sample Name	Predicted M.W kDa
1	IL6ST-3X N term Syntenin Cells	118
2	IL6ST-N term Syntenin Cells	91
3	IL6ST-Syndecan1 Cells	93
4	IL6ST-GCN4 L.Z-N term Syntenin Cells	94
5	IL6ST extracellular domain-PDGFR TM-N term Syntenin Cells	57
6	IL6ST Cells	77
7	IL6ST extracellular domain-ADRB2 TM-C term CD63 Cells	70
8	Ctrl Cells	
9	IL6ST extracellular domain-PDGFR TM Cells	43
10	IL6ST-TSG101 Cells	121

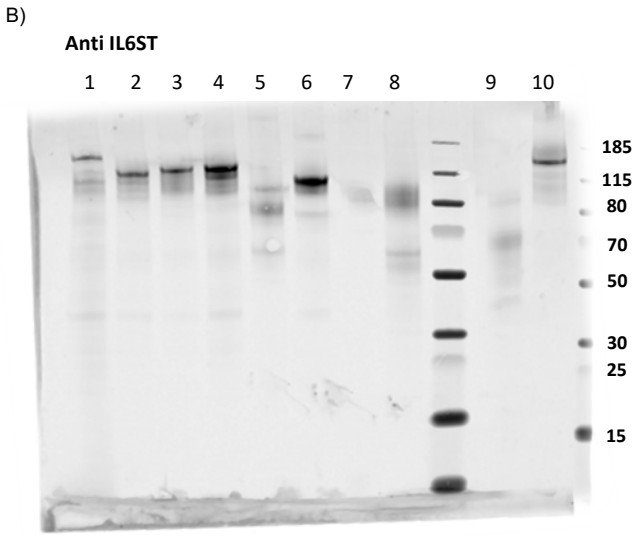

Lane	Sample Name	Predicted M.W kDa
1	IL6ST-3X N term Syntenin EVs	118
2	IL6ST-N term Syntenin EVs	91
3	IL6ST-Syndecan1 EVs	93
4	IL6ST-GCN4 L.Z-N term Syntenin EVs	94
5	IL6ST extracellular domain-PDGFR TM-N term Syntenin EVs	57
6	IL6ST EVs	77
7	IL6ST extracellular domain-ADRB2 TM-C term CD63 EVs	70
8	Ctrl EVs	
9	IL6ST extracellular domain-PDGFR TM EVs	43
10	IL6ST-TSG101 EVs	121

Supplementary Figure 3. WB probed against mouse IL6ST on **A)** engineered HEK293T cells and their **B)** respective EVs. Cells were transfected with indicated genetic constructs. Predicted molecular weight (kDa) values were calculated based on the amino acid sequence of the respective construct. Full length blot corresponding to **A** is included in Supp. Figure 17.

A)

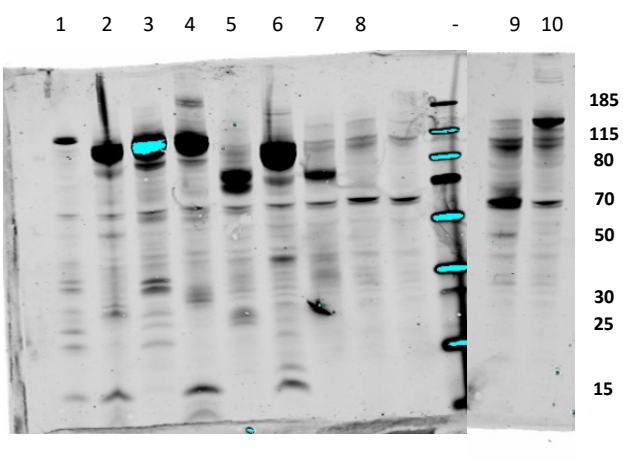

Lane	Sample Name	Predicted M.W kDa
1	IL6ST-3X N term Syntenin Cells	118
2	IL6ST-N term Syntenin Cells	91
3	IL6ST-Syndecan1 Cells	93
4	IL6ST-GCN4 L.Z-N term Syntenin Cells	94
5	IL6ST extracellular domain-PDGFR TM-N term Syntenin Cells	57
6	IL6ST Cells	77
7	IL6ST extracellular domain-ADRB2 TM-CD63 Cells	70
8	Ctrl Cells	
9	IL6ST extracellular domain-PDGFR TM Cells	43
10	IL6ST-TSG101 Cells	121

B)

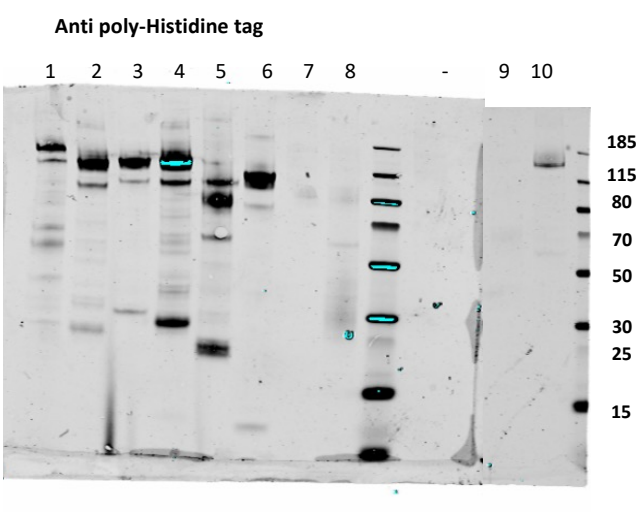

Lane	Sample Name	Predicted M.W kDa
1	IL6ST-3X N term Syntenin EVs	118
2	IL6ST-N term Syntenin EVs	91
3	IL6ST-Syndecan1 EVs	93
4	IL6ST-GCN4 L.Z-N term Syntenin EVs	94
5	IL6ST extracellular domain-PDGFR TM-N term Syntenin EVs	57
6	IL6ST EVs	77
7	IL6ST extracellular domain-ADRB2 TM-CD63 EVs	70
8	Ctrl EVs	
9	IL6ST extracellular domain-PDGFR TM EVs	43
10	IL6ST-TSG101 EVs	121

Supplementary Figure 4. WB probed against poly Histidine tag on **A)** engineered HEK293T cells and their **B)** respective EVs. Cells were transfected with indicated genetic constructs. Predicted molecular weight (kDa) values were calculated based on the amino acid sequence of the respective construct.

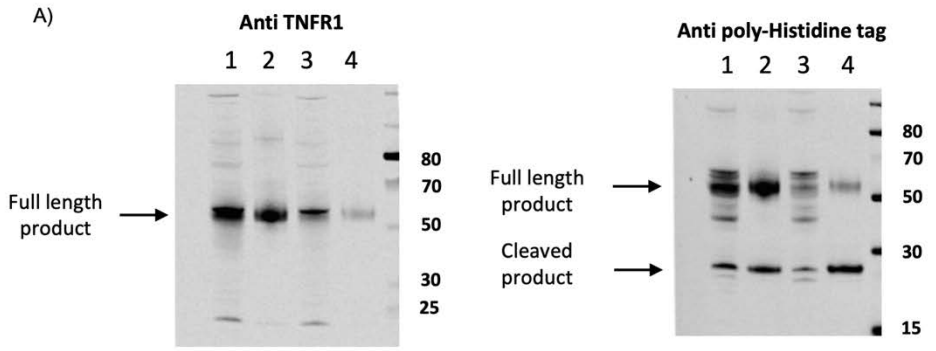

Lane	Sample Name	Predicted M.W kDa
1	TNFR1 MMP-N term Syntenin Cells	45
2	TNFR1 MMP-N term Syntenin EVs	45
3	TNFR1-N term Syntenin Cells	45
4	TNFR1-N term Syntenin EVs	45

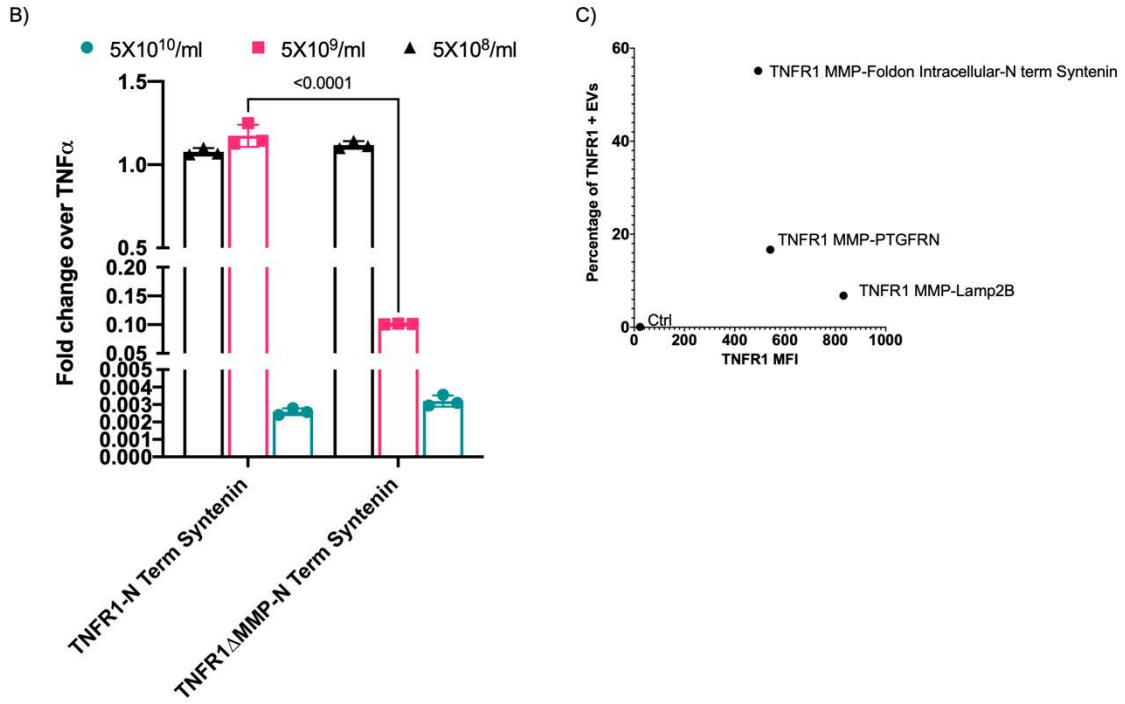

Supplementary Figure 5. A) WB probed against human TNFR1 and poly Histidine tag on engineered HEK293T EVs and their respective cells transfected with WT and Mutant TNFR1 fused to Syntenin. Predicted molecular weight (kDa) values were calculated based on the amino acid sequence of the respective construct. **B)** Engineered EVs displaying TNFR1 purified from HEK293T cells transfected with constructs listed in the figure legends, evaluated for TNFα decoy in an *in vitro* cell assay respondent to TNFα induced NF-ϰB activation. Data were normalized to control cells treated with TNFα (5ng/ml). Central Value = Mean, Error bars = S.D (*Biological replicate, n*=3). Statistical significance calculated by two-way ANOVA with Dunnett's post-test compared with response of Ctrl EVs at the respective dose. **C)** EV sorting efficiency of various TNFR1 display constructs used in Figure

2C determined by single vesicle flow cytometry. EVs purified from HEK293T cells transfected with the constructs as listed in the figure legend were stained with TNFR1-Alexa 647 antibody and analysed on single vesicle flow cytometry. X-axis represent percentage of EVs positive for TNFR1 and Y axis represent the median fluorescence intensity of TNFR1 staining on EVs.

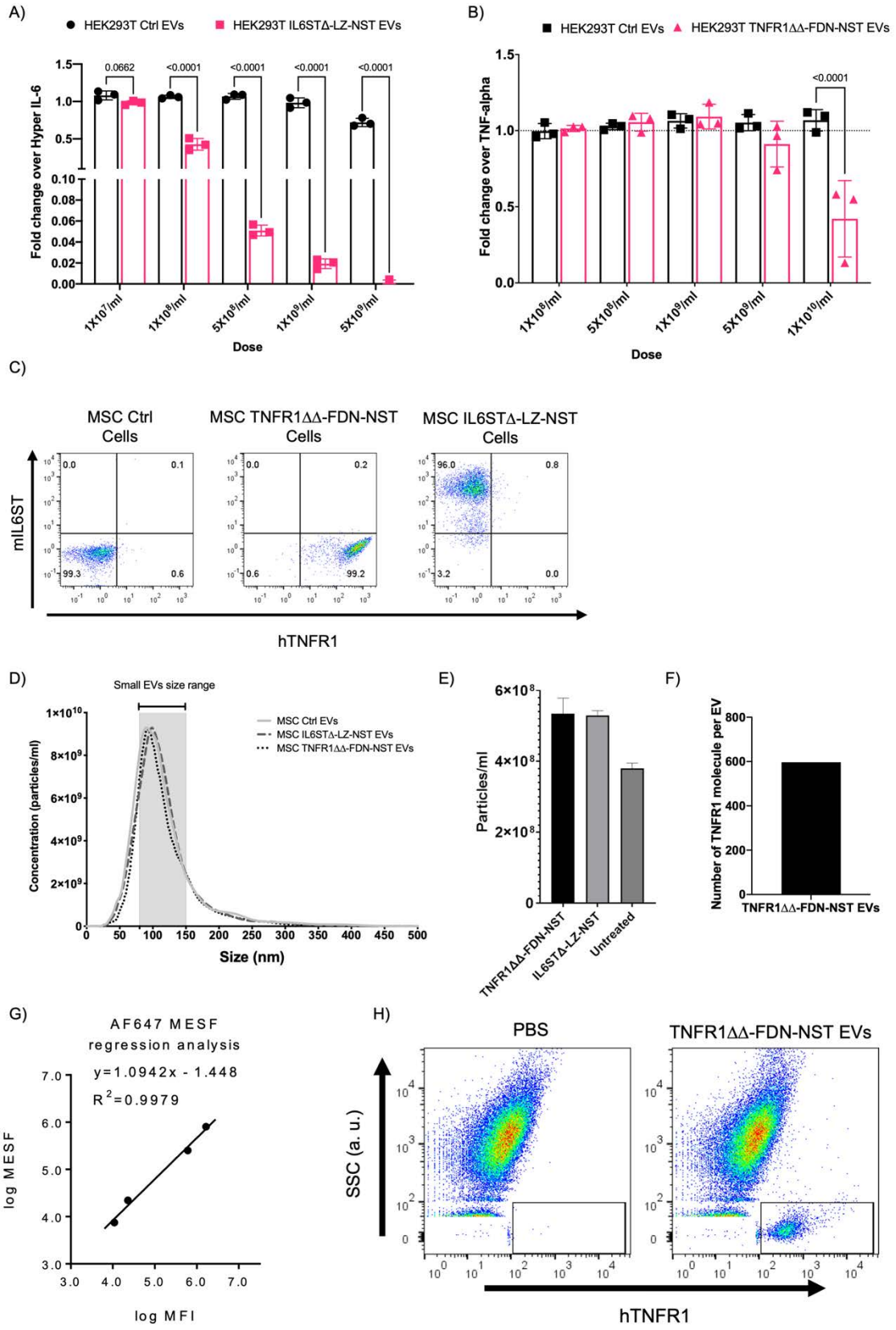

Supplementary Figure 6. A) IL6/IL6R induced STAT3 activation is reduced in a dose dependent manner by EVs purified from HEK293T cells stable expressing the optimized

IL6STΔ-LZ-NST display construct. Data were normalized to control cells treated with IL6/sIL6R (5 ng/ml). Central Value = Mean, Error bars = S.D (*Biological replicate, n*= 3). Statistical significance calculated by two-way ANOVA upon comparing response to Ctrl EVs at the respective dose. **B)** TNFα induced NF-ϰB activation is reduced in a dose dependent manner by EVs purified from HEK293T cells stable expressing the optimized TNFR1ΔΔ-FDN-NST display construct. Data were normalized to control cells treated with TNFα (5ng/ml). Central Value = Mean, Error bars = S.D (*Biological replicate, n*=3). Statistical significance calculated by two-way ANOVA upon comparing response to Ctrl EVs at the respective dose. **C)** Flow cytometry analysis of MSC TNFR1ΔΔ-FDN-NST, MSC IL6STΔ-LZ-NST cells stained with mouse IL6ST APC conjugated (y axis) and human TNFR1 PE (y axis) conjugated antibody. **D)** Size distribution determined by NTA of MSC Ctrl EVs, IL6STΔ-LZ-NST EVs and TNFR1ΔΔ-FDN-NST EVs. (*Technical replicate, n*= 5). **E)** Total number of particles detected by NTA in condition medium of WT MSC cells or MSC cells stable expressing the optimized TNFR1ΔΔ-FDN-NST or IL6STΔ-LZ-NST display construct. Central Value = Mean, Error bars = S.D (*Technical replicate, n*= 5). **F)** Total estimated number of TNFR1 receptors per EV estimated based on obtained mean fluorescence intensity values after fluorescence calibration of with AF647 MESF beads by single vesicle imaging flow cytometry on a Cellstream instrument and staining of TNFR1ΔΔ-FDN-NST EVs with TNFR1-Alexa 647 antibodies. **G)** Linear regression was applied to convert MFI into MESF units of absolute fluorescence to delineate the number receptors detected on the surface of the EVs shown in Supp. Fig. 7F. **H)** Single vesicle flow cytometry analysis (IFCM) with dot plots of HEK293T TNFR1ΔΔ-FDN-NST EVs stained with hTNFR1 AF647 conjugated antibody. PBS + antibodies were used for background adjustment and for determining the gating strategy.

A)

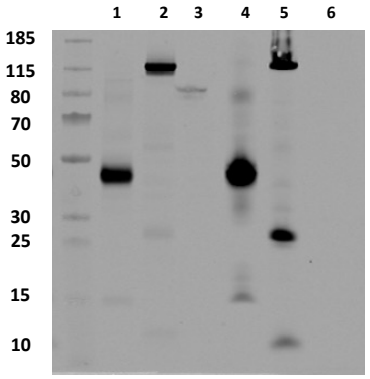

Lane	Sample Name	Predicted M.W kDa
1	MSC TNFR1ΔΔ-FDN-NST Cells	48
2	MSC IL6STΔ-LZ-NST Cells	94
3	MSC Ctrl Cells	-
4	MSC TNFR1ΔΔ-FDN-NST EVs	48
5	MSC IL6STΔ-LZ-NST EVs	94
6	MSC Ctrl EVs	-

B)

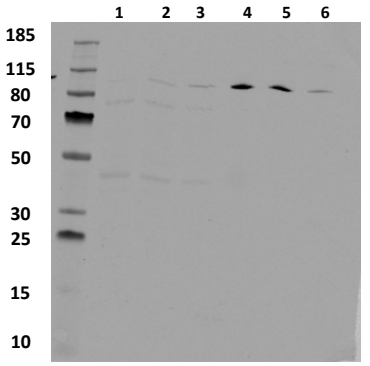

Lane	Sample Name
1	MSC TNFR1ΔΔ-FDN-NST Cells
2	MSC IL6STΔ-LZ-NST Cells
3	MSC Ctrl Cells
4	MSC TNFR1ΔΔ-FDN-NST EVs
5	MSC IL6STΔ-LZ-NST EVs
6	MSC Ctrl EVs

C)

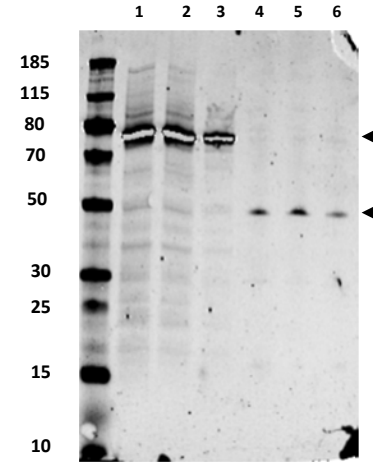

Lane	Sample Name
1	MSC TNFR1ΔΔ-FDN-NST Cells
2	MSC IL6STΔ-LZ-NST Cells
3	MSC Ctrl Cells
4	MSC TNFR1ΔΔ-FDN-NST EVs
5	MSC IL6STΔ-LZ-NST EVs
6	MSC Ctrl EVs

Supplementary Figure 7. A-C) Uncropped version of WB images as shown in Figure 3D.

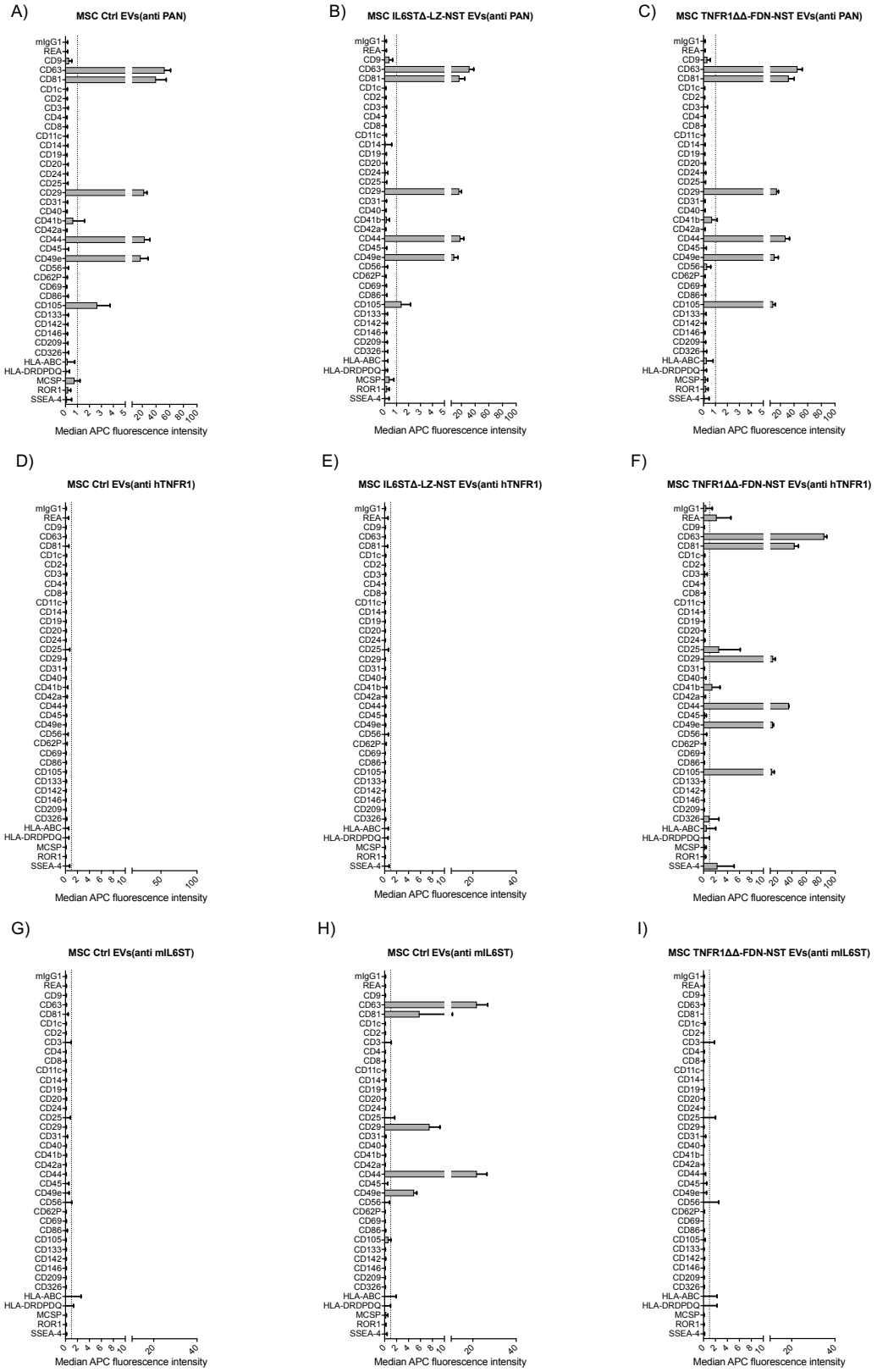

Supplementary Figure 8. A-I) Full expression profile of all the 37 different markers determined by multiplex bead-based assay for the same dataset as shown in Figure 3F-H. Error bars S.D, (*Technical replicate, n*= 5000-15000).

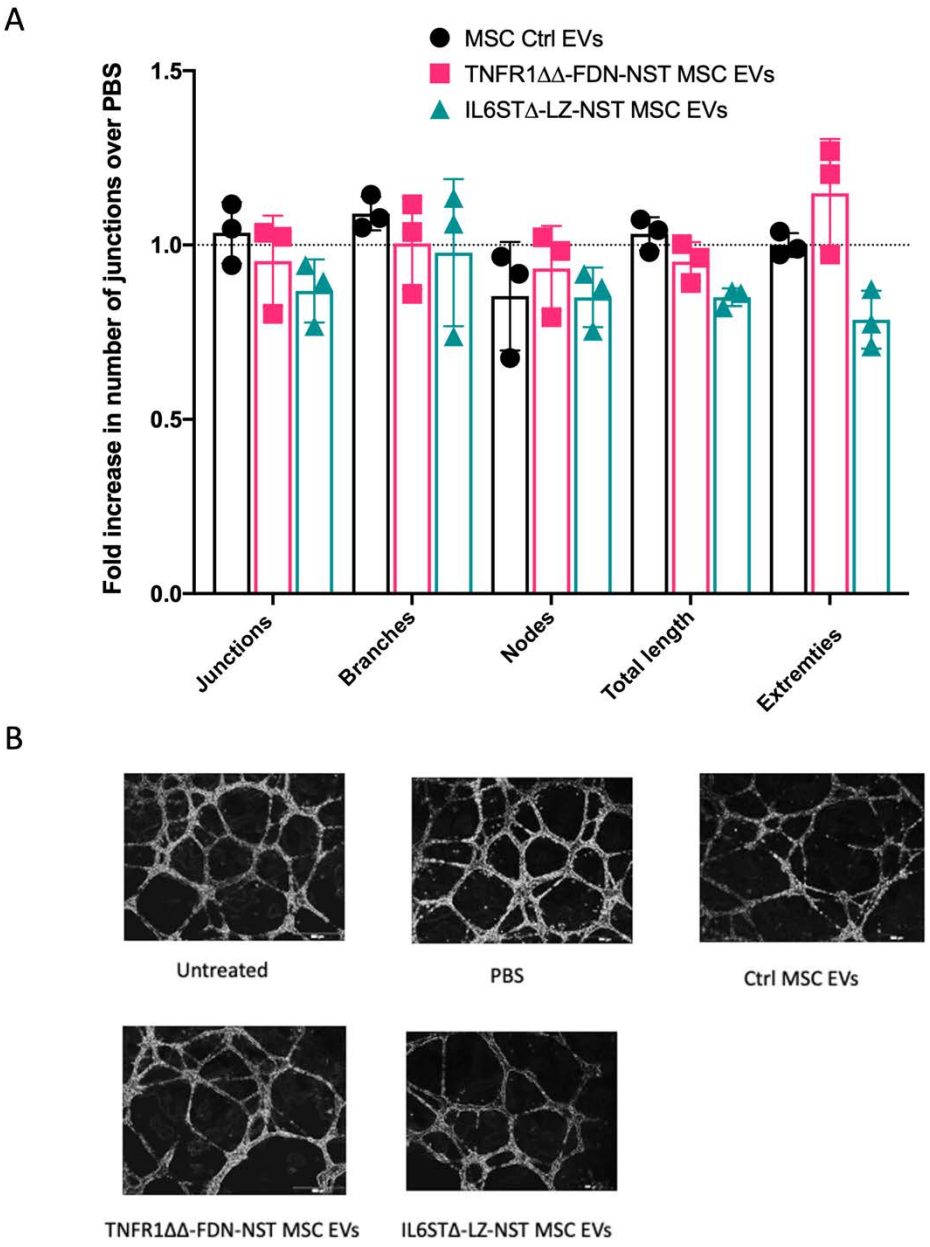

Supplementary Figure 9. A. Effect of EVs on Endothelial cell tube formation assay. Human heart aortic endothelial cells were cocultured with either PBS or $1X10^{10}$ EVs as indicated in the figure legend. **B**. Representative microscopy images of Human heart aortic endothelial cells treated with PBS or $1X10^{10}$ EVs.

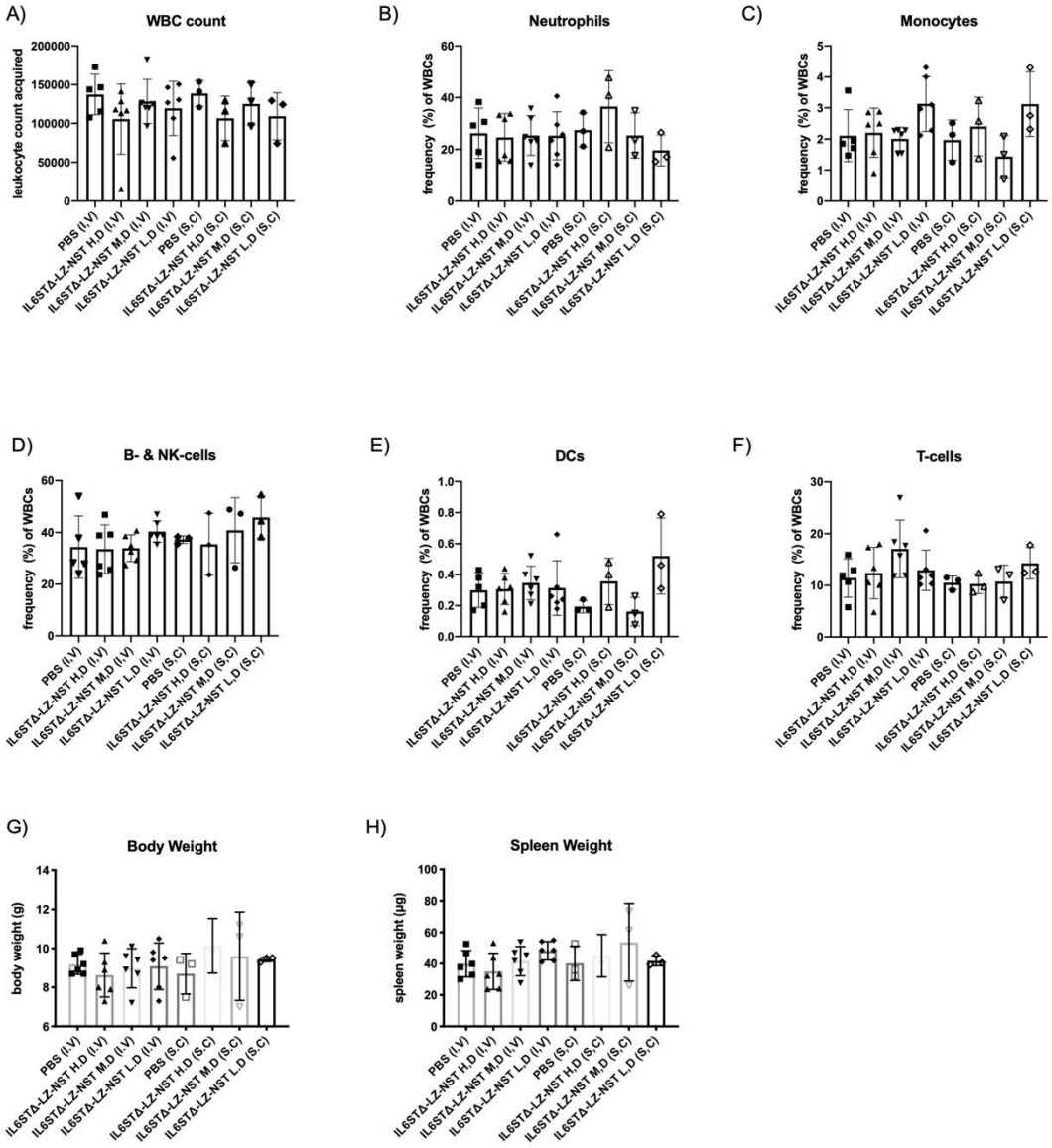

Supplementary Figure 10. *in vivo* toxicity profile of Engineered EVs. 2 weeks old mdx genotype mice were injected with either High dose (H.D) $3.75X10^{10}$, Medium dose (M.D) $7.5X10^{9}$ or Low dose (L.D) $3.75X10^{9}$ of IL6STΔ-LZ-NST MSC EVs either through I.V (n=6) or S.C (n=3) twice a week for two weeks. **A-F)** Whole blood assessment at the endpoint of the toxicity study did not reveal any differences in number of leukocytes (WBC), neutrophils, monocytes, B- and NK-cells, dendritic cells (DCs), or T-cells. Kruskal-Wallis test was used to calculate significance ($p<0.05$). **G-H)** Body weight and spleen weight at necropsy. No significant differences were seen between the groups. Kruskal-Wallis test was used to calculate significance ($p<0.05$).

A

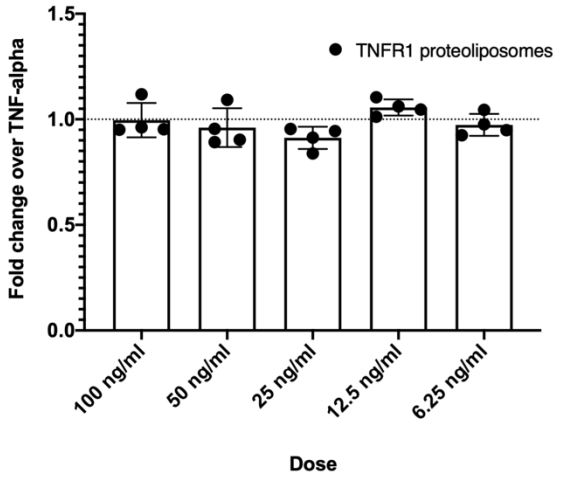

B

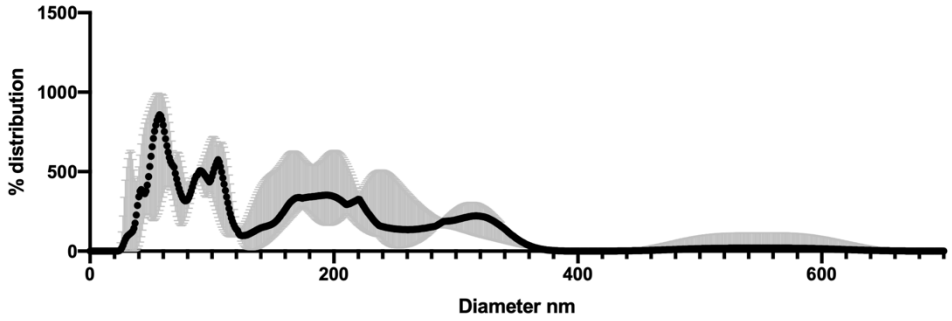

Supplementary Figure 11. A) Effect of Synthetic proteoliposomes displaying human TNFR1 on blocking TNFα induced NF-ϰB activation. Data were normalized to control cells treated with TNFα (5ng/ml). Central Value = Mean, Error bars = S.D (*Biological replicate, n*=3). **B)** Size distribution profile of Synthetic proteoliposomes displaying TNFR1 as determined by NTA analysis *(Technical replicate, n=5)*.

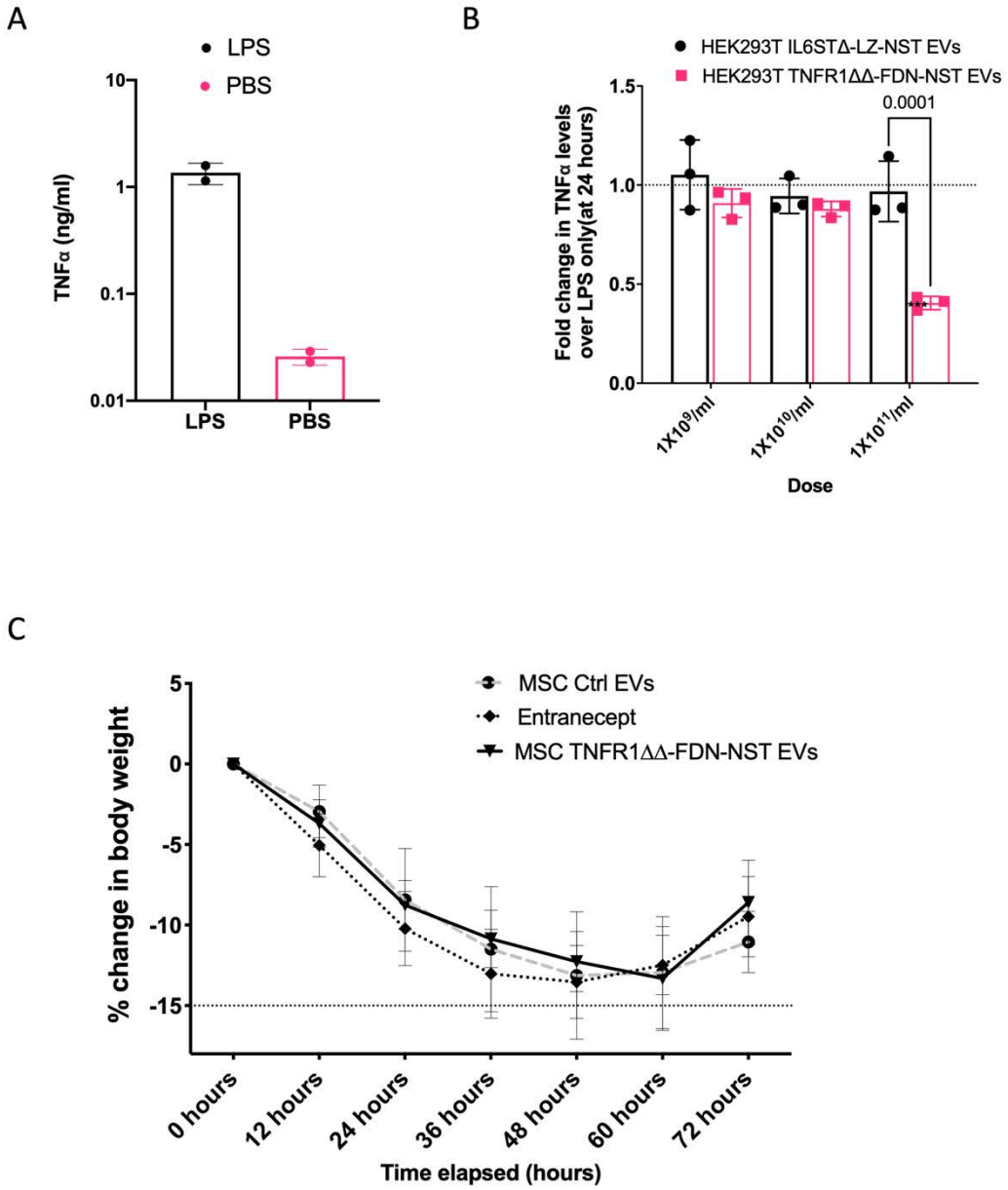

Supplementary Figure 12. A) TNFα levels in conditioned medium of RAW 246.7 macrophages 24 hours after stimulation with LPS (100ng/ml). **B)** Effect of HEK293T TNFR1ΔΔ-FDN-NST EVs and IL6STΔ-LZ-NST EVs on TNFα levels in conditioned medium determined by ELISA at 24 hours post LPS stimulation of RAW 246.7 macrophages. Data were normalized to control cells treated with LPS only. Central Value = Mean, Error bars = S.D (*Biological replicate*, n=3). Statistical significance calculated by one-way ANOVA upon comparing response between two different groups. **C)** Percentage change in bodyweight to initial bodyweight of mice induced with LPS (15 mg/kg) mediated systemic inflammation and treated I.V with either 1×10^{11} MSC TNFR1ΔΔ-FDN-NST EVs or 1×10^{11} MSC Ctrl EVs or 160 μg Etanercept 3 hours post LPS induction.

A)

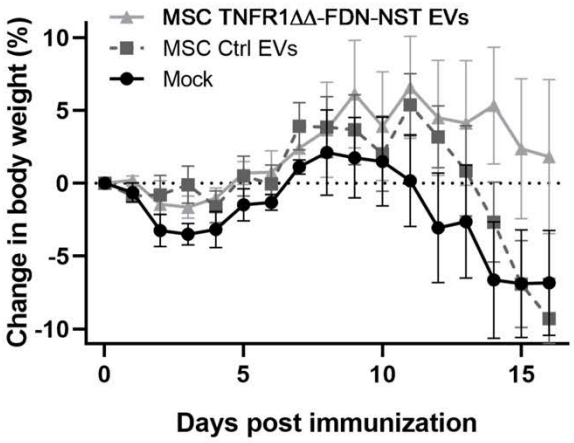

B)

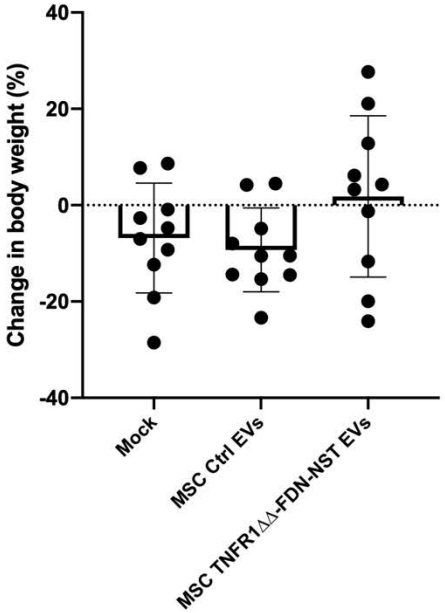

Supplementary Figure 13. A) Percent change in relative bodyweight to initial weight over the disease course and **B)** Percent change in body weight between day 0 to day 16 in mice induced with EAE using MOG_{35-55} peptide and treated with S.C administration of either 4×10^{10} MSC TNFR1ΔΔ-FDN-NST EVs (n=5) or MSC Ctrl EVs (n=5) or Saline (n=5) (On day 7, 10 & 13).

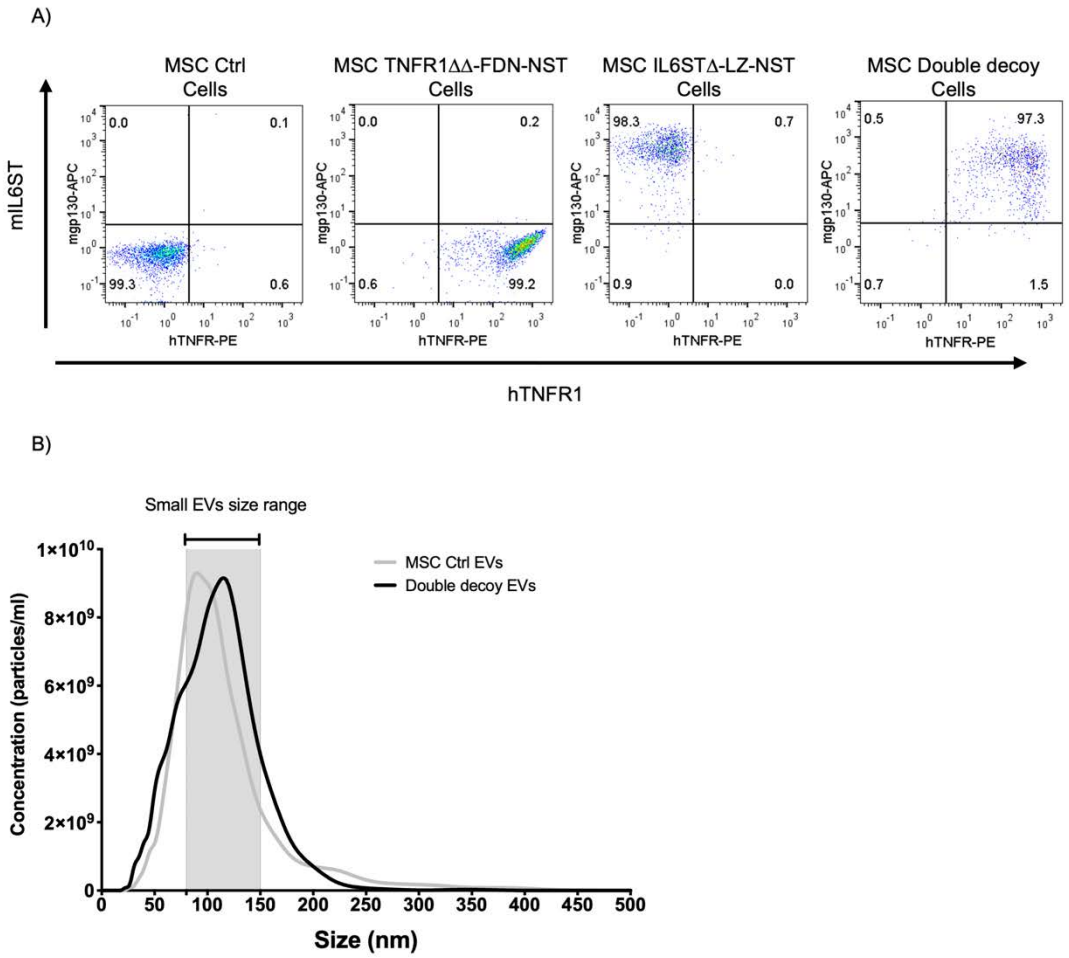

Supplementary Figure 14. A) Flow cytometry analysis of MSC TNFR1ΔΔ-FDN-NST, MSC IL6STΔ-LZ-NST and MSC double decoy cells stained with mouse IL6ST APC conjugated and human TNFR1 PE conjugated antibody. **B)** Size distribution determined by NTA of MSC Ctrl EVs and double decoy EVs *(Technical replicate, n=5)*.

A)

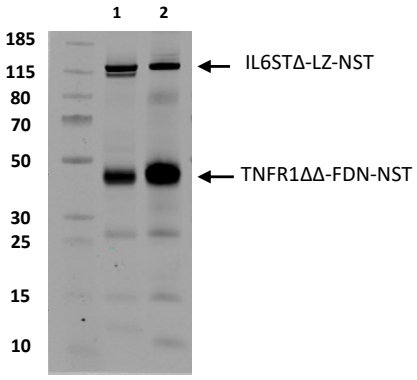

Lane	Sample Name	Predicted M.W kDa
1	MSC Double decoy Cells	94 and 48
2	MSC Double decoy EVs	94 and 48

B)

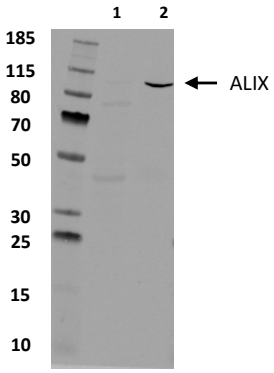

Lane	Sample Name
1	MSC Double decoy Cells
2	MSC Double decoy EVs

C)

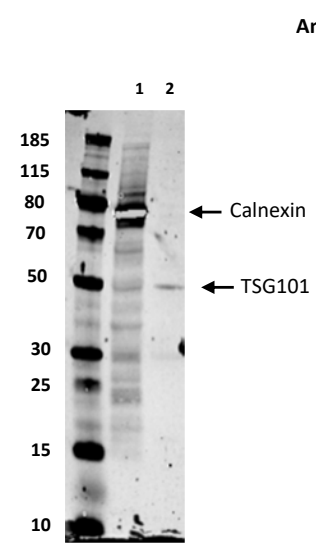

Lane	Sample Name
1	MSC Double decoy Cells
2	MSC Double decoy EVs

Supplementary Figure 15. A) WB of double decoy cells and EVs indicating the presence of both his-tagged decoy receptors; TNFR1ΔΔ-FDN-NST (48 kDa) and IL6STΔ-LZ-NST (94 kDa) in cells and EVs. The WB results further demonstrate the presence of **B)** classical EV

markers; ALIX (96 kDa), TSG101 (44 kDa) and **C)** absence of Calnexin (67 kDa) in the isolated EVs.

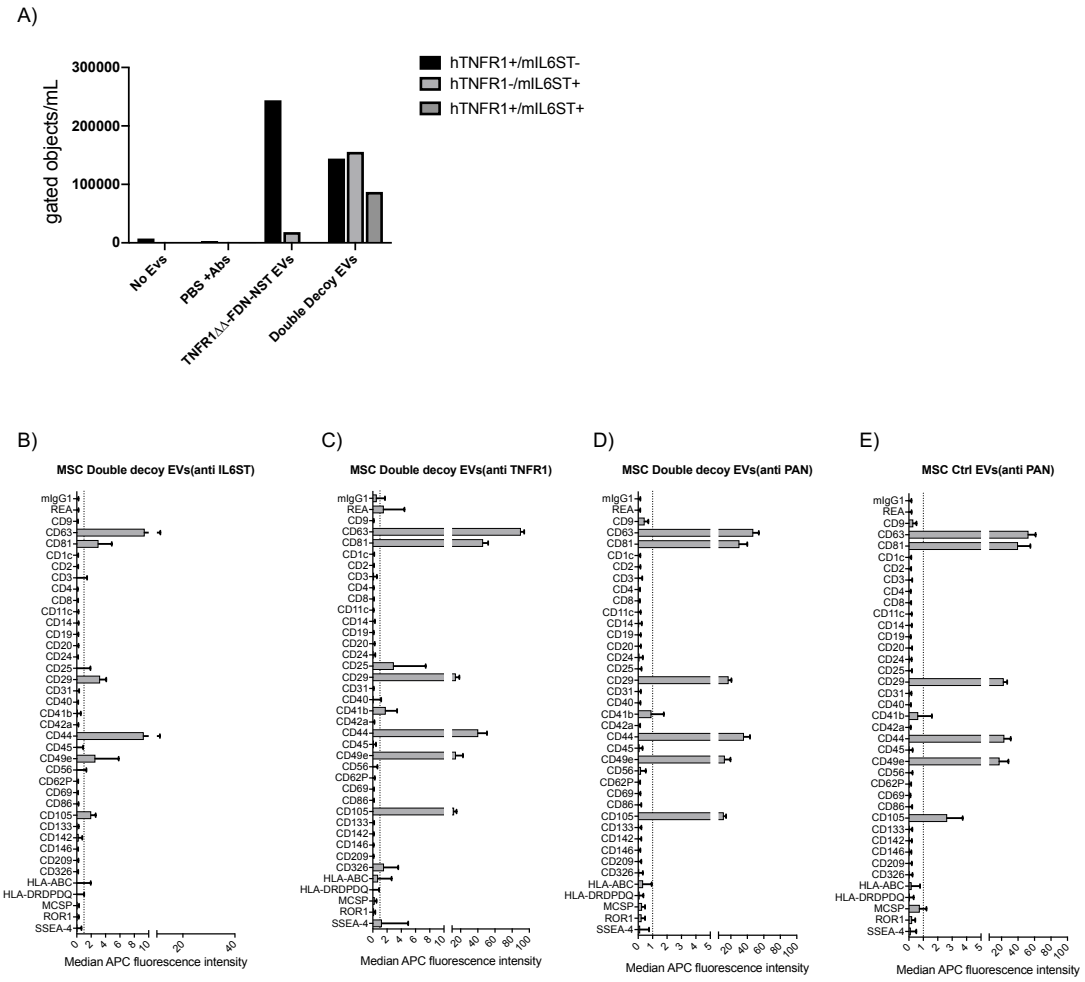

Supplementary Figure 16 A) Concentration of events in different gated population, for the same dataset as shown in Figure 6A and Extended Data Figure 4A. **B-E).** Full expression profile of all the 37 different markers determined by multiplex bead-based assay for the same dataset as shown in Figure 6D. Error bars S.D, (*Technical replicate, n=* 5000-15000).

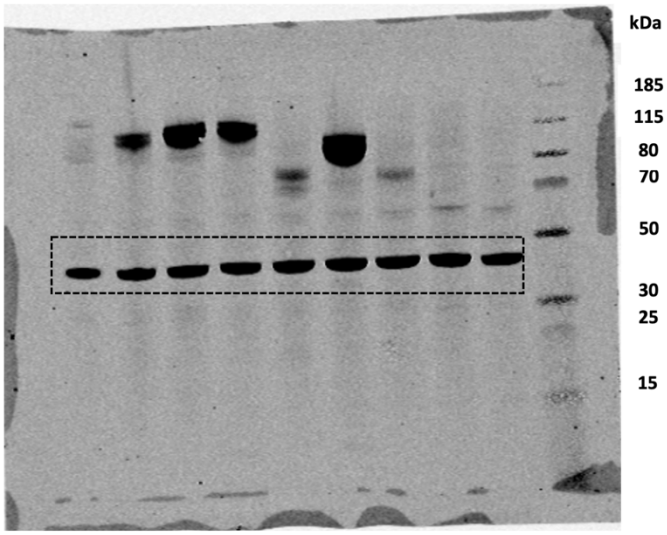

Supplementary Figure 17. Full length blot corresponding to Supp. Figure 3A.

Supplementary Table 1. EAE scoring system used in this study

EAE-Score	Clinical signs
0	No clinical signs
1	Partially limp tail
2	Paralyzed tail
3	Hind limb paresis, uncoordinated movement
4	One hind limb paralyzed
5	Both hind limbs paralyzed
6	Hind limbs paralyzed, weakness in forelimbs
7	Hind limbs paralyzed, one forelimb paralyzed

8	Hind limbs paralyzed, both forelimbs paralyzed
9	Moribund
10	Death

Supplementary Table 2. Amino acid sequence of the various genetic constructs used in this study.

Construct	Amino acid sequence
mIL6ST TSG101	MSAPRIWLAQALLFFLTTESIGQLLEPCGYIYPEFPVVQRGSNFTAICVLKEACLQHYYVNASYIVWKTNHAAVPREQVTVINRTTSSVTFTDVVLPS VQLTCNILSFGQIEQNVYGVTMLSGFPPDKPTNLTCIVNEGKNMLCQWDPGRETYLETNYTLKSEWATEKFPDCQSKHGTSCMVSYMPTYYVNI EVWVEAENALGKVSSESINFDPVDKVKPTPPYNLSVTNSEELSSILKLSWVSSGLGGLLDLKSDIQYRTKDASTWIQVPLEDTMSPRTSFTVQDLKP FTEYVFRIRSIKDSGKGYWSDWSEEASGTTYEDRPSRPPSFWYKTNPSHGQEYRSVRLIWKALPLSEANGKILDYEVILTQSKSVSQTYTVTGTELTV NLTNDRYVASLAARNKVGKSAAAVLTIPSPHVTAAYSVVNLKAFPKDNLLWVEWTPPPKPVSKYILEWCVLSENAPCVAmEDWQQEDATVNRT HLRGRLLESKCYQITVTPVFATGPGGSESLKAYLKQAAPARGPTVRTKKVGKNEAVLAWDQIPVDDQNGFIRNYSISYRTSVGKEMVVHVDSSHT EYTLSSLSSDTLYMVRMAAYTDEGGKDGPEFTFTTPKFAQGEIEAIVVPVCLAFLLTTLLGVLFCFNKRDLIKKHIWPNVPDPSKSHIAQWSPHTPPR HNFNSKDQGGGSGSGGSGSAVSESQLKKMVSKYKYRDLTVRETVNVITLYKDLKPVLDSYVFNDGSSRELMNLTGTIPVPYRGNTYNIPICLWLLDTY PYNPPICFVKPTSSMTIKTGKHVDANGKIYLPYLHEWKHPQSDLLGLIQVMIVVFGDEPPVFSRPISASYPPYQATGPPNTSYMPGMPGGISPYPS GYPPNPSGYPGCPYPPGGPYPATTSSQYPSQPPVTTVGPSRDGTISEDTIRASLISAVSDKLRWRMKEEMDRAQAELNALKRTEEDLKKGHQKLEE MVTRLDQEVAEVDKNIELLKKKDEELSSALEKMENQSENNDIDEVIIPTAPLYKQILNLYAEENAIEDTIFYLGEALRRGVIDLDVFLKHVRLLSRKQF QLRALMQKARKTAGLSDLYHHHHHH
mIL6ST N-term-Syntenin	MSAPRIWLAQALLFFLTTESIGQLLEPCGYIYPEFPVVQRGSNFTAICVLKEACLQHYYVNASYIVWKTNHAAVPREQVTVINRTTSSVTFTDVVLPS VQLTCNILSFGQIEQNVYGVTMLSGFPPDKPTNLTCIVNEGKNMLCQWDPGRETYLETNYTLKSEWATEKFPDCQSKHGTSCMVSYMPTYYVNI EVWVEAENALGKVSSESINFDPVDKVKPTPPYNLSVTNSEELSSILKLSWVSSGLGGLLDLKSDIQYRTKDASTWIQVPLEDTMSPRTSFTVQDLKP FTEYVFRIRSIKDSGKGYWSDWSEEASGTTYEDRPSRPPSFWYKTNPSHGQEYRSVRLIWKALPLSEANGKILDYEVILTQSKSVSQTYTVTGTELTV NLTNDRYVASLAARNKVGKSAAAVLTIPSPHVTAAYSVVNLKAFPKDNLLWVEWTPPPKPVSKYILEWCVLSENAPCVEDWQQEDATVNRTHLR GRLLESKCYQITVTPVFATGPGGSESLKAYLKQAAPARGPTVRTKKVGKNEAVLAWDQIPVDDQNGFIRNYSISYRTSVGKEMVVHVDSSHTEYTL SSLSSDTLYMVRMAAYTDEGGKDGPEFTFTTPKFAQGEIEAIVVPVCLAFLLTTLLGVLFCFNKRDLIKKHIWPNVPDPSKSHIAQWSPHTPPRHNF NSKDQGGGSGSGGSGSAVSESQLKKMVSKYKYRDLTVRETVNVITLYKDLKPVLDSYVFNDGSSRELMNLTGTIPVPYRGNTYNIPICLWLLDTY PYNPPICFVKPTSSMTIKTGKHVDANGKIYLPYLHEWKHPQSDLLGLIQVMIVVFGDEPPVFSRPISASYPPYQATGPPNTSYMPGMPGGISPYPS GYPPNPSGYPGCPYPPGGPYPATTSSQYPSQPPVTTVGPSRDGTISEDTIRASLISAVSDKLRWRMKEEMDRAQAELNALKRTEEDLKKGHQKLEE MVTRLDQEVAEVDKNIELLKKKDEELSSALEKMENQSENNDIDEVIIPTAPLYKQILNLYAEENAIEDTIFYLGEALRRGVIDLDVFLKHVRLLSRKQF QLRALMQKARKTAGLSDLYHHHHHH
mIL6ST	MSAPRIWLAQALLFFLTTESIGQLLEPCGYIYPEFPVVQRGSNFTAICVLKEACLQHYYVNASYIVWKTNHAAVPREQVTVINRTTSSVTFTDVVLPS VQLTCNILSFGQIEQNVYGVTMLSGFPPDKPTNLTCIVNEGKNMLCQWDPGRETYLETNYTLKSEWATEKFPDCQSKHGTSCMVSYMPTYYVNI EVWVEAENALGKVSSESINFDPVDKVKPTPPYNLSVTNSEELSSILKLSWVSSGLGGLLDLKSDIQYRTKDASTWIQVPLEDTMSPRTSFTVQDLKP FTEYVFRIRSIKDSGKGYWSDWSEEASGTTYEDRPSRPPSFWYKTNPSHGQEYRSVRLIWKALPLSEANGKILDYEVILTQSKSVSQTYTVTGTELTV NLTNDRYVASLAARNKVGKSAAAVLTIPSPHVTAAYSVVNLKAFPKDNLLWVEWTPPPKPVSKYILEWCVLSENAPCVEDWQQEDATVNRTHLR GRLLESKCYQITVTPVFATGPGGSESLKAYLKQAAPARGPTVRTKKVGKNEAVLAWDQIPVDDQNGFIRNYSISYRTSVGKEMVVHVDSSHTEYTL SSLSSDTLYMVRMAAYTDEGGKDGPEFTFTTPKFAQGEIEAIVVPVCLAFLLTTLLGVLFCFNKRDLIKKHIWPNVPDPSKSHIAQWSPHTPPRHNF NSKDQHHHHHH
mIL6ST Syndecan 1 x 3	MSAPRIWLAQALLFFLTTESIGQLLEPCGYIYPEFPVVQRGSNFTAICVLKEACLQHYYVNASYIVWKTNHAAVPREQVTVINRTTSSVTFTDVVLPS VQLTCNILSFGQIEQNVYGVTMLSGFPPDKPTNLTCIVNEGKNMLCQWDPGRETYLETNYTLKSEWATEKFPDCQSKHGTSCMVSYMPTYYVNI EVWVEAENALGKVSSESINFDPVDKVKPTPPYNLSVTNSEELSSILKLSWVSSGLGGLLDLKSDIQYRTKDASTWIQVPLEDTMSPRTSFTVQDLKP FTEYVFRIRSIKDSGKGYWSDWSEEASGTTYEDRPSRPPSFWYKTNPSHGQEYRSVRLIWKALPLSEANGKILDYEVILTQSKSVSQTYTVTGTELTV NLTNDRYVASLAARNKVGKSAAAVLTIPSPHVTAAYSVVNLKAFPKDNLLWVEWTPPPKPVSKYILEWCVLSENAPCVEDWQQEDATVNRTHLR GRLLESKCYQITVTPVFATGPGGSESLKAYLKQAAPARGPTVRTKKVGKNEAVLAWDQIPVDDQNGFIRNYSISYRTSVGKEMVVHVDSSHTEYTL SSLSSDTLYMVRMAAYTDEGGKDGPEFTFTTPKFAQGEIEAIVVPVCLAFLLTTLLGVLFCFNKRDLIKKHIWPNVPDPSKSHIAQWSPHTPPRHNF NSKDQGGGSGSGGSGSGGSGSRMKKKDEGSYSLEEPKQANGGAYQKPTKQEEFYAGGGSGSGGSGSGGSGSRMKKKDEGSYSLEEPKQANGG AYQKPTKQEEFYAHHHHHH
mIL6ST-GCN4 LZ-N-term-Syntenin	MSAPRIWLAQALLFFLTTESIGQLLEPCGYIYPEFPVVQRGSNFTAICVLKEACLQHYYVNASYIVWKTNHAAVPREQVTVINRTTSSVTFTDVVLPS VQLTCNILSFGQIEQNVYGVTMLSGFPPDKPTNLTCIVNEGKNMLCQWDPGRETYLETNYTLKSEWATEKFPDCQSKHGTSCMVSYMPTYYVNI EVWVEAENALGKVSSESINFDPVDKVKPTPPYNLSVTNSEELSSILKLSWVSSGLGGLLDLKSDIQYRTKDASTWIQVPLEDTMSPRTSFTVQDLKP FTEYVFRIRSIKDSGKGYWSDWSEEASGTTYEDRPSRPPSFWYKTNPSHGQEYRSVRLIWKALPLSEANGKILDYEVILTQSKSVSQTYTVTGTELTV NLTNDRYVASLAARNKVGKSAAAVLTIPSPHVTAAYSVVNLKAFPKDNLLWVEWTPPPKPVSKYILEWCVLSENAPCVEDWQQEDATVNRTHLR GRLLESKCYQITVTPVFATGPGGSESLKAYLKQAAPARGPTVRTKKVGKNEAVLAWDQIPVDDQNGFIRNYSISYRTSVGKEMVVHVDSSHTEYTL SSLSSDTLYMVRMAAYTDEGGKDGPEFTFTTPKFAQGEIEAIVVPVCLAFLLTTLLGVLFCFNKRDLIKKHIWPNVPDPSKSHIAQWSPHTPPRHNF NSKDQRMKQLEDKVEELLSKNYHLENEVARLKKLVGERGSGSGSGSGSSLYPSLEDLKVDKVIQAQTAYSANPASQAFVLVDASAALPPDGNLYP KLYPELSQYMGLSLNEAEICESMPMVSGAPAQGQLVARPSSVNYMVAPVTGNDAGIRRAEIKHHHHHH
mIL6ST PDGFR TM N-term-Syntenin	MSAPRIWLAQALLFFLTTESIGQLLEPCGYIYPEFPVVQRGSNFTAICVLKEACLQHYYVNASYIVWKTNHAAVPREQVTVINRTTSSVTFTDVVLPS VQLTCNILSFGQIEQNVYGVTMLSGFPPDKPTNLTCIVNEGKNMLCQWDPGRETYLETNYTLKSEWATEKFPDCQSKHGTSCMVSYMPTYYVNI EVWVEAENALGKVSSESINFDPVDKVKPTPPYNLSVTNSEELSSILKLSWVSSGLGGLLDLKSDIQYRTKDASTWIQVPLEDTMSPRTSFTVQDLKP FTEYVFRIRSIKDSGKGYWSDWSEEASGTTYEDSTASFAVGQDTQEVIVVPHSLPFKVVVISAILALVVLTIISLIILIMLWQKKPRGSGSGSGSGSSLY PSLEDLKVDKVIQAQTAYSANPASQAFVLVDASAALPPDGNLYPKLYPELSQYMGLSLNEAEICESMPMVSGAPAQGQLVARPSSVNYMVAPVT GNDAGIRRAEIKHHHHHHHHHHHH
mIL6ST ADRB2 TM CD63	MSAPRIWLAQALLFFLTTESIGQLLEPCGYIYPEFPVVQRGSNFTAICVLKEACLQHYYVNASYIVWKTNHAAVPREQVTVINRTTSSVTFTDVVLPS VQLTCNILSFGQIEQNVYGVTMLSGFPPDKPTNLTCIVNEGKNMLCQWDPGRETYLETNYTLKSEWATEKFPDCQSKHGTSCMVSYMPTYYVNI EVWVEAENALGKVSSESINFDPVDKVKPTPPYNLSVTNSEELSSILKLSWVSSGLGGLLDLKSDIQYRTKDASTWIQVPLEDTMSPRTSFTVQDLKP FTEYVFRIRSIKDSGKGYWSDWSEEASGTTYEDRPSRPPSFWYKTNPSHGQEYRSVRLIWKALPLSEANGKILDYEVILTQSKSVSQTYTVTGTELTV NLTNDRYVASLAARNKVGKSAAAVLTIPSPHVTAAYSVVNLKAFPKDNLLWVEWTPPPKPVSKYILEWCVLSENAPCVEDWQQEDATVNRTHLR GRLLESKCYQITVTPVFATGPGGSESLKAYLKQAAPARGPTVRTKKVGKNEAVLAWDQIPVDDQNGFIRNYSISYRTSVGKEMVVHVDSSHTEYTL SSLSSDTLYMVRMAAYTDEGGKDGPEFTFTTPKFASESPEPLSQQWTAGMGLLMALIVLLIVAGNVLVIVAIAKTPRLAVEGGMKCVKFLLYVLLL AFCACAVGLIAVGVGAQLVLSQTIIQGATPGSLLPVVIIAVGVFLFLVAFVGCCGACKENYCLMITFAIFLSLIMLVEVAAAIAGYVFRDKVMSEFNN NFRQQMENYPKNNHTASILDRMQADFKCCGAANYTDWEKIPSMSKNRVPDSCCINVTVGCGINFNEKAIHKEGCVEKIGGWLRKNVLVVAAA ALGIAFVEVLGIVFACCLVKSIRSGYEVMHHHHHH*
mIL6ST N-term-Syntenin X 3	MSAPRIWLAQALLFFLTTESIGQLLEPCGYIYPEFPVVQRGSNFTAICVLKEACLQHYYVNASYIVWKTNHAAVPREQVTVINRTTSSVTFTDVVLPS VQLTCNILSFGQIEQNVYGVTMLSGFPPDKPTNLTCIVNEGKNMLCQWDPGRETYLETNYTLKSEWATEKFPDCQSKHGTSCMVSYMPTYYVNI EVWVEAENALGKVSSESINFDPVDKVKPTPPYNLSVTNSEELSSILKLSWVSSGLGGLLDLKSDIQYRTKDASTWIQVPLEDTMSPRTSFTVQDLKP

	FTEYVFRIRSIKDSGKGYWSDWSEEASGTTYEDRPSRPPSFWYKTNPSHGQEYRSVRLIWKALPLSEANGKILDYEVILTQSKSVSQTYTVTGTELTV NLTNDRYVASLAARNKVGKSAAAVLTIPSPHVTAAYSVVNLKAFPKDNLLWVEWTPPPKPVSKYILEWCVLSENAPCVEDWQQEDATVNRTHLR GRLLESKCYQITVTPVFATGPGGSESLKAYLKQAAPARGPTVRTKKVGKNEAVLAWDQIPVDDQNGFIRNYSISYRTSVGKEMVVHVDSSHTEYTL SSLSSDTLYMVRMAAYTDEGGKDGPEFTFTTPKFAQGEIEAIVVPVCLAFLLTTLLGVLFCFNKRDLIKKHIWPNVPDPSKSHIAQWSPHTPPRHNF NSKDQGGGGSGGGGSGGGGSSLYPSLEDLKVDKVIQAQTAYSANPASQAFVLVDASAALPPDGNLYPKLYPELSQYMGLSLNEAEICESMPMVS GAPAQGQLVARPSSVNYMVAPVTGNDAGIRRAEIKGGGGSGGGGSGGGGSSLYPSLEDLKVDKVIQAQTAYSANPASQAFVLVDASAALPPDG NLYPKLYPELSQYMGLSLNEAEICESMPMVSGAPAQGQLVARPSSVNYMVAPVTGNDAGIRRAEIKGGGGSGGGGSGGGGSSLYPSLEDLKVD KVIQAQTAYSANPASQAFVLVDASAALPPDGNLYPKLYPELSQYMGLSLNEAEICESMPMVSGAPAQGQLVARPSSVNYMVAPVTGNDAGIRR AEIKHHHHHH*
mIL6ST Flottlin 1	MSAPRIWLAQALLFFLTTESIGQLLEPCGYIYPEFPVVQRGSNFTAICVLKEACLQHYYVNASYIVWKTNHAAVPREQVTVINRTTSSVTFTDVVLPS VQLTCNILSFGQIEQNVYGVTMLSGFPPDKPTNLTCIVNEGKNMLCQWDPGRETYLETNYTLKSEWATEKFPDCQSKHGTSCMVSYMPTYYVNI EVWVEAENALGKVSSESINFDPVDKVKPTPPYNLSVTNSEELSSILKLSWVSSGLGGLLDLKSDIQYRTKDASTWIQVPLEDTMSPRTSFTVQDLKP FTEYVFRIRSIKDSGKGYWSDWSEEASGTTYEDRPSRPPSFWYKTNPSHGQEYRSVRLIWKALPLSEANGKILDYEVILTQSKSVSQTYTVTGTELTV NLTNDRYVASLAARNKVGKSAAAVLTIPSPHVTAAYSVVNLKAFPKDNLLWVEWTPPPKPVSKYILEWCVLSENAPCVEDWQQEDATVNRTHLR GRLLESKCYQITVTPVFATGPGGSESLKAYLKQAAPARGPTVRTKKVGKNEAVLAWDQIPVDDQNGFIRNYSISYRTSVGKEMVVHVDSSHTEYTL SSLSSDTLYMVRMAAYTDEGGKDGPEFTFTTPKFAQGEIEAIVVPVCLAFLLTTLLGVLFCFNKRDLIKKHIWPNVPDPSKSHIAQWSPHTPPRHNF NSKDQGSGSGSGSGSFFTCGPNEAMVVSGFCRSPPVMVAGGRVFVLPCIQQIQRISLNTLTLNVKSEKVYTRHGVPISVTGIAQVKIQGQNKEML AAACQMFLGKTEAEIAHIALETLEGHQRAIMAHMTVEEIYKDRQKFSEQVFKVASSDLVNMGISVVSYTLKDIHDDQDYLHSLGKARTAQVQKD ARIGEAEAKRDAGIREAKAKQEKVSAQYLSEIEMAKAQRDYELKKAAYDIEVNTRRAQADLAYQLQVAKTKQQIEEQRVQVQVVERAQQVAVQE QEIARREKELEARVRKPAEAERYKLERLAEAEKSQLIMQAEAEAASVRMRGEAEAFAIGARARAEAEQMAKKAEAFQLYQEAAQLDMLLEKLPQ VAEEISGPLTSANKITLVSSGSGTMGAAKVTGEVLDILTRLPESVERLTGVSISQVNHKPLRTAHHHHHH*
mIL6ST-Fragment X-N-term-Syntenin	MSAPRIWLAQALLFFLTTESIGQLLEPCGYIYPEFPVVQRGSNFTAICVLKEACLQHYYVNASYIVWKTNHAAVPREQVTVINRTTSSVTFTDVVLPS VQLTCNILSFGQIEQNVYGVTMLSGFPPDKPTNLTCIVNEGKNMLCQWDPGRETYLETNYTLKSEWATEKFPDCQSKHGTSCMVSYMPTYYVNI EVWVEAENALGKVSSESINFDPVDKVKPTPPYNLSVTNSEELSSILKLSWVSSGLGGLLDLKSDIQYRTKDASTWIQVPLEDTMSPRTSFTVQDLKP FTEYVFRIRSIKDSGKGYWSDWSEEASGTTYEDRPSRPPSFWYKTNPSHGQEYRSVRLIWKALPLSEANGKILDYEVILTQSKSVSQTYTVTGTELTV NLTNDRYVASLAARNKVGKSAAAVLTIPSPHVTAAYSVVNLKAFPKDNLLWVEWTPPPKPVSKYILEWCVLSENAPCVEDWQQEDATVNRTHLR GRLLESKCYQITVTPVFATGPGGSESLKAYLKQAAPARGPTVRTKKVGKNEAVLAWDQIPVDDQNGFIRNYSISYRTSVGKEMVVHVDSSHTEYTL SSLSSDTLYMVRMAAYTDEGGKDGPEFTFTTPKFAQGEIEAIVVPVCLAFLLTTLLGVLFCFNKRDLIKKHIWPNVPDPSKSHIAQWSPHTPPRHNF NSKDQETIETFDNNEEESSYSYEEINDQTNDNITARLDRIDEKLSEILGMLHTLVVASAGPTSARGSGSGSGSGSSLYPSLEDLKVDKVIQAQTAYSA NPASQAFVLVDASAALPPDGNLYPKLYPELSQYMGLSLNEAEICESMPMVSGAPAQGQLVARPSSVNYMVAPVTGNDAGIRRAEIKHHHHHH*
mIL6ST-2XGCN4 LZ-N-term-Syntenin	MSAPRIWLAQALLFFLTTESIGQLLEPCGYIYPEFPVVQRGSNFTAICVLKEACLQHYYVNASYIVWKTNHAAVPREQVTVINRTTSSVTFTDVVLPS VQLTCNILSFGQIEQNVYGVTMLSGFPPDKPTNLTCIVNEGKNMLCQWDPGRETYLETNYTLKSEWATEKFPDCQSKHGTSCMVSYMPTYYVNI EVWVEAENALGKVSSESINFDPVDKVKPTPPYNLSVTNSEELSSILKLSWVSSGLGGLLDLKSDIQYRTKDASTWIQVPLEDTMSPRTSFTVQDLKP FTEYVFRIRSIKDSGKGYWSDWSEEASGTTYEDRPSRPPSFWYKTNPSHGQEYRSVRLIWKALPLSEANGKILDYEVILTQSKSVSQTYTVTGTELTV NLTNDRYVASLAARNKVGKSAAAVLTIPSPHVTAGSGSGSGSGSGSRMKQLEDKVEELLSKNYHLENEVARLKKLVGERGSGSGSGSGSDNKFNKEQ QNAFYEILHLPNLNEEQRNAFIQSLKDDPSQSANLLAEAKKLNDAQAPKAAPARGPTVRTKKVGKNEAVLAWDQIPVDDQNGFIRNYSISYRTSV GKEMVVHVDSSHTEYTLSSLSSDTLYMVRMAAYTDEGGKDGPEFTFTTPKFAQGEIEAIVVPVCLAFLLTTLLGVLFCFNKRDLIKKHIWPNVPDPS KSHIAQWSPHTPPRHNFNSKDQGSGSGSGSGSGSRMKQLEDKVEELLSKNYHLENEVARLKKLVGERGSGSGSGSGSSLYPSLEDLKVDKVIQAQTA YSANPASQAFVLVDASAALPPDGNLYPKLYPELSQYMGLSLNEAEICESMPMVSGAPAQGQLVARPSSVNYMVAPVTGNDAGIRRAEIKHHHHH HH*
mIL6ST-GCN4 LZ-Tfr Endosomal domain	MSAPRIWLAQALLFFLTTESIGQLLEPCGYIYPEFPVVQRGSNFTAICVLKEACLQHYYVNASYIVWKTNHAAVPREQVTVINRTTSSVTFTDVVLPS VQLTCNILSFGQIEQNVYGVTMLSGFPPDKPTNLTCIVNEGKNMLCQWDPGRETYLETNYTLKSEWATEKFPDCQSKHGTSCMVSYMPTYYVNI EVWVEAENALGKVSSESINFDPVDKVKPTPPYNLSVTNSEELSSILKLSWVSSGLGGLLDLKSDIQYRTKDASTWIQVPLEDTMSPRTSFTVQDLKP FTEYVFRIRSIKDSGKGYWSDWSEEASGTTYEDRPSRPPSFWYKTNPSHGQEYRSVRLIWKALPLSEANGKILDYEVILTQSKSVSQTYTVTGTELTV NLTNDRYVASLAARNKVGKSAAAVLTIPSPHVTAAYSVVNLKAFPKDNLLWVEWTPPPKPVSKYILEWCVLSENAPCVEDWQQEDATVNRTHLR GRLLESKCYQITVTPVFATGPGGSESLKAYLKQAAPARGPTVRTKKVGKNEAVLAWDQIPVDDQNGFIRNYSISYRTSVGKEMVVHVDSSHTEYTL SSLSSDTLYMVRMAAYTDEGGKDGPEFTFTTPKFAQGEIEAIVVPVCLAFLLTTLLGVLFCFNKRDLIKKHIWPNVPDPSKSHIAQWSPHTPPRHNF NSKDQRMKQLEDKVEELLSKNYHLENEVARLKKLVGERGSGSGSGSGSMDQARSAFSNLFGGEPLSYTRFSLARQVDGDNSHVEMKLAVDEEE NADNNTKANVTKPKHHHHHH*
hTNFR1	MGLSTVPDLLLPLVLLELLVGIYPSGVIGLVPHLGDREKRDSVCPQGKYIHPQNNSICCTKCHKGTYLYNDCPGPGQDTDCRECESGSFTASENHLR HCLSCSKCRKEMGQVEISSCTVDRDTVCGCRKNQYRHYWSENLFQCFNCSLCLNGTVHLSCQEKQNTVCTCHAGFFLRENECVSCSNCKKSLECT KLCLPQIENVKGTEDSGTTVLLPLVIFFGLCLLSLLFIGLMYRYQRWKSKLYSIVCGKSTPEKEGELEGTTTKPLAPNPSFSPTPGFTPTLGFSPVPSSTF TSSSTYTPGDCPNFAAPRREVAPPYQGADPILATALASDPIPNGGGGSGRVILEGGHHHHHH*
hTNFR1-Linker-Syndecan 1	MGLSTVPDLLLPLVLLELLVGIYPSGVIGLVPHLGDREKRDSVCPQGKYIHPQNNSICCTKCHKGTYLYNDCPGPGQDTDCRECESGSFTASENHLR HCLSCSKCRKEMGQVEISSCTVDRDTVCGCRKNQYRHYWSENLFQCFNCSLCLNGTVHLSCQEKQNTVCTCHAGFFLRENECVSCSNCKKSLECT KLCLPQIENVKGTEDSGTTVLLPLVIFFGLCLLSLLFIGLMYRYQRWKSKLYSIVCGKSTPEKEGELEGTTTKPLAPNPSFSPTPGFTPTLGFSPVPSSTF TSSSTYTPGDCPNFAAPRREVAPPYQGADPILATALASDPIPNGGGGSGRKDEGSYSLEEPKQANGGAYQKPTKQEEFYALEGGHHHHHH*
hTNFR1 C-term-CD63	MGLSTVPDLLLPLVLLELLVGIYPSGVIGLVPHLGDREKRDSVCPQGKYIHPQNNSICCTKCHKGTYLYNDCPGPGQDTDCRECESGSFTASENHLR HCLSCSKCRKEMGQVEISSCTVDRDTVCGCRKNQYRHYWSENLFQCFNCSLCLNGTVHLSCQEKQNTVCTCHAGFFLRENECVSCSNCKKSLECT KLCLPQIENVKGTEDSGTTVLLPLVIFFGLCLLSLLFIGLMYRYQRWKSKLYSIVCGKSTPEKEGELEGTTTKPLAPNPSFSPTPGFTPTLGFSPVPSSTF TSSSTYTPGDCPNFAAPRREVAPPYQGADPILATALASDPIPNGGGGSGRCCLVKSIRSGYEVMCCLLEGGHHHHHH*
hTNFR1 C-term-CD63 X 2	MGLSTVPDLLLPLVLLELLVGIYPSGVIGLVPHLGDREKRDSVCPQGKYIHPQNNSICCTKCHKGTYLYNDCPGPGQDTDCRECESGSFTASENHLR HCLSCSKCRKEMGQVEISSCTVDRDTVCGCRKNQYRHYWSENLFQCFNCSLCLNGTVHLSCQEKQNTVCTCHAGFFLRENECVSCSNCKKSLECT KLCLPQIENVKGTEDSGTTVLLPLVIFFGLCLLSLLFIGLMYRYQRWKSKLYSIVCGKSTPEKEGELEGTTTKPLAPNPSFSPTPGFTPTLGFSPVPSSTF TSSSTYTPGDCPNFAAPRREVAPPYQGADPILATALASDPIPNGGGGSGRCCLVKSIRSGYEVMCCLVKSIRSGYEVMLEGGHHHHHH*
hTNFR1 N-term-Syntenin	MGLSTVPDLLLPLVLLELLVGIYPSGVIGLVPHLGDREKRDSVCPQGKYIHPQNNSICCTKCHKGTYLYNDCPGPGQDTDCRECESGSFTASENHLR HCLSCSKCRKEMGQVEISSCTVDRDTVCGCRKNQYRHYWSENLFQCFNCSLCLNGTVHLSCQEKQNTVCTCHAGFFLRENECVSCSNCKKSLECT KLCLPQIENVKGTEDSGTTVLLPLVIFFGLCLLSLLFIGLMYRYQRWKSKLYSIVCGKSTPEKEGELEGTTTKPLAPNPSFSPTPGFTPTLGFSPVPSSTF TSSSTYTPGDCPNFAAPRREVAPPYQGADPILATALASDPIPNGGGGSGRSLYPSLEDLKVDKVIQAQTAFSANPANPAILSEASAPIPHDGNLYPR LYPELSQYMGLSLEGGHHHHHH*
hTNFR1 CD63	MAVEGGMKCVKFLLYVLLLAFCACAVGLIAIGVAVQVVLKQAITHETTAGSLLPVVIIAVGAFLFLVAFVGCCGACKENYCLMITFAIFLSLIMLVEV AVAIAGYVGGSRIHPSGVTGLVPSLGDREKRDSLCPQGKYVHSKNNSICCTKCHKGTYLVSDCPSPGRDTVCRECEKGTFTASQNYLRQCLSCKTC RKEMSQVEISPCQADKDTVCGCKENQFQRYLSETHFQCVDCSPCFNGTVTIPCKETQNTVCNCHAGFFLRESECVPCSHCKKNEECMKLCLPPPL ANVTNPQDSGTEFGGIHTQGCVETIAIWLRKNILLVAAAALGIAFVEVLGIIFSCCLVKSIRSGYEVMDPPDLDN*
hTNFR1 delta MMP Intracellular-Foldon N-term-Syntenin	MGLSTVPDLLLPLVLLELLVGIYPSGVIGLVPHLGDREKRDSVCPQGKYIHPQNNSICCTKCHKGTYLYNDCPGPGQDTDCRECESGSFTASENHLR HCLSCSKCRKEMGQVEISSCTVDRDTVCGCRKNQYRHYWSENLFQCFNCSLCLNGTVHLSCQEKQNTVCTCHAGFFLRENECVSCSNCKKSLECT KLCLPQGTEDSGTTVLLPLVIFFGLCLLSLLFIGLMYRYQRWKGTGYIPEAPRDGQAYVRKDGEWVFLSTFLSPANGGGGSGRSLYPSLEDLKVDKVI QAQTAFSANPANPAILSEASAPIPHDGNLYPRLYPELSQYMGLSLEGGHHHHHH*
hTNFR1 delta MMP N-term-Syntenin	MGLSTVPDLLLPLVLLELLVGIYPSGVIGLVPHLGDREKRDSVCPQGKYIHPQNNSICCTKCHKGTYLYNDCPGPGQDTDCRECESGSFTASENHLR HCLSCSKCRKEMGQVEISSCTVDRDTVCGCRKNQYRHYWSENLFQCFNCSLCLNGTVHLSCQEKQNTVCTCHAGFFLRENECVSCSNCKKSLECT KLCLPQGTEDSGTTVLLPLVIFFGLCLLSLLFIGLMYRYQRWKNGGGGSGRSLYPSLEDLKVDKVIQAQTAFSANPANPAILSEASAPIPHDGNLYPR LYPELSQYMGLSLEGGHHHHHH*
hTNFR1 delta MMP extracellular-Foldon N-term-Syntenin	MGLSTVPDLLLPLVLLELLVGIYPSGVIGLVPHLGDREKRDSVCPQGKYIHPQNNSICCTKCHKGTYLYNDCPGPGQDTDCRECESGSFTASENHLR HCLSCSKCRKEMGQVEISSCTVDRDTVCGCRKNQYRHYWSENLFQCFNCSLCLNGTVHLSCQEKQNTVCTCHAGFFLRENECVSCSNCKKSLECT KLCLNGGGGSGRGYIPEAPRDGQAYVRKDGEWVFLSTFLSPANGGGGSGRPQGTEDSGTTVLLPLVIFFGLCLLSLLFIGLMYRYQRWKGTNGGG GSGRGYIPEAPRDGQAYVRKDGEWVFLSTFLSPANGGGGSGRSLYPSLEDLKVDKVIQAQTAFSANPANPAILSEASAPIPHDGNLYPRLYPELSQ YMGLSLEGGHHHHHH*MGLSTVPDLLLPLVLLELLVGIYPSGVIGLVPHLGDREKRDSVCPQGKYIHPQNNSICCTKCHKGTYLYNDCPGPGQDT

	DCRECESGSFTASENHLRHCLSCSKCRKEMGQVEISSCTVDRDTVCGCRKNQYRHYWSENLFQCFNCSLCLNGTVHLSCQEKQNTVCTCHAGFFL RENECVSCSNCKKSLECTKLCLNGGGGSGRGYIPEAPRDGQAYVRKDGEWVFLSTFLSPAPQGTEDSGTTVLLPLVIFFGLCLLSLLFIGLMYRYQR WKGTNGGGGSGRSLYPSLEDLKVDKVIQAQTAFSANPANPAILSEASAPIPHDGNLYPRLYPELSQYMGLSLEGGHHHHHHHHHHHH*
hTNFR1 delta MMP Extra and Intracellular-Foldon N-term-Syntenin	MGLSTVPDLLLPLVLLELLVGIYPSGVIGLVPHLGDREKRDSVCPQGKYIHPQNNSICCTKCHKGTYLYNDCPGPGQDTDCRECESGSFTASENHLR HCLSCSKCRKEMGQVEISSCTVDRDTVCGCRKNQYRHYWSENLFQCFNCSLCLNGTVHLSCQEKQNTVCTCHAGFFLRENECVSCSNCKKSLECT KLCLNGGGGSGRGYIPEAPRDGQAYVRKDGEWVFLSTFLSPANGGGGSGRPQGTEDSGTTVLLPLVIFFGLCLLSLLFIGLMYRYQRWKGTNGGG GSGRGYIPEAPRDGQAYVRKDGEWVFLSTFLSPANGGGGSGRSLYPSLEDLKVDKVIQAQTAFSANPANPAILSEASAPIPHDGNLYPRLYPELSQ YMGLSLEGGHHHHHH*